POLITECNICO DI MILANO

Determination of Electron Phonon Coupling from RIXS Spectral Intensity

Relatore:
Prof. Giacomo GHIRINGHELLI

Autore:
Mattia PAGETTI

Facoltà di Ingegneria Industriale e dell'Informazione

Corso di Laurea Magistrale in Ingegneria Fisica

Anno accademico 2017-2018

"La verità è sempre inverosimile [...]. Per rendere la verità più verosimile, bisogna assolutamente mescolarvi della menzogna. La gente ha sempre fatto così."

Fëdor Dostoevskij, *I Demoni*

POLITECNICO DI MILANO

Abstract

Scuola di Ingegneria dell'Informazione
Dipartimento di Fisica

Physics Engeenering

Determination of Electron Phonon Coupling from RIXS Spectral Intensity

by Mattia PAGETTI

Ho lavorato alla presente tesi all'interno del gruppo di ricerca guidato dal professor Giacomo Ghiringhelli, presso il dipartimento di fisica del Politecnico di Milano, a cavallo tra l'autunno del 2018 e la primavera del 2019.
Il gruppo possiede una lunga e consolidata tradizione nell'ambito della spettroscopia realizzata attraverso radiazione di sincrotrone e finalizzata allo studio delle proprietà magnetiche ed elettroniche della materia. Negli ultimi venti anni, infatti, l'attività del gruppo è ruotata attorno alla spettroscopia d'emissione di raggi X, ed in particolare alla tecnica sperimentale che prende il nome di RIXS - Resonant Inelastic X-rays Scattering. I dati da questa ottenuti, eventualmente integrati con quelli di altre tecniche affini e complementari (XAS, XLD, XMCD), permettono di studiare, quindi di caratterizzare in termini di vettor d'onda ed energia, le eccitazioni del materiale - manifestazioni dirette ed univoche della struttura atomica ed elettronica. Contribuendo allo sviluppo tecnico tanto quanto a quello teorico del RIXS, l'intenso lavoro del gruppo ha, a partire dal nuovo millennio, aperto la strada ad una nuova e più fine comprensione di fenomeni e dinamiche microscopiche della materia, offrendo a tutti gli effeti un nuovo punto di vista complementare (e per molti versi peculiare) nel panorama delle tecniche sperimentali fino ad allora presenti (INS, Inelastic Neutron Scattering, su tutte).
A partire dal 2009, inoltre, la ricerca del gruppo si è concentrata attorno ai metalli di transizione $3d$, con particolare enfasi per quanto riguarda i cuprati, materiali estremamente singolari caratterizzati da una struttura quasi bidimensionale (relativamente ai piani CuO_2 in essi presenti), rimarchevoli per essere superconduttori ad alta temperatura; più di ogni altra cosa, però, ancora enigmatici (la vera natura della superconduttività ad alte temperature non trova a tutt'oggi una spiegazione convincente) ed adatti ad essere studiati attraverso la RIXS.
In questo ambito si inserisce la mia tesi - incomincerò quindi da una breve introduzione riguardo i cuprati (approfondendone due in particolare, LCO e NBCO, e spendendo prima qualche parola sui superconduttori in generale e sui sistemi fortemente correlati), soffermandomi quindi sull'importanza dei fononi all'interno del meccanismo che si pensa regoli la superconduttività ad alte temperature, per poi dedicare un intero capitolo al RIXS, approfondendone aspetti teorici e tecnici quanto basta ed aggiungendo considerazioni di stampo prettamente pratico.
Il terzo capitolo rappresenta il corpo principale del mio lavoro: interamente dedicato alle dinamiche fononiche caratterizzabili attraverso il RIXS, ne si affronta prima la teoria (seguendo le tracce già date dalla letteratura), passando poi alla simulazione di quelli che, date le dovute premesse e approsimazioni, dovrebbero essere gli spettri RIXS associabili alle diverse eccitazioni fononiche presenti nei materiali.
Infine, l'ultimo capitolo è un'analisi dei risultati ottenuti durante l'esperimento condotto a ESRF sulla beamline ID32. Perticolare enfasi è posta sul metodo con cui le analisi sono condotte - aspetto preponderante nell'ambito del RIXS più di quanto lo sia in altre tecniche sperimentali.

I have worked on this thesis within the group of professor Giacomo Ghiringhelli, at the physics department of Politecnico di Milano, between the autumn of 2018 and the spring of 2019.
The group has a long and consolidated tradition in synchrotron based spectroscopy, aimed at the study of magnetic and electronic properties of the materials. In the last twenty years, indeed, the activity of the group has been focused on X-rays emission spectroscopy, and in particular on the experimental technique denominated RIXS - Resonant Inelastic X-rays Scattering. The data obtained from it, possibly complemented with the ones obtained from other techniques (XAS, XLD, XMCD), allow us to study, and thus to characterize in energy and momentum, the material's excitations - which are direct and unequivocal manifestations of the atomic and electronic structure. Participating in both the technical and theoretical development of RIXS, the intensive work of the group have, since the beginning of the new millennium, paved the way to a new and more sharp understanding of matter's microscopic phenomena and dynamics, providing a new and complementary point of view (endued with many peculiarities) in the landscape of the already present experimental techniques (INS, Inelastic Neutron Scattering, most notably).
Since 2009, more in particular, the group research has been focused on $3d$ transition-metal compounds, with greater emphasis on cuprates, exceptionally unique materials characterized by a quasi bidimensional structure (given by CuO_2 layers), notable for being high temperature superconductors; and most importantly, puzzling (the true nature of high temperature superconductivity is nowadays still missing a coherent explanation) and suitable to be investigated through RIXS.
My thesis can be placed in this contest - I will thus begin from a brief introduction on cuprates (paying particular attention to LCO and NBCO, and mentioning the most important characteristic of superconductors and strongly correlated systems), spending some words on the importance of phonons in the mechanism which is thought to be at the basis of high temperature superconductivity, to then dedicate a whole Chapter (the second one) to the RIXS technique, with a focus on theoretical and technical aspects, and incorporating some practical consideration.
The third Chapter is the main body of the thesis: it is devoted to the phononic dynamics which can be characterized through a RIXS investigation. In first place, the theory is shown (following the tracks already given by the literature), and then RIXS spectra are simulated, accounting for the premises and for the assumptions - given the phononic excitations in the sample, those spectra are what we expect as a result from a RIXS experiment.
Finally, the last chapter is an analysis of the results obtained during the experiment that we carried out at ESRF on the beamline ID32. Particular emphasis is given on the analysis method - this is a predominant aspect in RIXS technique, more than in othes experimental techniques.

Acknowledgements

Innanzitutto ed in particolare devo ringraziare Giacomo, che sin dal primo giorno ha sempre trovato il tempo, il modo e soprattutto la pazienza di guidarmi all'interno di quel mondo per me completamente nuovo che è la ricerca scientifica. A tutti gli effetti, è un esempio da cui ho tratto grande ispirazione.
Grazie anche al resto del gruppo: Lucio, Marco, Matteo, Riccardo e Roberto, per la compagnia ed il supporto nelle nottati insonni trascorse in beamline; per l'incoraggiamento ed i consigli.
Ringrazio i miei compagni di laboratorio, pure, per aver fin troppo pazientemente sopportato i miei assai frequenti sfoghi.
E poi, ovviamente, tutti i miei amici - e mi limiterò a dire di essere fin troppo fortunato ad averne abbastanza da essere vinto dalla pigrizia nel momento di doverli ringraziare uno ad uno; tuttavia mi conoscono, e spero mi perdoneranno.
Infine grazie alla mia famiglia, a cui questa tesi è dedicata, e senza il cui costante supporto non sarei ciò che sono.

Contents

List of Figures

Alla Mia Famiglia

Chapter 1

Cuprates

1.1 Summary

Cuprates superconductors have been discovered in late 1986 [1] (see Figure 1.1 for an historical prospective), when the improvements in samples quality and the development and refinement of sophisticated experimental techniques made their discovery possible. Their high critical temperature - which we define as the maximum temperature at which we observe the emergence of the superconductive state - has immediately raised a great interest in the scientific community, due to the possible revolutionary technological applications.
With RIXS, we have the possibility to investigate many interesting properties of the solids (as we will see more in detail in the next Chapter). In particular, adopting soft X-rays, we are able to work with the K edge of O and $L_{2,3}$ absorption peaks of $3d$ transition-metal compounds, which are in general very interesting materials with many technological applications – and for what concerns transition metals compounds, among the most interesting ones we found cuprates. They are in fact endued with an extremely rich physics which basically relies on their complex electronic structure – and this structure is still to be completely understood. Given this premises, it is quite immediate to understand why the research of the group in which i have worked on this thesis has been focused on cuprates for the last ten years.
In approaching this brief discussion of the cuprates, I add nothing new to what has been done, for example, in [2] or [3], following the track here given in order to achieve a clear presentation.

1.2 High T_c Superconductors

Superconductors are systems which, under a certain critical temperature, undergo a phase transition to the superconducting state, characterized by an identically null resistance and a magnetic field repellent condition - although this is true only in first approximation: in principle we should distinguish type I and type II superconductors, and admit that phenomena like Abrikosov vortex (magnetic fluxes passing through the material) are possible for the latter category. Still, in this section we will have only an introductory discussion; for more details, see [4].

High Temperature Superconductivity, more specifically, is a definition that has been coined in 1986, when Bednorz and Muller discovered that a certain class of material - cuprates, indeed - undergo a superconducting phase transition at a temperature which was forbidden by the BCS theory (BCS stand for Barter-Cooper-Schriffer, author of the theory which explain the canonical superconductivity [4]). The BCS theory, in fact, relies on a well understood mechanism of phonon-mediated coupling of the electrons, which lead to a breakdown of the resistance below T_c - but once we try to apply that mechanism to high temperature superconductors, nor the superconductive state or the unexpected high T_c seems to find a justification.
For example, while in a conventional (always in the sense that can be explained through the BCS theory) superconductor the superconduncting electrons wavefunctions have the same symmetry of the underlying lattice, in high temperature superconductors cuprates they have a so called "d-wave" symmetry, which implies that the wavefunctions changes sign upon rotations of 90°, arising what is called an "unconventional pairing" [5]. This "unconventional pairing" leads to thermodynamic properties which are different from those of conventional superconductors (for more details, see [6]). Even if this is now well understood, the fact that in cuprates, superconductors endued with unconventional symmetries (which were thought to be extremely fragile, in the sense that even small concentrations of impurities were enough to break the superconductive state) the superconductivity is resistant to many disorder manifestations is a puzzle which has still to be solved.
As one could expect, this generated a great enthusiasm, and many attempts were made in order to understand the mechanism behind high temperature superconductivity. After many years, even if many progress have been made, a final and coherent explanation is still missing. Moreover, in the last months, made a great impact the discovery of a material which, although at enormous pressure conditions, exhibit a superconductive state transition at a nearly room temperature [7] - but the mechanism, in this case, is well understood: it is in fact a conventional BCS superconductor, in which the phonons are endued with an exceptional energy.
Anyway, cuprates clearly represented a breakthrough in the physics of superconductivity, with a maximum T_c (at atmospheric pressure condition) of about 138 K.

In order to discover the mechanism behind high temperature superconductors, eventually, it is also crucial to underline the importance of an understanding of the unconventional physics characterizing the normal state from which the superconducting state emerges, where correlations between spin, orbital and charge degrees of freedom lead to the emergence of ordering phenomena and exotic phases (see Figure 1.6 and 1.10).

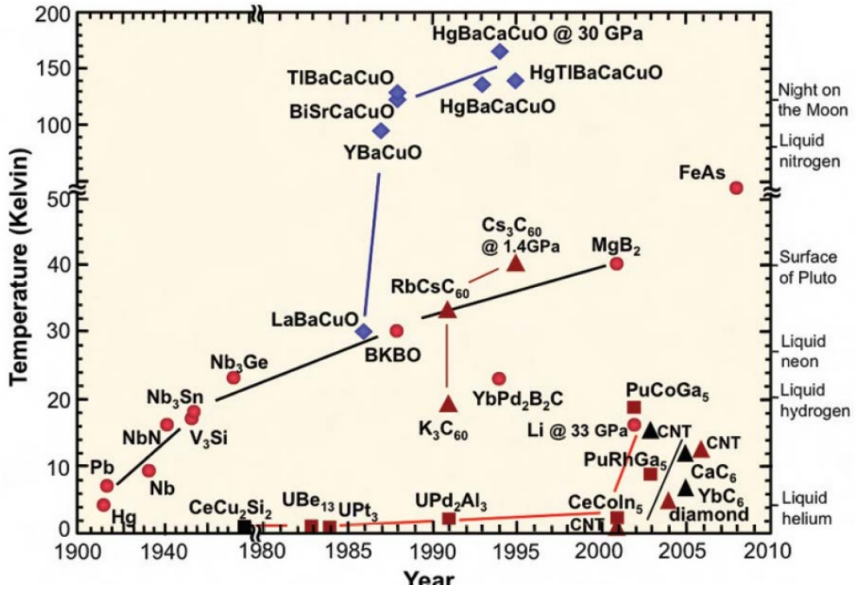

FIGURE 1.1: Historical development of superconducting materials. Figure from [3].

1.3 Correlated Electron Systems

Cuprates superconductors are defined as *strongly correlated electron systems*, because of the non negligible electron-electron interaction which is found in the valence state, where usually the single particle description issued from the Bloch state works well. Cuprates belongs in fact to that class of materials for which one-electron theories fail to describe the observed properties.
When we write one-electron theories, we are referring to theories in which we only consider one electron per time - or, more technically, the Hamiltonian is considered to be equal for every electron, decoupling in this way the wave function of each one through the use of a mean-field approach to account for their mutual interactions. When this approach fails to describe the experimental properties of the material, is simply because in those materials the interactions between the electrons are too complex to be accurately described through a mean-field approach.
When the single electron approach fails, we have that materials which are theoretically predicted as endued with a metallic band structure (in the framework of one-electron theories calculations) could behave, for example, as insulators with very large band gaps, at least at room temperature; and this is the case of ceramic high temperature superconductors, based on CuO_2 layers and exhibiting a poorly conducting antiferromagnetic phase at room temperature and a superconductive phase below a critical temperature T_c.
In principle, many-body calculations are needed. Those approaches are in general very complicated, and rely on very technical mathematical models (such as, for example, the DFT - density functional theory, see [8]) .
An option is to develop a model Hamiltonian which assign a certain coupling between the electrons only for a specific triggers: for example, the Hubbard

model [9], developed in 1963 and probably the simplest of the many body calculations, assign a certain Coulomb repulsion U only when two electrons occupy the same site in the solid. This means to consider a Hamiltonian of the form (exploiting the second quantization formalism):

$$H = -t \sum_{<i,j>,\sigma} c^{+}_{i,\sigma} c_{j,\sigma} + U \sum_{i=1}^{N} n_i \tag{1.1}$$

The term t is here intended to be the overlapping term (in a tight banding approximation sense) between the wave functions of two electrons localized over nearby atoms (where we suppose, for non neighbouring atoms, $t \simeq 0$). There is thus a conflict between two opposite tendencies of the electron - the localization over a single atom and the propagation through the material. The decisive ratio is here $\frac{U}{t}$ - but again: U is a term which single electron calculations do not account for.
Still, even if the Hubbard model is an improvement from single-electron models, it fails in many complex systems descriptions, and more detailed approaches are needed. For example, we could account for the spin part of the wave functions - this is what the Mott model does. Even more, we could refine our picture taking into account also the role of O atoms in our conduction mechanism - and this is done by the Zaanen-Sawatzky-Allen scheme.
An insulating correlated system can be, depending on the magnitude of those different contributions to its insulating character, a Mott-Hubbard insulator or a charge-transfer insulator.
A general discussion of the electronic structure of transition-metal oxides, evidently correlated electron systems, is found in [10], and is behind the purposes of this thesis.

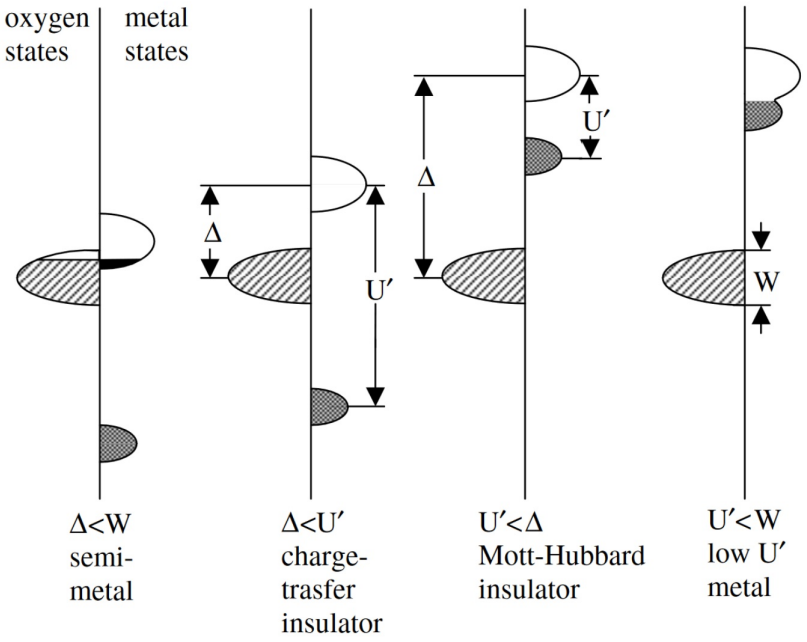

FIGURE 1.2: Schematic diagram for the Zaanen, Sawatzky and Allen theory framework. W is the bandwidth of the occupied oxygen 2*p* states, Δ is the energy difference between the 2*p* oxygen band and the lowest unoccupied metal orbital and U' is the energy difference between the lowest unoccupiedmetal orbital and the highest occupied metal orbital. Depending on the relative magnitude of those three parameter, our material will show different properties (for what concerns the electric conduction). A great number of perovskite oxide compunds have been explained on the basis of such a model. Figure from [32].

1.4 Insulating Layered Cuprates

The most evident peculiarity of cuprates is their electronic structure. Differently from most of the materials composed by transition metals, where the conduction takes place in bands which are originated (again, in the sense of a tight-bending calculation approach) from the 3d orbitals, in cuprates the conduction band has non null contributions from both the 3*d* orbitals of copper and the 2p orbital of oxygen; and this is a distinctive (and non common) result arising from the very narrow energy difference between those orbitals. As we will see later, the CuO_2 plane is at the core of this thesis.

In the CuO_2 plane the copper is in a Cu^{2+} ionization state, and thus with an electronic configuration of $3d^9$, where nine of the ten 3d orbitals are filled. Due to the oxygen ligands surrounding the copper, both in plane and out of plane (where we can have octahedral, pyramidal or squared coordination polyhedra), the 3d orbitals are non degenerate in energy.

The geometrical coordination of the ligands lower the spherical symmetry of the ion and lifts degeneracy in energetic levels endued with the same quantum numbers. In particular, considering an octahedral geometry of the

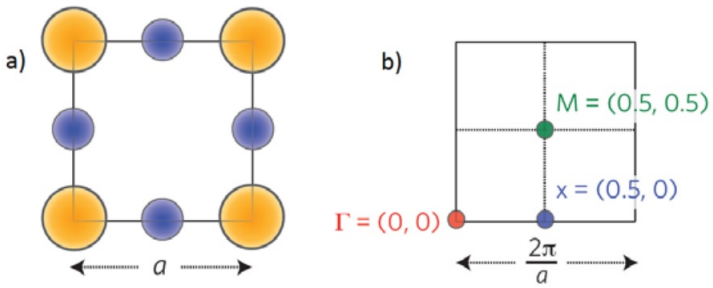

FIGURE 1.3: (a) Basic structural unit of cuprates, where $a \simeq 3.8$ A. (b) The correspondent reciprocal space. M is the antiferromagnetic scattering vector. The periodicity of the spin lattice is in fact double respect to the one of the non magnetic lattice, and thus the magnetic Brillouin zone will be half the size of the canonical one. Moreover, the directions of its basis are rotated of 45 degrees compared to the basis of the real lattice, and this is why the point M is found along the diagonal direction. See Figure 2.5. Figure from [3].

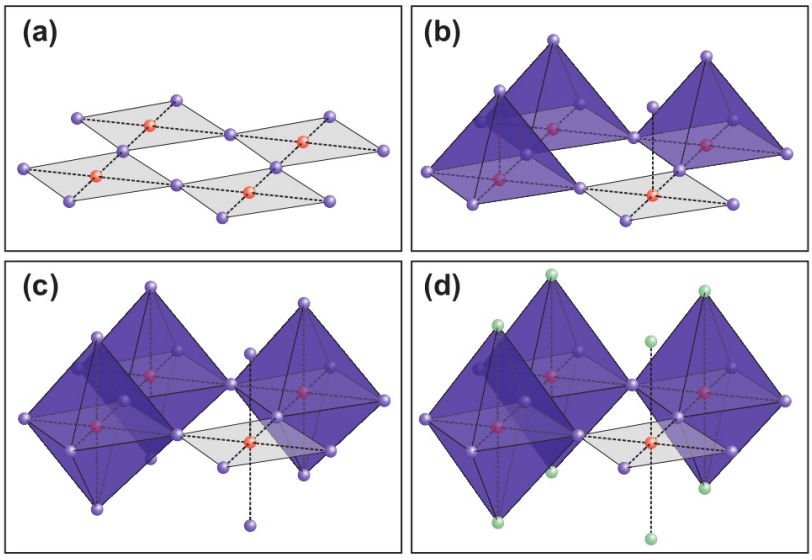

FIGURE 1.4: Some of the possible coordination polyhedra in cuprates. In (a) we have the CuO_2 plane. In (b), (c), (d) we have different geometrical coordination of the ligands. (b) is the case of NBCO, while (c) is the effective coordination geometry of LCO (which are the interesting materials for this thesis, see next Sections). Figure from [11].

ligands surrounding oxygen atoms, we find, assuming the correspondent crystal field in a perturbation theory approach, a splitting of the five $3d$ orbitals in two groups, t_{2g} and e_g, with respect to their symmetry.

The t_{2g} orbitals are obviously the lowest in energy, since the electron spatial distribution is such to reduce the Coulomb repulsion with ligand's crystal

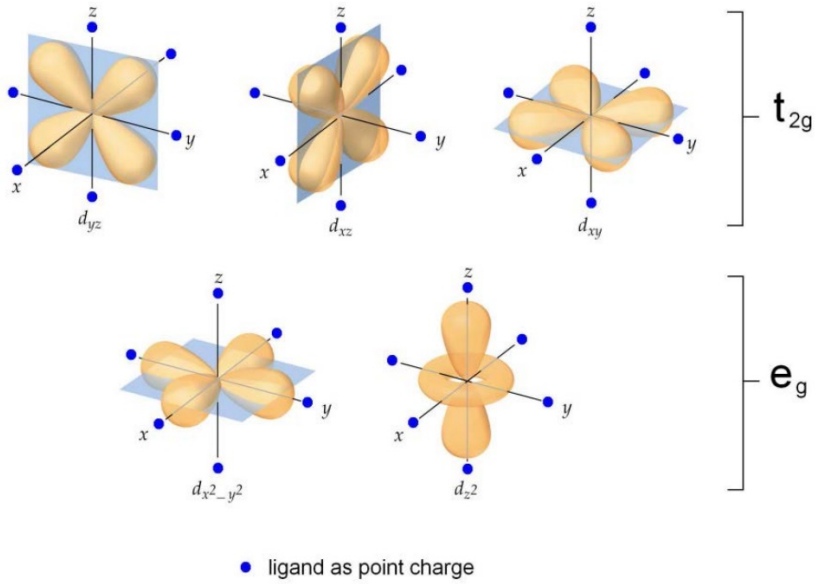

FIGURE 1.5: Cu d orbitals splitting in energy due to the lower symmetry of the system, using a crystal field approach. As it is intuitive, electronic configurations which minimize the Coulomb repulsion between ligands and copper electrons are preferred. Figure from [3].

field. For a specular reason, e_g orbitals hold the highest energy (see Figure 1.5). Moreover, since in cuprates the crystalline field is not cubic, we found that also the different t_{2g} and e_g orbitals are not degenerated in energy with respect to each other.
A standard one-electron theory would predict a metallic behaviour of the material, since we have a not completely filled outer shell of the ion. But this does not happen - layered cuprates are in fact insulators at ambient temperature - and we already knows that it is because cuprates are intrinsically strong correlated electron systems. The reason is that the addition of another electron in the t_{2g} orbital require a non negligible amount of extra energy, which, for example, in the Hubbard model is given by U (1.1), and is not taken in account in one electron calculations.
Speaking about magnetic properties, we have that the insulating layered compounds (which are the parent compounds of high T_c superconductors, in the sense that they become potential superconductors only once doped, as we will see later) have a spin $\frac{1}{2}$ for each Cu^{2+} in the CuO_2 plane. Those spins follow an antiferromagnetic ordering, with a super-exchange mechanism [12](and thus an exchange interaction mediated by oxygen) that can be well described by a bi-dimensional Heisenberg model. They are oriented parallel to the CuO_2 plane (see, for example, [11], and Figure 2.5 for a more general description). The Néel ordering temperature is of about 300 K (which can be considered high, and implies a strong super-exchange mediated coupling, of the order of 140 meV).
As we have mentioned before, when an insulating parent compound (namely an insulating layered cuprate) is doped with extra hoels or electron in the

CuO_2 plane (by modification of the chemical composition outside the planes), we have the emergence of the superconductive state (naturally under the correspondent critical temperature).
This happen only for a certain range of doping, and in this situation we have that the long-range spin order, namely the antiferromagnetic order, is destroyed (but overall spin fluctuations are still found, see [11]). As we can see in Figure 1.6, the general phase diagram of cuprates as a function of doping and temperature is endued with a lot of complexity - in general we have a lot things going on, depending on the doping: the pseudo-gap phase and the antiferromagnetic order are just the most prominent phenomena (for a review of the pseudo-gap state, see [13]). In this thesis we will only briefly see, as significant cases and between others, charge density waves and spin density waves (see [14]).

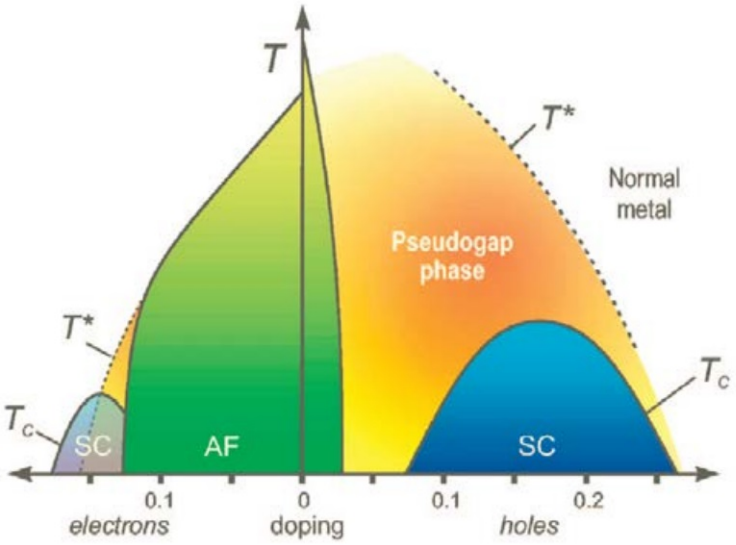

FIGURE 1.6: Phase diagram for cuprates, as a function of doping and temperature. Notably, antiferromagnetic and superconductive phase are shown. As is evident, those systems are sensitive to the sign (i.e. hole or electrons) of the doping. A more exhaustive phase diagram can be found in 1.10. Figure from [15].

In cuprates, we have an intercalation of the CuO_2 plane with other layers, which are called *charge reservoir layers*. The number of electrons available to be put in the electronic states of the CuO_2 (which is also defined as the "effective doping") is imposed, through chemistry, by those layers, which also can isolate or connect each layer with the others. The manipulation of those charge reservoir layer can be accomplished by partial substitution of one atom of higher or lower valence (see Figure 1.7) or by adding oxygen.
We define as the optimal doping as the doping which guarantee the emergence of the superconductive state at the highest temperature.

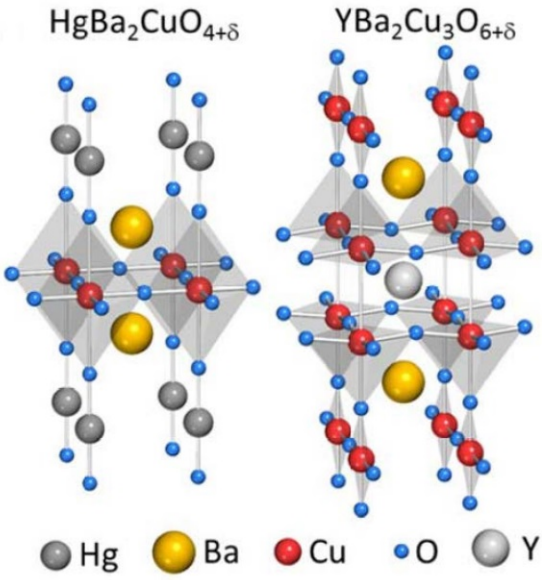

FIGURE 1.7: Schematic representation of crystal structure and charge reservoir layers for two cuprates. In this case the interstitial oxygen variation, which also set the overall doping, is denoted by δ. Figure from [3].

1.4.1 LCO and NBCO

LCO stands for La_2CuO_4. We investigated its properties - paying particular attention to his phononic behaviour, as we will see in Chapter 4 - during our RIXS experiment at the ID32 beam line at ESRF.
It is characterized by an octahedral geometrical organization of the ligands (see Figure 1.3). The parent compound of this family, undoped La_2CuO_4, is a Mott insulator that orders antiferromagnetically, with a Néel temperature of approximately 325 K. This antiferromagnetic order vanish for a doping of about $x \simeq 0.02$. LCO is part of the so called "214 cuprates" family, which are characterized by a composition $La_{2-x-y}(Sr,Ba)_x(Nd,Eu)_yCuO_4$.
NBCO stands for $NdBa_2Cu_3O_7$. We investigated NBCO through RIXS during our experiment at the Diamond Light Source - once again, we focused mainly on the phononic behaviour.
Differently from LCO, it belongs to the "123 cuprates" family, since its composition and crystal structure is the one of the *R*BCO materials (where *R* stands for a Rare Earth).

It is worth to spend a few words about the interesting and peculiar ordering phenomena that we can find in those families, following the track given in [16]. A specific phase diagram, more detailed that the one shown in Figure 1.6, that also account for those ordering phenomena, is found in Figure 1.10.
In the 214 cuprates family, we can think of each doping hole as to a magnetic impurity in the two dimensional antiferromagnetically ordered lattice.

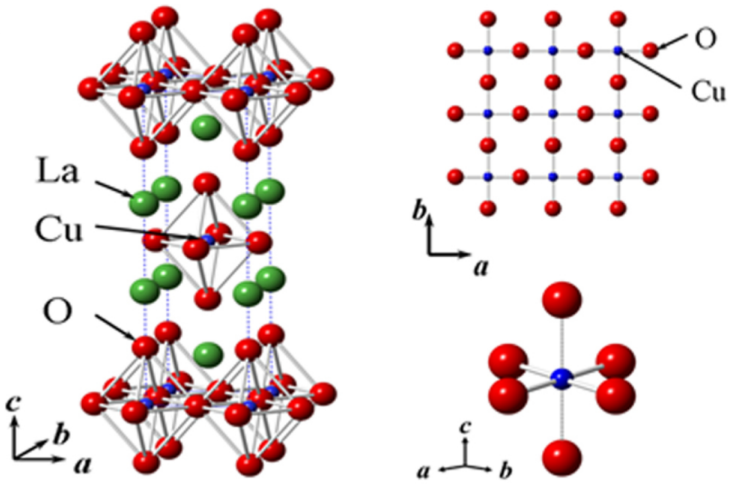

FIGURE 1.8: LCO structure, both in and out the CuO_2 plane. Figure from [3].

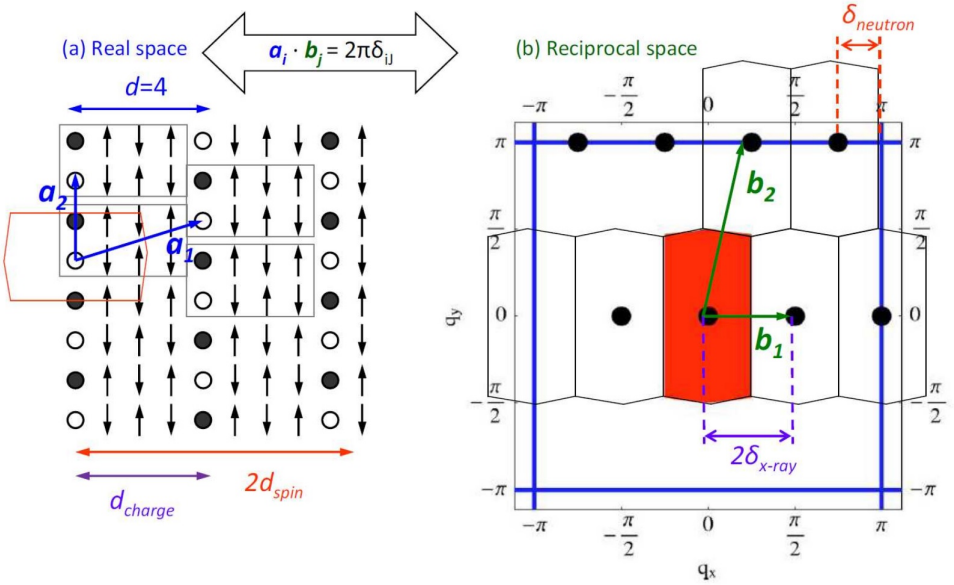

FIGURE 1.9: Rapresentation of half filled stripes in CuO_2 plane, for the minimum allowed distance between the stripes. The reciprocal lattice reflection points generated by charge stripes ordering are indicated, with distinction between the ones associated to the spin order (detectable by INS - a technique that, as we will see in Chapter 2, investigate the Brillouin zone around the $[\pi, \pi]$ point) and the ones associated to charge orders (to which RIXS is sensible). Figure from [16]

.

Considering both the energy needed to break the antiferromagnetic order between neighbouring Cu^{2+} (given by a super-exchange mechanism) and the Coulomb repulsion between the doping holes, the most energetically convenient configuration for those extra charges is a stripes-like one, as shown in Figure 1.9 (see [17]). The filling of those stripes (defined as the number of

added hole per Cu site along each one) is found to minimize the energy for a value of 0.5 - it means that along the stripes we have half hole per Cu ion. Moreover, upon increasing doping, it is more convenient for the system to increase the density of stripes rather than their filling, until the stripes reach a distance between each other of four lattice parameters. This new order will imply new elastic reflection points in the Brillouin zone, in addition to the canonical Bragg ones. Inelastic Neutron Scattering (INS) and Resonant Inelastic X-Rays Scattering (RIXS) experiments probe different points - INS is sensitive to the spin reordering with respect to the antiferromagnetic lattice (see Chapter 2) and instead of finding the typical in plane reflection associated to antiferromagnetic order at (π, π), we will find incommensurate peaks at a distance δ from (π, π); while RIXS is sensitive to charge modulations, and will sense a peak at a wavevector that is twice the one of INS experiments (as it is clearly seen in Figure 1.9). Eventually, we have that $\delta = \frac{1}{2d}$, which also allows us (δ can be thought of as a doping linear dependent parameter: $\delta(p) = p$) to track down the position of those peaks as a function of the doping (see [18] for more details) - when peaks are not found in the expected positions, fluctuating stripes are seen as an explanation.
Still, even if the phenomenology of the stripes in 241 cuprates is well known, their competition with respect to the high temperature superconductivity (made evident by the "anomaly" around doping $p = \frac{1}{8}$ found in the diagram phase - see Figure 1.10 - which associates the characteristic $d = 4$ parameter, as we have just said) is puzzling.
In 123 cuprates family, instead, working in underdoped conditions (which is to say, with a smaller doping than the optimal one), we observe a strong enhancement of the elastic signal around incommensurate wave vectors ([0.31,0,L], intended as the total transferred momentum). No elastic peak is found through INS experiment (as in the case of 214 family), and thus we can deduce that no magnetic ordering is present - charge stripes are no more an option. Still, nothing prevent us from admitting a purely charge ordering to which RIXS in sensible, but INS is not. More in particular, we refer to this charge order which generates such elastic signal at points in the Brillouin zone which are incommensurable to the real lattice as to charge density waves (CDW) phenomena (for more details, see [19]).

1.5 Phonons in Cuprates

We will now have a brief introduction about the importance of phonons dynamic in cuprates, since phonons themselves will be the main subject of this thesis.

The main physical phenomenon behind superconductivity is pairing, which can we define as the process responsible for the creation of Cooper pairs. Roughly speaking, a Coopers pair is a state of a system composed by two electron, bounded together at low temperature through the action of a potential - which will be in general considered and defined as the pairing mechanism. The superconductive state emerges when we have an adequate density

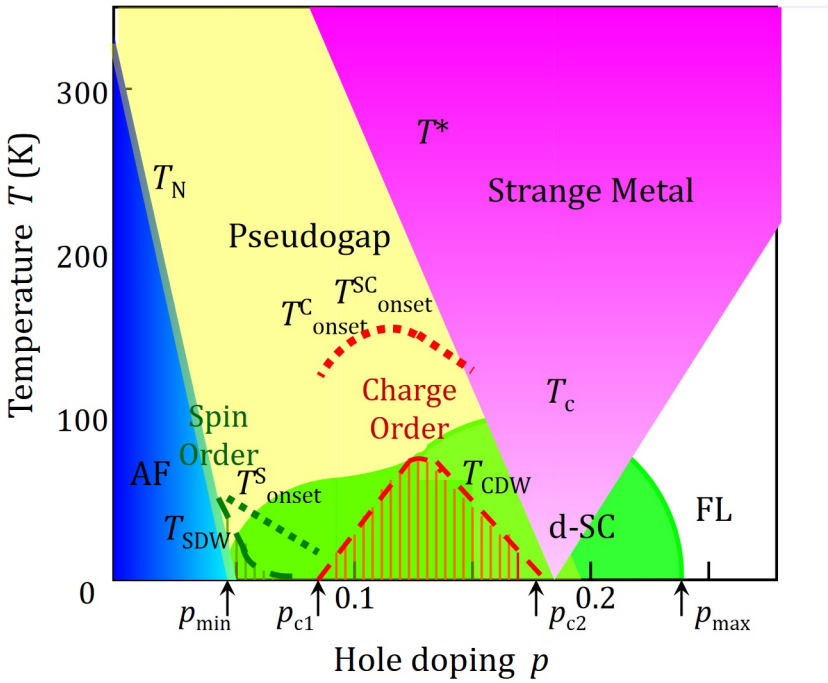

FIGURE 1.10: Complete phase diagram, in which we can also see the region characterized by the presence of charge density waves (CDW) and spin density waves (SPW). FL stands for Fermi Liquid, d-SC for d-wave superconductivity. The temperatures marked as onset fix the temperature at which precursor orders or fluctuations become apparent. Figure from [6]

of Cooper pairs (the literature here is abundant; see, for example, [20])
The conventional superconductivity is mediated by phonons (for an intuitive understanding, see Figure 1.11), in the sense that the potential responsible for the pairing mechanism is intrinsically associated to the lattice dynamic - the critical temperature itself scales with the strength of electron-phonon coupling, and in most cases it is possible to find particular modes which are strongly coupled to electrons. Those modes are identified by the fact that are experimentally seen (eg, through INS experiments) as broader and softer than predicted by lattice dynamic models. This is all well explained by the BCS theory.
But when we start to consider high temperature superconductivity, the situation is more complex. The already mentioned very nature of the "d-wave" pairs wavefunctions suggest the existence of a pairing mechanism induced by a spin-based interaction, and not by phonons as in canonical superconductivity. Relatively recent accumulations of experimental results (from Raman spectroscopy, INS and penetration depth measurement, see [21]), anyway, suggest that the electron-phonon interaction still play an important role. Nowadays, the most plausible hypothesis is that both a spin related interaction and a more canonical electron-phonon interaction contribute to the pairing mechanism - but the the problem is still very open and puzzling.
But if we want to find evidence of strong electron-phonon coupling in the

high temperature superconductors, we immediately face many problems: due to the extremely large unitary cell, the cuprates have a large number of phononic modes. Furthermore the standard theory can not identify the soft acoustic ones, and their identification must be done by "blind search". The large single crystal necessary to map the dispersion relations through INS, moreover, became available only years after the first discovery of high temperature superconductivity.
In this context we can find the reason of this thesis, and more in general of the electron-phonon interaction investigation through RIXS (as we will see in Chapters 2 and 3). Through RIXS we have in fact a way to probe the strength of the electron-phonon coupling. Of course we will need to adopt more or less drastic approximations, and for the moment we can just estimate the overall magnitude of the interaction and its general shape as a function of the phonons moment (which is already a great result) - but RIXS is theoretically endued with all the potential to deeply investigate this coupling: its magnitude, its momentum dependence, its peculiarities toward each phononic mode; but we will deeply investigate this topic along all the thesis.

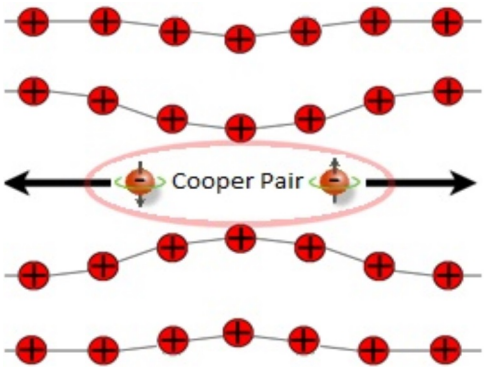

FIGURE 1.11: A naive picture of the pairing mechanism mediated by phonons. The interactions between electrons is provoked by lattice oscillations, and is thus given by phonons' dynamic. It is also remarkable the fact that the electrons involved in the pairing are endued with opposite momenta and opposite spin - more technically, they are found in a singlet state. The Cooper pairs can thus be considered bosons (they have zero spin), and at sufficiently low temperature (below the critical temperature) we can found an adequate numbers of them in the same ground state (since they are bosons, they follow the Bose-Einstein distribution, not the Fermi one): the macroscopic effect is the emergence of the superconductive state.

Chapter 2

Resonant Inelastic X-Rays Scattering

2.1 A Brief Overview

In first place, it is useful to have a quick recap of RIXS technique: how it is implemented, which are its features, which are its limitations and which are the fundamental excitations accessible through it. In this exposure, i will basically add nothing new to what has been done , for example, in [22], [11] and [2].
After a first, more qualitative approach, a more quantitative study is needed: in first place for completeness, and in second place because the results will be the starting point when we will begin to focus our attention on phonons, in Chapter 3. In our tractation of the subject, we will follow the track given by [22].

2.1.1 Summary

RIXS (Resonant inelastic x-rays scattering) is a photon in-photon out, synchrotron-based technique, which aims to probe elementary excitations inside the matter.
Basically, we have a photon flux which hits the sample. The light-matter interaction causes the photon to be scattered in an arbitrary direction, with a certain change in its energy, momentum and polarization state. This implies that a certain energy, momentum and angular momentum (which is related to the polarization state of the photon) have been transferred to the sample, which is thus left in an excited state. Carefully comparing the initial and final state of the photons (thus experimentally characterizing their energy, momentum and polarization), and in particular studying the inelastic features of the RIXS spectra, one is theoretically able to deduce, as we will show later, the elementary excitations which are left in the sample as a consequence the scattering event - this means that we can characterize, by the means of the conservation laws, their energy and momentum dependency.
If we want to write some preliminary, simple equation, we have:

$$\hbar\omega_i = \hbar\omega_o + E_{exc} \tag{2.1}$$

$$\hbar\mathbf{k}_i = \hbar\mathbf{k}_o + \hbar\mathbf{q}_{exc} \tag{2.2}$$

Moreover, RIXS is a resonant technique: this means that the energy of the phonon is tuned to a resonant energy of the system. In the specific case, an electron from an atomic core level is promoted into an excited (and thus empty) state in the proximity of the Fermi level. This level can be thought of as an atomic level (in a single ion approach) or a conduction band state (a generally more realistic representation - but still the goodness of the single-ion approximation depends on the excitation that we are dealing with). After a usually short time (in the order of the fs), the hole left in the core level is filled by another (or the same) electron. This produces the outgoing photon. A resonant process, between other advantages that we will see later, enhance of many order of magnitude the overall cross-section of the process (as every second order process, RIXS scattering is a relatively unlikely event, and the technique itself results to be photon-hungry, which means that we need an high flux of photons in order to achieve a significant statistic for our results). As suggested in [22], good overviews of RIXS technique are [23] and [24].

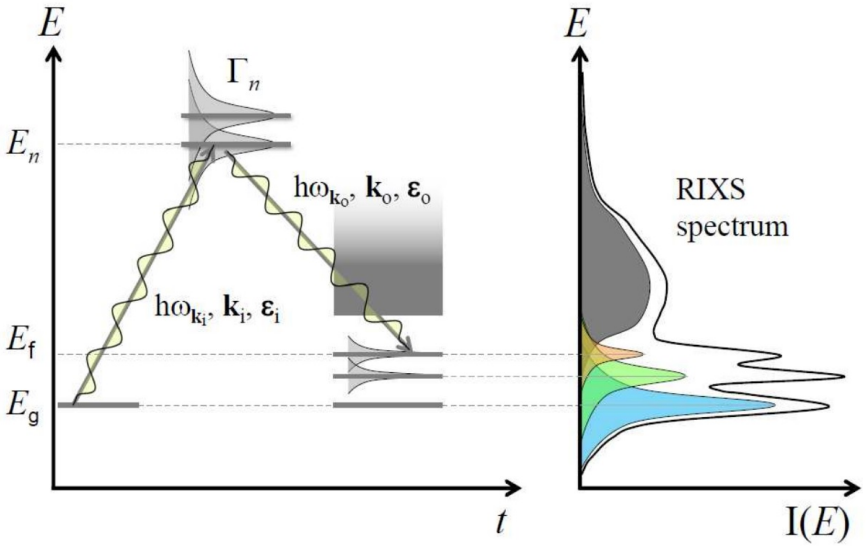

FIGURE 2.1: A schematic representation of the *direct* RIXS scattering process (see section "*Theory of Electron Photon Coupling*"). An *indirect* RIXS process would imply a scattering event (in which an excitation is generated) while the system is found in the intermediate state. Figure from [11].

2.1.2 RIXS characteristics

The basic idea of RIXS is to measure the energy and momentum given to the sample by the scattering event through a comparison between the energy and momentum of the ingoing and outgoing photons. We have many

features which distinguish RIXS from other widely used experimental techniques, like INS (Inhelastic Neutron Scattering) or ARPES (Angle Resolved Photo Emission Spectroscopy).
In first place, as we have already said, we are able to measure the energy and momentum dependence of excitations over a wide portion of the first Brillouin zone, allowing us to study the dispersion of those excitations (this is, obviously, the most important and striking feature - in the field of elementary excitations, RIXS, togheter with INS, is the main experimental technique which allow such a systematic investigation).
We can also measure the polarization of the incident and outgoing radiation [25], which allows us to investigate the angular momentum dependence of the excitations (the polarization of the radiation, as we will see later, enters the cross-section calculations in a very "clean" and well understood manner, see [11]).
We are also aware, once we set the energy of the incident photon and thus the resonant energy of the system (resonances energies are called "edges"), of which electronic transition we are exciting (and thus the atom at which the excited core electron belongs) - and this is often called *chemical sensitivity*.
Another very important feature is related to the penetration length of the photon, which is, in general, an universal curve not dependent on the sample composition but only on the photon energy. In the soft X-ray regime, the penetration length is of the orders of micrometers. This is enough to reach and thus study the bulk of the material, and not only the surface.
Eventually, we also have an high flux of photons assured by the synchrotron sources, and thus we are actually allowed to use smaller sample than, for example, in inelastic neutron scattering.

But, of course, adopting RIXS also mean to have limitations. The main two problems that we have to face in working with RIXS are related to energy resolution and the time required to have a good measurement.
The first one is intimately related to the difference between the photon energy and the energy of the excitations in the sample, which force us to work at a very high resolving power. The state of the art resolution is nowadays of 35 meV, and it is the result of a continuous improvement over the last twenty years (See Figure 2.2).

The time required to have a good measurement, instead, must be large in order to have a good count of photon collected - we have always to remember that inelastic scattering is a second order process, and thus its cross-section, even at resonance, is intrinsically small.

Considering very briefly other techniques, a very close relative of RIXS is IXS (inelastic X-rays scattering): the difference is that in IXS we exploit a non-resonant process - and this means that IXS rquire a generally high time of acquisition in order to obtain results endued with a sufficient statistic.
XAS (X-ray absorption spectroscopy) can be thought as a part of the RIXS process: initially, in fact, we have to check that the photon energy is the one which maximize the ratio of absorbed photons, and thus is the exact resonant

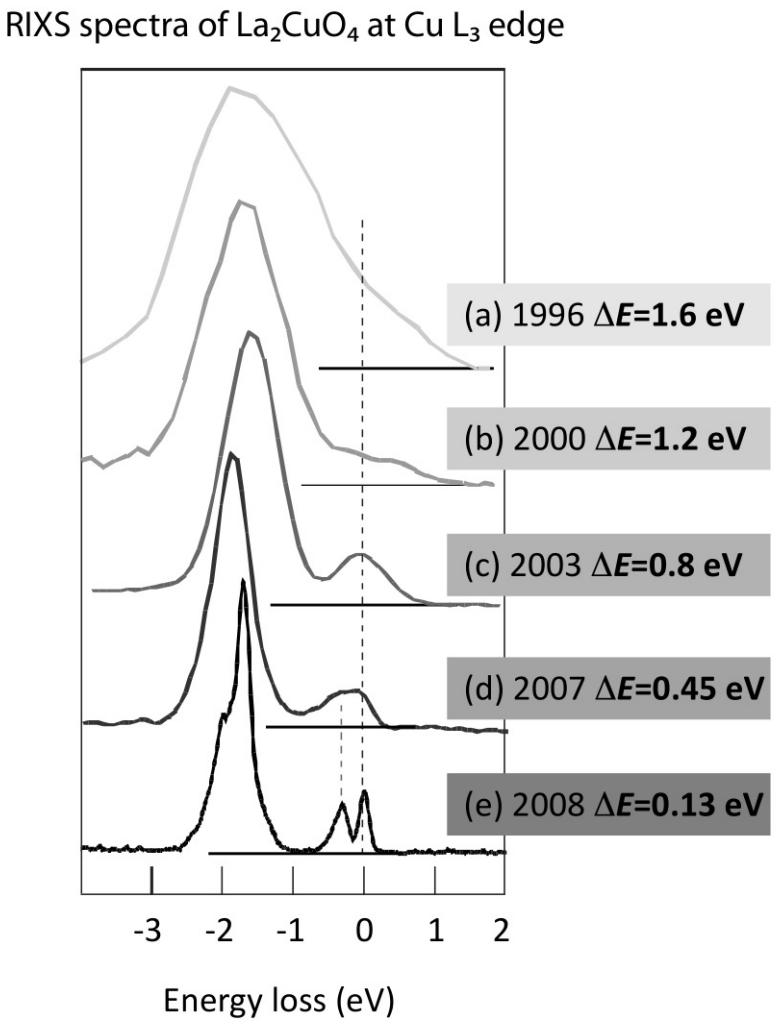

FIGURE 2.2: Progress in RIXS resolution at the Cu L edge ($\simeq$931 eV). Figure by G. Ghiringhelli and L. Braicovich, from [22].

energy.
Raman light scattering, with respect to RIXS, is confined at (almost) zero momentum transfer, due to the low energy of the photons (in fact, Raman scattering only probe the center of the Brillouin zone).
INS (inelastic neutron scattering), that we have already mentioned, is a technique which relies on the scattering of neutron; RIXS is more efficient in term of cross-section (it makes no sense to talk about resonances in the INS case), and more versatile to probe magnetic excitations, since photons carry a unitary spin while neutrons carry a $\frac{1}{2}$ spin. Anyway, RIXS and INS can be considered as complementary techniques - they both probe elementary excitations and they both have advantages and disadvantages respect each other.
For a long time, anyway, INS has been the only experimental technique able to probe the phonons ad magnons dispersion. Even now, it is the only option for those material in which X-Rays investigations do not work properly.

2.1.3 Acessible Excitations

Another very important matter is which excitations we are allowed to investigate through RIXS.
The first thing to notice is that we will always find an elastic component of our spectra, which is to say that some photon will be elastically scattered. From the very well known theory of elastic scattering in X-rays (see, for example, [26]) we know that elastic reflection of X-rays is obtained for fixed angles (set by the lattice parameters and the photon energy); we will refer to them as to the Bragg reflections. Theoretically, elastic scattering is allowed only for fixed angles (see section 2.3), but non ideal structures (i.e. defects) in the materials also allow the existence of an elastic component away from the exact Bragg reflection conditions. Many times the elastic component of the RIXS spectra obscures the low energy excitations components - it is one of the practical problems, still to be resolved (hopefully with a resolution improvement), in the studying of low energy excitations (i.e. phonons) through RIXS (see Chapter 3 and Chapter 4).

Now, the main excitations accessible to RIXS are:

Charge Transfer Excitations. In an insulator, or better in a Mott insulator (and thus in a strongly correlated system) electrons are very localized, blocking each other way. A charge excitation is a transfer of an electron from a lattice point in which it was localized (i.e. from an atom) to another one - more in particular, from the oxygen atom to the metallic ion, which is eventually found with less charge than in the ground state. The energy required is the one setted by the Coulomb repulsion between electrons [27], typically higher than 2 eV.

Orbital Excitations. The excited electron, when it is promoted in first place an when it decays at the end of the RIXS process in second place, can occupy different orbitals of the atom. Thus, the orbital configuration can be view as an effective degree of freedom. This orbital degree of freedom affects many physical properties of the solid: if the initial and the final orbital of the electron happen to not be the same, we have that the emitted photon will be less energetic than the absorbed one, and the difference will be the same amount of energy of which the two orbitals differs of. Orbital excitations are also called (at least in cuprates, where the interested orbitals are the d orbitals) *dd excitations*. These excitations are found at about 1 eV energy loss. See, for example, [11].

Magnetic Excitations. The magnetic moments of ions interact with each other, resulting in a magnetic order (antiferromagnetic, in the case of LCO) which break the most generic symmetry of the material. In cuprates, the spin interactions are mainly super-exchange interactions. The result of a magnetic order is also the emergence of collective perturbations (magnons and spinons) - in the case of magnetic order, we can think at its perturbations as to be endued with a wave-like shape, and thus assume that a connection

exist between their momentum and their energy. Through RIXS we can investigate the dispersion relations of this excitations. The magnetic moments interactions (which are, naturally, associated to each spin) determine the low temperature magnetic properties. Considering a single-ion model, we can think of a pure magnetic excitation as provoked by an electron that, once decaying from an excited intermediate state, return to his original orbital, but with its spin flipped. This is the perturbation of the equilibrium which originate the magnons (see [12]). They are found, in cuprates, at around 0.4 eV. It is notable that their periodicity is dictated by the magnetic reciprocal space (see Chapter 1), which differs from the conventional Brillouin zone.

Phonons. Phonons are the main object of this thesis. They are usually found at very low energies, less than 100 meV. There will be a more detailed discussion in the next chapter.

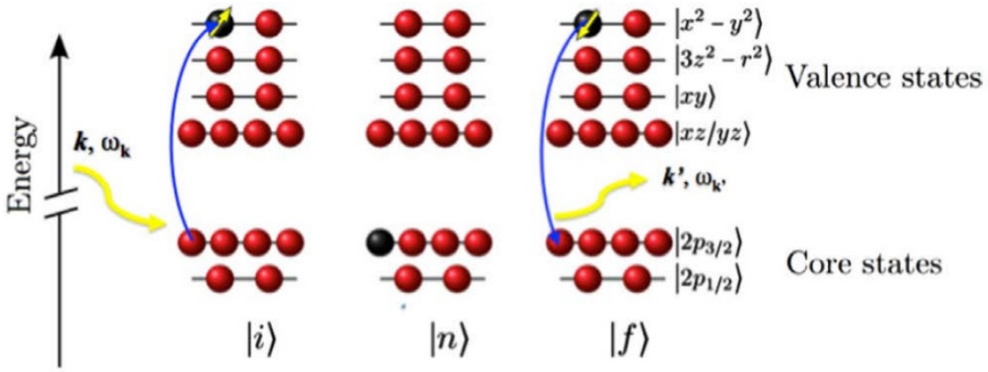

FIGURE 2.3: RIXS process at the Cu L_3 resonant edge. In this particular case, we have the excitation of a magnon: the final state is equivalent to the initial one, but with flipped spin. We are implicitly accepting a single ion approximation - in general we should suppose the electron to be promoted in an empty band, and not in a single ion orbital. Figure from [28].

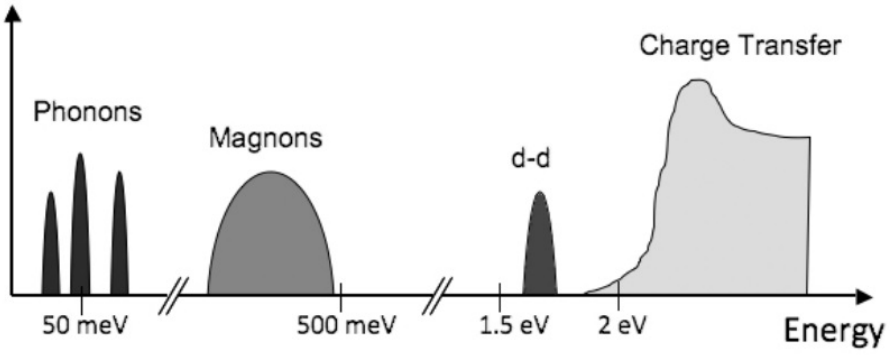

FIGURE 2.4: Schematic representation of a canonical RIXS spectrum for cuprates. Figure from [22].

2.2 For a Theory of RIXS: Electron-Phonon Coupling

2.2.1 Summary

What we are going to do in this chapter is to obtain a quantitative cross-section for the RIXS event - technically, an excitation of a core electron into a valence state, which brings the whole system in a excited intermediate state, and the successive filling of the core hole by a valence electron. We will consider, coherently with our purpose to describe a RIXS process at X-rays energy (where the lifetime of the intermediate is very short) only *direct* RIXS scattering events: which is to say that, while the system is in the intermediate state, no scattering events occur - we do not expect to have transitions to and from different intermediate states.
To consider a direct RIXS scattering, in fact, means considering the transition of the system (usually a solid, in some case the molecule or a single atom) from an initial state to an intermediate state, and then, from that exact intermediate state, a transition to the final state. Technically, the phonon RIXS is an indirect RIXS process, since the excitation of the phonon happens in the intermediate state, and this imply that the intermediate state itself will not be the same before and after the phonon creation. But, as it is noticed in [22], the phonon process is anyway well described by an elastic process, since the phonons only slightly modify the electronic intermediate state. In other words, we consider that the electronic state does not evolve during the intermediate state despite the creation of one or more electrons.
In the order, we will have a brief look at the basis of electron-photon coupling (in the low energy expansion of the QED) to obtain a Hamiltonian which we will later insert in the Fermi golden rule equation for second order transitions, and as result we will have the Kramers-Heisenberg equations. We will eventually use some approximation to obtain a more compact form.
This section follows strictly the discussion in [22].

2.2.2 Electron-Photon Coupling

The first order expansion for the QED Hamiltonian is:

$$H = \frac{1}{2m}(\mathbf{p} + e\mathbf{A})^2 + \frac{eh}{2m}\sigma \cdot \mathbf{B} - e\phi \tag{2.3}$$

where ϕ and $\mathbf{A}$ are the electric and vector potential of the electromagnetic field associated to the photon and σ is a vector whose components are the Pauli matrices. The second order expansion results to be (of course, the first order expansion will be included in this):

$$H = \frac{(\mathbf{p} + e\mathbf{A})^2}{2m} + \frac{eh}{2m}\sigma\mathbf{B} - e\phi + \frac{e^2h}{(2mc)^2}\sigma\mathbf{E} \times \mathbf{A} + \frac{1}{2}\frac{eh^2\rho}{(2mc)^2\epsilon_0} + \frac{eh}{(2mc)^2}\sigma \cdot (\mathbf{E} \times \mathbf{p} - \mathbf{p} \times \mathbf{E}) \tag{2.4}$$

where term proportional to ρ is called the Darwin term, and the last term is the relativistic spin-orbit coupling.
We could also exploit the third order expansion, but no new significant term would appear (for all the details, always rely on [22]).
We have to consider an initial and final state for the scattering process, and we will assume (decoupling the photon and the material wave functions):

$$|G\rangle = |g, \mathbf{k}\epsilon\rangle, |F\rangle = |f, \mathbf{k}'\epsilon'\rangle \tag{2.5}$$

where $\mathbf{k}$ and ϵ are the wave vector and the polarization vector of the photon. By splitting the total Hamiltonian in $H = H_o + H'$, where the whole electron-photon interaction is contained in H' (which is a part of (2.4)), $|G\rangle$ and $|F\rangle$ are eigenstates of H_o (a term affecting only the photon or only the electron state) with energies $E_g + h\omega_{\mathbf{k}}$ and $E_f + h\omega_{\mathbf{k}}$.
The photons appears in the QED Hamiltonian through the second quantization formalism. Expanding $\mathbf{A}(\mathbf{r})$, which is found in (2.4):

$$\mathbf{A}(\mathbf{r}) = \sum_{\mathbf{k},\epsilon} \sqrt{\frac{h}{2V\epsilon_0\omega_{\mathbf{k}}}}(\epsilon a_{\mathbf{k},\epsilon} e^{i\mathbf{kr}} + \epsilon^* a^\dagger_{\mathbf{k},\epsilon} e^{i\mathbf{kr}}) \tag{2.6}$$

where we used the usual formalism of second quantization, with creation and annihilation operators.
Now, considering the way in which creation and annihilation operators work on the photon eigenstates, in order to obtain the transition ratio from the ground state to a final state, considering the possibility to have a transition through an intermediate state $|n\rangle$, we have to exploit the Fermi golden for second order transitions ((2.4) can be treated as a perturbation to H_0 since electron-photon interactions are controlled, in terms of intensity, by the fine structure costant):

$$w = \frac{2\pi}{h}\sum_f [\langle F|H'|G\rangle + \sum_n \frac{\langle G|H'|n\rangle\langle n|H'|F\rangle}{E_g - E_n}]^2 \delta(E_f - E_g) \tag{2.7}$$

$|n\rangle$ is the intermediate state with energy E_n (we will indicate with $|n\rangle$ both the total state and the electron state alone, but it will be clear by the context). Usually, the first order amplitude dominates the second order one, but when the energy of the incoming photon is in resonance with a certain transition ($E_g \simeq E_n$) we have a strong enhancement of the second order amplitude - this is the key of RIXS, and this is the physical meaning of the resonance.

2.2.3 Kramer-Heisenberg Equation

Since we are considering a RIXS process, we are interested in processes in which we have a phonon in and a phonon out. We can reach this result in basically two ways: with a first order process in which the work (in terms of action on the photon state made by the creator and annihilation operators) is done by the term $\mathbf{A}^2$, or with a second order process (our resonant process, which is basically a two step process in which a phonon is created and annihilated in two different moments) where the two relevant terms can be linear with $\mathbf{A}$.
Looking again at our electron-photon interaction terms in (2.4), the first quadratic terms in $\mathbf{A}$ give raise to a non resonant scattering, while the fourth is at the origin of a magnetic non resonant scattering. The terms linear in $\mathbf{A}$, as we have said, can give rise to a resonant, second order process. In particular, considering the terms which contributes to the first order amplitude, the first one is proportional to the derivative of $\mathbf{A}$ (remembering that $\mathbf{E} = \frac{\partial \mathbf{A}}{\partial t}$) - that is $\sigma \cdot (\frac{\partial \mathbf{A}}{\partial t}) \times \mathbf{A}$. This term is smaller than $\mathbf{A}^2$ of a factor $\frac{h\omega}{mc^2} << 1$, and will be neglected. $\mathbf{A}^2$ itself, also, can be neglected, as result from LDA (local density approximation) calculations, see [29].
The term proportional to $\sigma \cdot \nabla\phi \times \mathbf{A}$, moreover, turns out to be irrelevant (for all details, once again rely on [22]).
Considering all of this, the remaining meaningful terms for a RIXS scattering event are only the ones which contribute to the resonant second order process:

$$H' = \sum_{i=1}^{N} [\frac{e}{m}\mathbf{A}(\mathbf{r}_i) \cdot \mathbf{p}_i + \frac{eh}{2m}\sigma_i \cdot \nabla \times \mathbf{A}(\mathbf{r}_i)] \tag{2.8}$$

At this point, we have to consider that the intermediate state is not a stable state - we account for that assuming $E_n \longrightarrow E_n - i\Gamma_n$, where, if τ is the lifetime, $\Gamma \simeq \frac{h}{\tau}$.
Now, considering (2.6) and (2.8) (for all the calculations, [30], or again [22]):

$$\begin{aligned}\frac{\langle G|H'|n\rangle\langle n|H'|F\rangle}{E_G - E_n + i\Gamma_n} =& \frac{e^2 h}{2m^2 V \epsilon_0 \sqrt{\omega_{\mathbf{k}}\omega_{\mathbf{k}'}}} \sum_n \sum_{i,j=1}^{N} \frac{\langle f|e^{-i\mathbf{k}'\cdot\mathbf{r}_i}(\epsilon'^* \cdot \mathbf{p}_i - \frac{ih}{2}\sigma_i \cdot \mathbf{k}' \times \epsilon'^*)|n\rangle}{E_g + h\omega_{\mathbf{k}} - E_n + i\Gamma_n} \\ & \cdot \frac{\langle n|e^{-i\mathbf{k}\cdot\mathbf{r}_i}(\epsilon \cdot \mathbf{p}_i + \frac{ih}{2}\sigma_i \cdot \mathbf{k} \times \epsilon)|g\rangle}{E_g + h\omega_{\mathbf{k}} - E_n + i\Gamma_n}\end{aligned} \tag{2.9}$$

Which is the resonant part of (2.7).
The part of the Hamiltonian (2.8) which held the Pauli matrices is indeed a magnetic term, accounting for the spin interaction with the field associated to the phonon (in (2.8) we can notice that it is the reformulation of the classical and more recognizable term $-\mu B$); in (2.9) it is again found as associated to the Pauli matrices. At 1 keV the exponential $e^{-i\mathbf{k}'\cdot\mathbf{r}_i}$ can be expanded (and is thus close to unit); this means that the X-ray energy is tuned to a dipole transition (here written in term of momentum, i.e. $\simeq \frac{\langle\psi_a|\mathbf{p}|\psi_b\rangle}{E_a-E_b}$). The magnetic term can then be neglected, because it generates only very small dipole transitions.
Defining now:

$$D = \frac{1}{im\omega_{\mathbf{k}}} \sum_{i=1}^{N} e^{-i\mathbf{k}'\cdot\mathbf{r}_i} \epsilon \cdot \mathbf{p}_i \tag{2.10}$$

The differential cross section can be written by multiplying (2.7) for the density of photon in the solid angle, and dividing from by the incident photon flux:

$$\frac{d^2\sigma}{dh\omega d\Omega} \propto \sum_f |F_{fg}|^2 \delta(e_g - E_f + h\omega) \tag{2.11}$$

Here $h\omega$ plays the role of the energy given by the photon to the system and D is defined as (from (2.7), (2.8) and (2.10)):

$$F_{fg}(\mathbf{k}, \mathbf{k}', \epsilon, \epsilon', \omega_{\mathbf{k}}, \omega_{\mathbf{k}'}) = \sum_n \frac{\langle f|D'^{\dagger}|n\rangle\langle n|D|g\rangle}{E_g + h\omega_{\mathbf{k}} - E_n + i\Gamma} \tag{2.12}$$

Pushing the equations a little bit further, we can take the polarization vector out of the definition (2.10), obtaining a new operator **D** such that :

$$D = \epsilon \cdot \mathbf{D} \tag{2.13}$$

This operator can be reduced to the known operator that causes electronic transition (a very nice property in order to expand the equation (2.12)):

$$\langle n|\mathbf{D}|g\rangle \simeq \sum_{i=1}^{N} e^{-i\mathbf{k}\cdot\mathbf{r}_i} \langle n|\mathbf{r}_i|g\rangle \tag{2.14}$$

Where we have switched the momentum representation of the dipole operator to a position representation, accounting that $h\omega_{\mathbf{k}} \simeq E_n - E_g$.
Using now the second quantization formalism, we call $\phi_{n\nu}$ the v^{th} Wannier function on the site n, and $c_{n\nu}$ the corresponding creation operator. What we obtain is:

$$\mathbf{D} = \sum_{i=1}^{N} e^{i\mathbf{k}\cdot\mathbf{r}_i} \sum_{n,\nu,m,\mu} c_{n\nu}^{\dagger} \langle\phi_{n\nu}|\mathbf{r}_i|\phi_{m\mu}\rangle c_{m\mu} \tag{2.15}$$

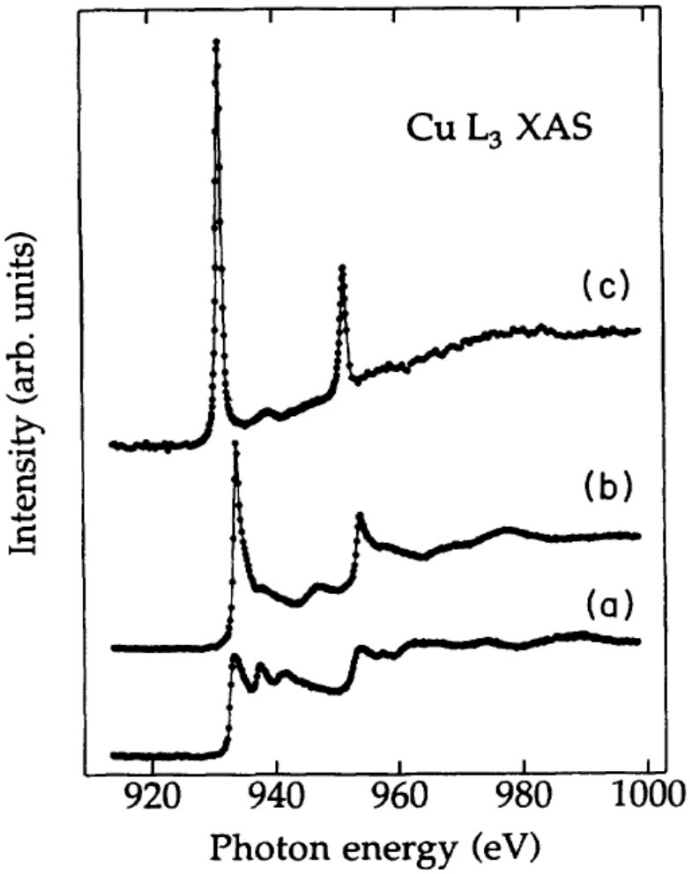

FIGURE 2.5: Typical Cu $L_{2,3}$ edges of (a) copper metal, (b) CuO_2 (Cu^{1+}) and (c) CuO_2 (Cu^{2+}). Those spectra are representative of the possible intermediate state ($|n\rangle$) that we can reach during a RIXS experiment - more in particular, we notice how the nature of those states depend on the chemical and structural configuration of our sample. Figure from [16].

Considering that the core states (which must be the first and final steps of the double dipole transition) are very much localized, we can consider also the excited states as localized on the same ion (i.e $n = m$, this is the single ion approximation). This reduces the operator **D** to:

$$\mathbf{D} \simeq \sum_{\nu,\mu} \langle \phi_\nu | \mathbf{r}_i | \phi_\mu \rangle \sum_i e^{i\mathbf{k}\cdot\mathbf{R}_i} c^\dagger_{i\nu} c_{i\mu} \tag{2.16}$$

And eventually we are able to write the Kremers-Heisenberg equation in its final forms. Always relying on (2.11) for the calculation of the cross section (which is the real important experimental parameter), we have the amplitude of the transition from a ground state to a final (possibly excited) state - and thus the amplitude for a resonant inelastic scattering event - as (from (2.12) and (2.16)):

$$F_{fg} = \sum_{\nu',\mu',\nu,\mu} T_{\nu'\mu'\nu mu}(\epsilon,\epsilon') \sum_i e^{i\mathbf{q}\cdot\mathbf{R}_i} \sum_n \frac{\langle f|c^\dagger_{i\mu'}c_{i\nu'}|n\rangle\langle n|c^\dagger_{i\nu}c_{i\mu}|g\rangle}{E_g + h\omega_{\mathbf{k}} - E_n + i\Gamma} \tag{2.17}$$

With a so called polarization factor:

$$T_{\mu'\nu'\mu\nu}(\epsilon,\epsilon') = \langle\phi_{\mu'}|\epsilon'^* \cdot \mathbf{r}|\phi_{\nu'}\rangle\langle\phi_\nu|\epsilon\cdot\mathbf{r}|\phi_\mu\rangle \tag{2.18}$$

In a direct RIXS event, $\nu = \nu'$; in an elastic one $\nu = \nu'$ and $\mu = \mu'$.
It is evident why it is called polarization factor: it depends only on the polarization of the emitted and absorbed photon. It is, fundamentally, the term which reveals if the dipole transition (or better, the double dipole transition) is allowed (and we must remember that we have neglected non-dipole transitions, since their amplitude is in general much smaller than the dipole ones). Once we have that the second order dipole transition between the initial and the intermediate state is allowed, we can look at the second term of the equation (2.18), which contain all the further physic - the resonance and the excitations.
As a matter of fact, in many cases for strongly correlated electron systems, where electronic wavefunctions relevant for the scattering process are very much localized on the atom, we can use atomic functions in place of Wannier functions when running calculations (in a single ion model this is of course true - for this kind of calculations, see [11]).

2.3 Experimental Setup

The experimental RIXS setup is in general very complex, and technical details may vary from a beamline to another. It will not be treated along this thesis, but the main thing to notice is that, in order to obtain a radiation of good quality in the energetic range of X-rays (in terms of brilliance - which is a multi comprehensive and fundamental parameter, since RIXS is a second order process and thus very photon-hungry), we need a synchrotron radiation. The main problem is then to have enough resolving power: we need to detect variation of energy in the order of 50 meV for photons around 1000 eV. More details and implementation can be found in, for example, [16], [31], [2] - many smart and sophisticated technical solutions have been adopted in order to achieve the present state of art.

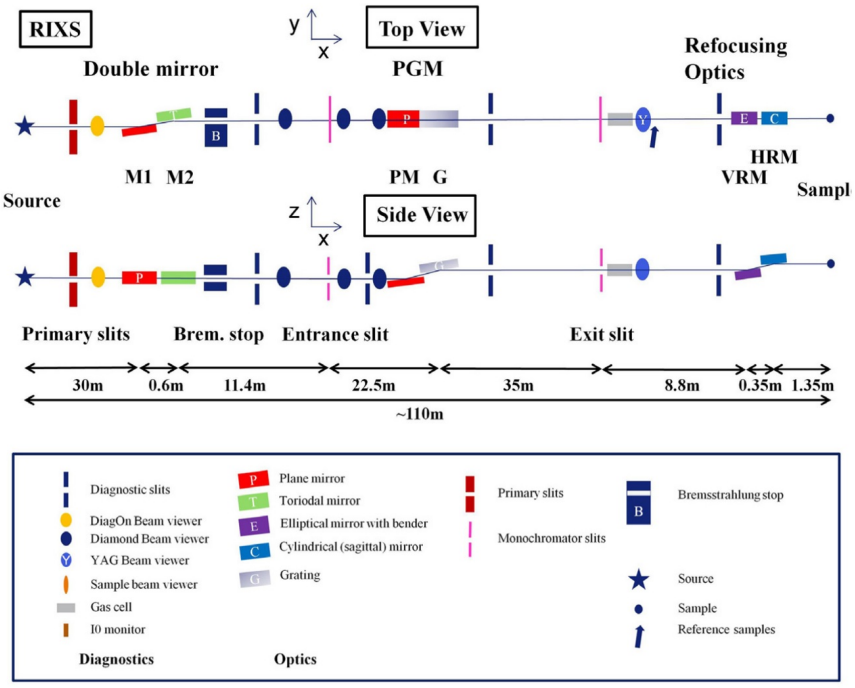

FIGURE 2.6: Here we have a representation of the optical apparatus needed (in this case at ID32 beam line at ESRF) to collimate the high energy X-rays beam on the sample. Since we want our photon to have a well defined energy, a monochromating element (in this case it is the grating) is of course needed. Figure from [31].

For our introductory presentation, it is enough to know that the synchrotron radiation is in first place focused on the sample (see Figure 2.5), scattered and then direct, through a slit, on a diffraction grating, which will diffract each photon with an angle dependent on its energy (this passage is crucial - is here that the extreme resolving power is reached), see Figure 2.6; eventually, the signal will be collected by a CCD detector - which will need to be enough sensitive to account for the signal generated by single photons.

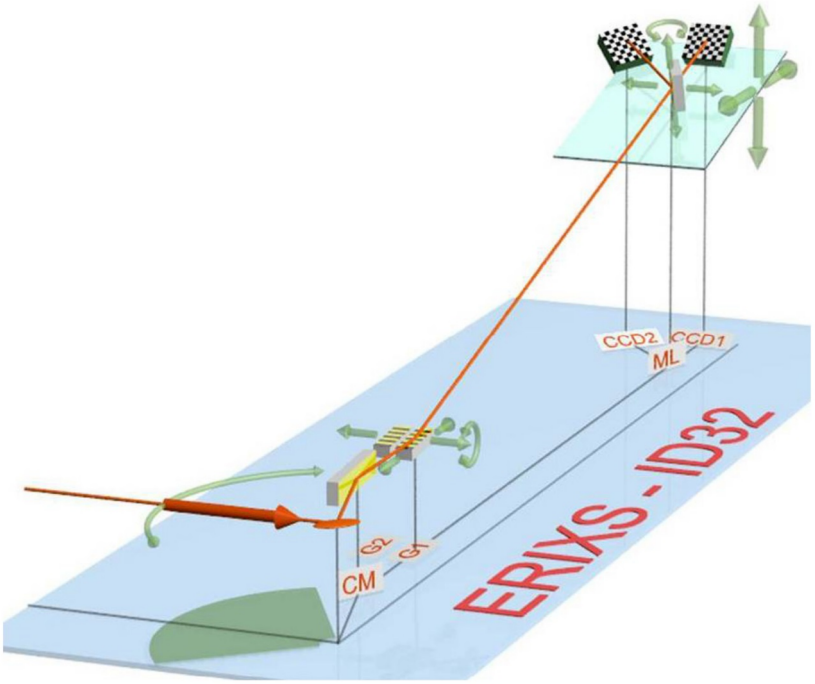

FIGURE 2.7: Here we have a schematic representation of the experimental setup which allows the scattered photons to be collected by the CCD detectors. This, in particular, is the layout, again, of ID32. The diffraction grating is the critical and maybe more complex element, also in the new generation spectrometers. Figure from [31].

Naturally, all the radiation propagation must happen in vacuum, more in particular in ultra high vacuum conditions ($\simeq 10^{-9}$ mbar).

What is crucial (and way more simple) to understand is the *geometry* of the experiment - which is to say how we are able to fix the momentum given to the sample excitations.

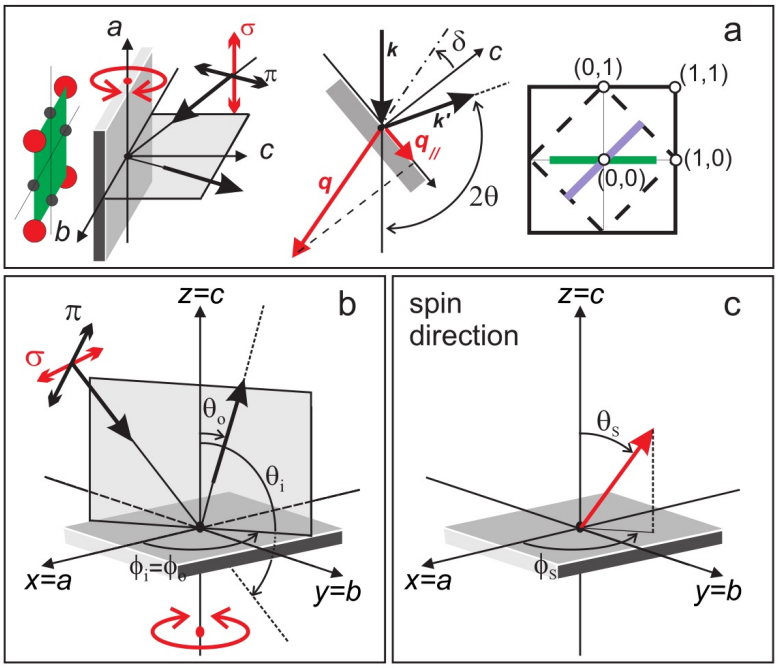

FIGURE 2.8: Here we have the typical experimental geometry. It is important to notice that χ is not depicted, and it is assumed to be identically fixed to zero. (a) also shows a sketch of the first Brillouin zone, in which we distinguish the two main directions [1,0] and [1,1] (in r.l.u.; in this thesis those directions will be indicated as $[-\pi, \pi]$ and $[0, \pi]$). (c) also shows the coordinates relative to the spin orientation in the plane, which would be useful in order to calculate matrix elements for the magnetic excitations cross section - in this thesis, anyway, we will never take advantage of them. Figure from [11].

We will suppose to be interested in cuprates, that, as we said in the previous chapters, are quasi 2D materials. This means that we are only interested in the transferred momentum along the CuO_2 plane. Also, the reciprocal lattice basis of this plane are parallel to the basis of the real lattice - otherwise, calculations would be less straightforward. Labelling the real lattice basis as **a**, **b**, **c**, where the vectors **a** and **b** identify the CuO_2 plane (accordingly to Figure 2.5, on which we will always rely on from now on), the reciprocal lattice basis vectors will be oriented accordingly, with modulus $\frac{2\pi}{a}, \frac{2\pi}{b}, \frac{2\pi}{c}$.
It is now common to define the reciprocal lattice units by setting $[\frac{2\pi}{a}, \frac{2\pi}{b}, \frac{2\pi}{c}] = [1, 1, 1]$. However, in this thesis we set $[\frac{1}{a}, \frac{1}{b}, \frac{1}{c}] = [1, 1, 1]$, which means to set $a = 1$ (in cuprates the dimension a is equivalent to the dimension b) and thus to write the total momentum transferred in units of $\frac{1}{a}$, where $a \simeq 3.8$ A. Our Brillouin zone will thus be included between π and $-\pi$.
$\mathbf{k}_{in}$ and $\mathbf{k}_{out}$ are the wave vectors belonging to the ingoing and outgoing radiation. The angle 2θ is fixed by the relative orientation of $\mathbf{k}_{in}$ and $\mathbf{k}_{out}$, and the same goes for the scattering plane. As we have already said, the CuO_2 plane is identified by the vectors **a**, **b**. We can define the linear polarization of the incoming and outgoing radiation with respect to the scattering plane (if

it belongs to the scattering plane, it is π. It is σ otherwise), even if along this thesis we will never use it. The angles θ_{in} and θ_{out} are defined as the angles between the wave vectors $\mathbf{k}_{in}$ and $\mathbf{k}_{out}$ and the CuO_2 plane. They are thus changed by rotations around the axe b. We also define a ϕ angle, which is zero when the scattering plane is the one identified by a, c. Finally, we can also define an angle χ, which is zero when the scattering plane is perpendicular to the plane identified by a, b. Neglecting misalignments (which can be due, in the case of angles θ, to not perfect alignment betweens the a, b plane and the holder plane) we can write the following relations:

$$\delta = \frac{\theta_{in} - \theta_{out}}{2} \tag{2.19}$$

$$\theta_{out} = 2\theta - \theta_{in} \tag{2.20}$$

And thus

$$\delta = \theta_{in} - \frac{2\theta}{2} \tag{2.21}$$

Once the alignment of the experimental apparatus is done (with respect to the Bragg reflections, as it will be clear by the end of this Section), we know θ_{in}, ϕ, χ and 2θ.
Intuitively, if for a moment we ignore the angle χ (and thus we supposed it to be fixed as identically equal to zero - which is also the case depicted in Figure 2.5), we can think that to know the momentum transferred into the CuO_2 plane it is enough to know θ, while if we also want to know the relative orientation of that given momentum into the CuO_2 plane we also need to include in our calculations ϕ.
Considering $\lambda_{in} \simeq \lambda_{out}$ (which is of course true, since we are talking of meV energy variations on the top of an overall energy which is in the order of hundreds of eV, and $\lambda = \frac{hc}{E}$) it is true that:

$$|\mathbf{k}_{in} - \mathbf{k}_{out}| \simeq 2|\mathbf{k}| \sin\left(\frac{2\theta}{2}\right) = |\mathbf{q}| \tag{2.22}$$

Where $\mathbf{q}$ is the total momentum transferred. We define the total momentum transferred as positive if $\theta_{in} > \theta_{out}$, negative otherwise. As we said before, we can now write:

$$|\mathbf{k}_{in} - \mathbf{k}_{out}| \simeq 2|\mathbf{k}| \sin\left(\frac{2\theta}{2}\right) = |\mathbf{q}| \tag{2.23}$$

$$q_{||} = 2|\mathbf{k}| \sin\left(\frac{2\theta}{2}\right) \sin(\delta) \tag{2.24}$$

$$q_{\perp} = 2|\mathbf{k}| \sin\left(\frac{2\theta}{2}\right) \cos(\delta) \tag{2.25}$$

More in particular, as we said before, we can also have the orientation of the momentum transferred parallel to the plane (and thus *in* the plane)

exploiting ϕ:

$$q_a = 2|\mathbf{k}| \sin\left(\frac{2\theta}{2}\right) \cos(\delta) \cos(\phi) \tag{2.26}$$

$$q_b = 2|\mathbf{k}| \sin\left(\frac{2\theta}{2}\right) \cos(\delta) \sin(\phi) \tag{2.27}$$

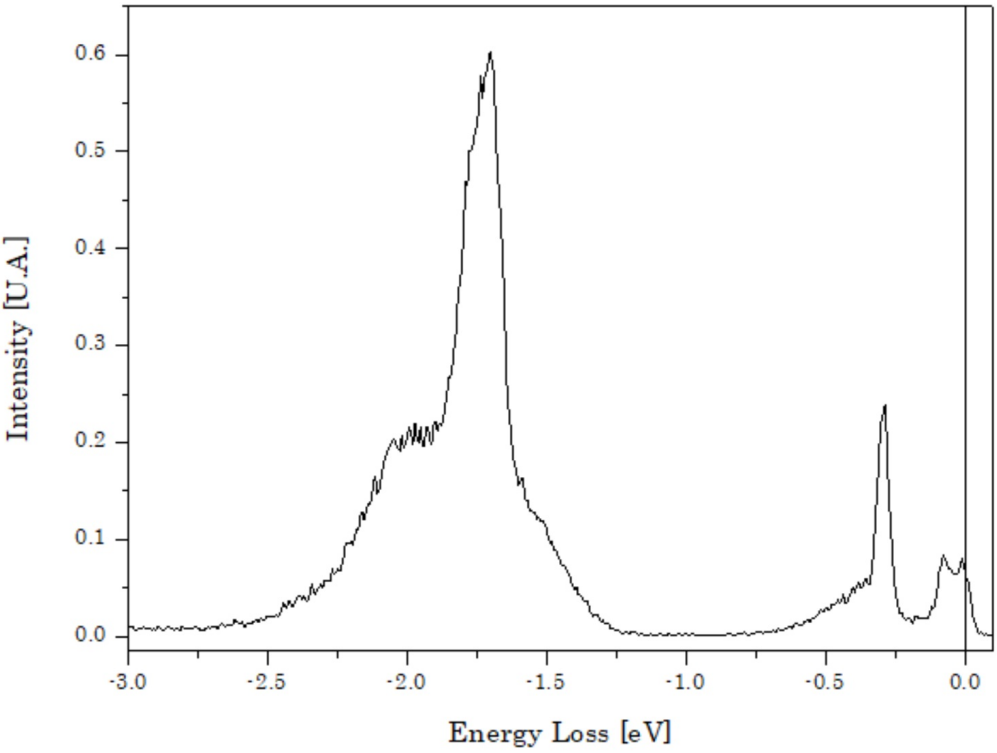

FIGURE 2.9: An example of a raw RIXS spectrum. In this particular case, it is the spectrum of an antiferromagnetic sample of LCO, at the L_3 edge (which imply an energy of $\simeq$ 931 eV), with a total transferred momentum $\mathbf{q} = [0.30,0,1.296]$ - it is one of the spectra that we have obtained at ESRF, and that we are going to study in Chapter 4. We can notice all the features that we have mentioned in the Chapter (and which are already schematized in Figure 2.4). Since we are quite away from the Bragg peak, the elastic peak intensity is comparable to the phonons peaks one.

If we would consider a possible angle χ, thought, the situation would be more complicated, and in the most general case we have to write:

$$q_a = 2|\mathbf{k}| \sin\left(\frac{2\theta}{2}\right) \cos(\delta) \cos(\phi) \tag{2.28}$$

$$q_b = 2|\mathbf{k}| \sin\left(\frac{2\theta}{2}\right) (\cos(\delta) \sin(\phi) \cos(\chi) - \cos(\delta) \sin(\chi)) \tag{2.29}$$

$$q_c = 2|\mathbf{k}| \sin\left(\frac{2\theta}{2}\right)(\sin(\delta)\sin(\phi)\sin(\chi) + \cos(\delta)\cos(\chi)) \tag{2.30}$$

$$k = |\mathbf{k}| = (\frac{2\pi}{hc})E = \frac{2\pi}{\lambda} \tag{2.31}$$

The equations (2.28), (2.29), (2.30), and (2.31) are the components of a complete set of equations which always allow us to extract the total transferred momentum (both in modulus and in direction).

What we can do now in order to test the equations (2.28), (2.29) and (2.30) is to search for Bragg reflections (see [14]), characterized by a great enhancement of the elastic signal. We expect one of them, namely $[0, 0, n]$ to happen for $\delta = 0$ and thus $\theta_{in} = \theta_{out}$ - in fact, it also called *specular* reflection. If we also suppose $\chi = 0$, then q_a and q_b disappear, leaving with momentum transferred in only one direction - (2.30):

$$q_c = 2|\mathbf{k}| \sin\left(\frac{2\theta}{2}\right) \tag{2.32}$$

In order for the Bragg condition to be respected, in r.l.u., this momentum must be an integer (i.e. it must be equal to a reciprocal lattice vector):

$$q_c = 2|\mathbf{k}| \sin\left(\frac{2\theta}{2}\right)(\frac{c}{2\pi}) = n \tag{2.33}$$

Exactly the Bragg condition.
Operatively, what we do during the alignment of an experiment session is to search in first place for a Bragg reflection. Ideally, this should be found at χ equal to zero and δ equal to zero - but, as we said, this could not be the case. So, we define offsets for every angle (for the δ angles, it imply that $\theta_{in} \neq \theta_{out}$), such that the Bragg peak will be found at those offset values - and the effective angle that we will consider in order to estimate the transferred momentum will be the "instrumentation" angle corrected by the offset angle.

Also, looking at (2.31), is once again evident why we need photons with energy in the range of X-rays - their associated wavelength is in the order of magnitude of the inter atomic distances, and is thus adequate to investigate the dispersive characteristics of excitations with typical atomic length, which is another way to say that we are able to probe the Brillouin zone of our materials - an electromagnetic probe of the microscopic structure of a solid must fall in the X-rays energetic range.

Chapter 3

Phonon investigation thorough RIXS

3.1 Introduction

3.1.1 Phonons

Strictly speaking, a phonon is a quasi particle. It is the quantum of atomic vibrations inside solids, and thus of the vibration of the crystal lattice. Phonons play a crucial role in the heat transport properties of the material, in the BCS mechanism on which the conventional superconduction rely on and, supposedly, they also play an important role in the high temperatures superconductors (see Chapter 1).
Approximating the potential between the ions in a crystal lattice as characterized by an harmonic shape (which is a very good approximation for small displacement of the ions), it is immediate to notice how the displacement of an ion will provoke a perturbation in the order of the lattice. This perturbation will behave like a wave (or at least, solutions of the perturbation dynamic are found in a wave-like shape), and thus endued with its dispersion, which fixes the relation between the wavevectors of the perturbation and the frequency (which uniquely associate an energy) of the displacement which it carries.
This means that the phonons are the quanta of waves which in real space are described as:

$$\mathbf{u}_\lambda^i = Re[\epsilon_\lambda^i(\mathbf{k})e^{\mathbf{k}\cdot\mathbf{R}-\omega_\lambda(\mathbf{k})t}] \tag{3.1}$$

where ϵ is the polarization vector, and the index i runs over every atom of the lattice (supposing a mono atomic lattice), which is located at $\mathbf{R}_i$ (the index is suppressed in the formula).
In general, treating a problem in N dimensions with n atoms per unit cell implies to find Nn normal modes, or branch - which is to say that Nn dispersion relations are allowed for the propagation of the perturbation waves (or, also, that we have Nn modes, Nn possible phonons with different energies, for each $\mathbf{k}$) - for the general calculation approach, see [26]. Those branches can be acoustic, if the energy (directly proportional to the amplitude) of the wave becomes zero for the wave vector also going to zero (i.e. we do not have stationary modes), or optical, otherwise.

Using the second quantization formalism, we can say that phonons are the quanta of the perturbations, which can always be reduced to a linear combinations of normal modes (the branches which emerges from the calculations). The allowed wavevectors are ruled out by the Born-Von Karman boundary condition (in one dimension in the first Brillouin zone we have a number of allowed wavevectors equal to the number of unitary cells in the solid), and are another way to see the emergence of the quantization. The wavevectors of the phonons are limited to the first Brillouin zone.
They are bosons, and they thus obey to the Bose-Einstein distribution (this is fundamental in order to understand their behaviour in the heat transportation, as in the Debye model).
A complete discussion - with a very useful analytic derivation - is given in [26] (here we reported the most elementary and important details).

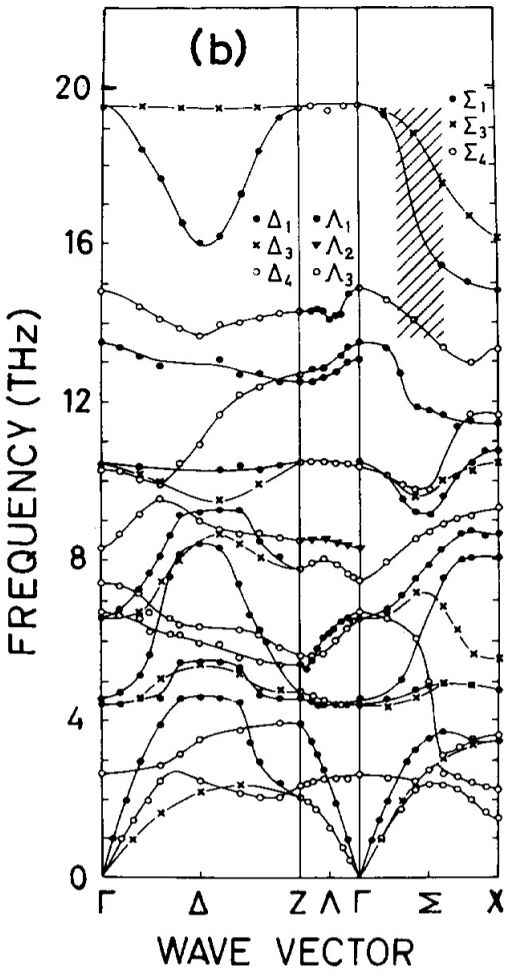

FIGURE 3.1: An example of INS measurement of phonons' dispersion relations. In this particular case, they are referred to La_2NiO_4. Figure from [32] (in the same article, measured phonons dispersion relation in LCO are found too).

3.2 Electron-Phonon Coupling

In this chapter, once again, we will follow the track given by [22], in order to derive the results with which we will later work.
RIXS couple to phonons, in a very intuitive way, because of the change in the charge spatial distribution which occurs in the intermediate state. This influences the lattice, inducing vibrations. Once the phonon is generated, the energy of the intermediate state is lowered (by the exact amount of energy given to the phonon), and this energy loss is detected in the transition from the intermediate to the final state.
Most of the core holes decay very rapidly, and there is not enough time to fully react to the charge distribution variation; this short duration of the intermediate state act as a suppression for the multi-phonon excitations, proportionally to the lifetime broadening Γ.
The Hamiltonian for the electron-phonon coupling is given in [33]:

$$H = \sum_{\mathbf{k}} [\omega_{\mathbf{k}} b^{\dagger}_{\mathbf{k}} b_{\mathbf{k}} + \sum_{i} (b_{\mathbf{k}} + b^{\dagger}_{-\mathbf{k}}) e^{i\mathbf{k}\cdot\mathbf{R}_i} \sum_{\mathbf{G}} m_{\mathbf{k}+\mathbf{G}} \eta(\mathbf{k}+\mathbf{G}) e^{i\mathbf{G}\cdot\mathbf{R}_i}] \tag{3.2}$$

Where we never write the branch index (which should follow each $\mathbf{k}$), nor we will do it later, and the excited electron is intended to be localized at $\mathbf{R}_i$. $b_{\mathbf{k}}$ are the creation and annihilation operators for the phonon with wave vector $\mathbf{k}$ and associated momentum $h\mathbf{k}$, and $h\omega_{\mathbf{k}}$ is its energy (which is to say that $\omega_{\mathbf{k}}$ is the dispersion relation of the mode at which the phonon belongs). h is setted equal to the unity. The functions used in (3.2) are:

$$m_{\mathbf{k}+\mathbf{G}} = -(\mathbf{k}+\mathbf{G}) \cdot \xi_{\mathbf{k}} \sqrt{\frac{h}{2\rho V \omega_{\mathbf{k}}}} V_{ei}(\mathbf{k}+\mathbf{G}) \tag{3.3}$$

$$\eta(\mathbf{k}+\mathbf{G}) = \int d\mathbf{r} e^{i\mathbf{G}\cdot\mathbf{R}_i} \Delta\rho(\mathbf{r}) \tag{3.4}$$

Where $\Delta\rho(\mathbf{r})$ is the change in the spatial charge distribution (and thus the difference between the square modulus of the ground and of the intermediate state wave function, multiplied by the elementary charge), and $V_{ei}(\mathbf{k})$ is the Fourier transform of an ion potential (with respect to the electron) placed at the origin. $\xi_{\mathbf{k}}$ is the polarization of the phonon (which is a vector with the dimensionality of the lattice that we are considering). We will say more about those terms in next chapters.

With the formalism of second quantization, assuming that the the cell is chosen to have the core hole a its centre $\mathbf{R}_i \cdot \mathbf{G} = 0$ and considering only direct RIXS events (the dynamic of the intermediate state is forgotten, we already said it in Chapter 2 and we will return on this concept soon), we have $e^{i\mathbf{k}\cdot\mathbf{R}} = \sum_i d^{\dagger}_i d_i e^{i\mathbf{k}\cdot\mathbf{R}_i}$ (see [22] and [33]), where $d^{\dagger}_i$ (d_i) is the creation (or annihilation) operator of a photo-excited electron at site i, and we can rewrite the Hamiltonian as:

$$H = \sum_{\mathbf{k}} [\omega_{\mathbf{k}} b^{\dagger}_{\mathbf{k}} b_{\mathbf{k}} + M_{\mathbf{k}} \sum_{\mathbf{p}} d^{\dagger}_{\mathbf{p}} d_{\mathbf{p}-\mathbf{k}} (b_{\mathbf{k}} + b^{\dagger}_{-\mathbf{k}}) \tag{3.5}$$

This is written in momentum space. We have defined:

$$M_{\mathbf{k}} = \sum_{\mathbf{G}} m_{\mathbf{k}+\mathbf{G}} \eta(\mathbf{k}+\mathbf{G}) \tag{3.6}$$

Since the phonons modify the electrons wave functions slightly, the polarization factor (2.18) is well approximated by the elastic process (at least in a process in which only phonons are excited), i.e. the initial and final state states of the electron are the same (we will label it by ψ), and the intermediate state to be considered is the $d_{x^2-y^2}$ one (at least in canonical cuprates at L_3 Cu edge).
We can rewrite the polarization factor as:

$$T_{el}(\epsilon', \epsilon) = \sum_{\psi} T_{\psi}(\epsilon', \epsilon) \tag{3.7}$$

3.2.1 Non Dispersive Phonons

In the Einstein model, we consider a single non-dispersive phonon per site of frequency ω_0.
We do not have branches, and, as we will see later, it does not even make sense to talk about a Brillouin zone - there is no need, indeed, to label the wave vector $\mathbf{k}$, since we have no dispersion (like in Raman scattering).
The e-p Hamiltonian reduces to:

$$H = \sum_{i} \omega_0 b^{\dagger}_i b_i + M d^{\dagger}_i d_i (b^{\dagger}_i + b_i) \tag{3.8}$$

i runs over different atoms.
Now, we can diagonalize the Hamiltonian through a canonical transformation ([34]). Defining:

$$S_i = \frac{M}{\omega_0} (b^{\dagger}_i - b_i) \tag{3.9}$$

$$S = \sum_{i} d^{\dagger}_i d_i S_i \tag{3.10}$$

We have the transformation as $H^* = e^S H e^{-S}$. The results is:

$$H^* = \sum_{i} \omega_0 b^{\dagger}_i b_i - \frac{M^2}{\omega_0} \tag{3.11}$$

Now, from (2.17), and defining $z = h\omega_{\mathbf{k}} - E_{res} + i\Gamma$ (in this particular case, $\omega_{\mathbf{k}} = \omega_0$):

$$F_{fg} = T_{el}(\epsilon', \epsilon) \sum_i e^{i\mathbf{q}\cdot\mathbf{R}_i} \sum_{n_i=0}^{\infty} \frac{\langle n_i'|e^{-S_i}|n_i\rangle\langle n_i|e^{S_i}|n_i^0\rangle}{z + \frac{M^2}{\omega_0} - n_i\omega_0} \tag{3.12}$$

Developing calculations (for all details, see appendix of [22]), we obtain, considering in the initial state zero phonons to be present (the index i run over all atomic sites, and $\mathbf{q}$ is intended to be the transferred momentum, which for Einstein phonons is identically zero):

$$F_{fg} = T_{el}(\epsilon', \epsilon) \sum_i e^{i\mathbf{q}\cdot\mathbf{R}_i} [\sum_{n=0}^{n_i'} \frac{B_{n_i'n}(g)B_{n0}(g)}{z + (g-n)\omega_0} + \sum_{n=n_i'+1}^{\infty} \frac{B_{nn_i'}(g)B_{n0}(g)}{z + (g-n)\omega_0}] \tag{3.13}$$

With

$$g = \frac{M^2}{\omega_0^2} \tag{3.14}$$

And the Franck-Condon factor is defined as:

$$B_{ab}(g) = \sqrt{e^{-g}a!b!} \sum_{l=0}^{b} \frac{(-1)^a(-g)^l\sqrt{g}^{a-b}}{(b-l)!l!(a-b+l)!} \tag{3.15}$$

Eventually, plugging this result into (2.11) to obtain the cross-section (which, we empathize, is the significant quantity in an RIXS experiment - $I \propto \frac{d^2\sigma}{d\omega d\Omega}$), we obtain:

$$\begin{aligned}\frac{d^2\sigma}{d\omega d\Omega} &\propto \sum_f |F_{fg}|^2\delta(\omega - n'\omega_0) = \\ &= NT^2 \sum_{n'=0}^{\infty} |\sum_{n=0}^{n'} \frac{B_{n'n}(g)B_{n0}(g)}{z + (g-n)\omega_0} + \sum_{n=n'+1}^{\infty} \frac{B_{nn'}(g)B_{n0}(g)}{z + (g-n)\omega_0}|^2\delta(\omega - n'\omega_0)\end{aligned} \tag{3.16}$$

Here there are a few important things to notice. In first place, a final state is identified by the number of phonons excited: $f \to n'$. The phonons could be localized on every atom, according to the Einstein model, and this is denoted by the factor N which is the result of the sum over i.
The $\mathbf{q}$ dependence is lost, according to the localized nature of the Einstein phonons.

Basically, each final state (identified by the number n' of phonons excited) is endued with a certain amplitude, and the total RIXS cross section will be directly proportional to the sum of those amplitudes (and in fact the sum over f turns out to be a sum over n'). But we must keep in mind that what we are talking about is an energy spectrum - each final state state will associate an energy (the term $\delta(\omega - n'\omega_0)$, where $h = 1$) at which its "part of cross

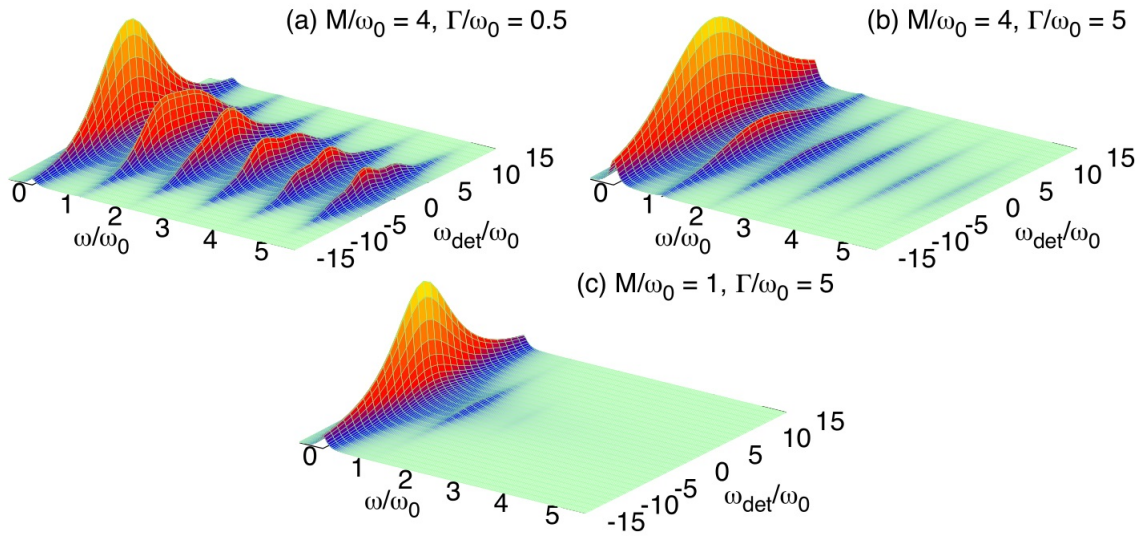

FIGURE 3.2: Simulations for different parameters choice of formula (3.16). This is a different plotting of the result that we will later obtain (see Figure 3.5), where different combinations of parameters are shown. Figure from [22].

section" (directly proportional to its amplitude squared) will be found. In the particular case of Einstein phonons, those will be multiple of ω_0, since all the phonons have the very same energy.
The RIXS spectrum will be a series of peaks, each one associated to a certain number of phonons which can be found in the final state, each one with an intensity directly proportional to the probability of exciting those number of phonons (according to (3.16), the intensity is directly proportional to the cross-section), and each one located at the energy loss necessary to excite that number of phonons.

3.2.2 A Better Approximation: Dispersive Phonons

For the dispersive phonons (which is the real case, where we have interacting atoms and thus dispersive excitations) the things are much more complicated, at least numerically: we will have to consider, in the most general case, that a Brillouin zone exist, and phonons "live" in it. Each one will be endued with a certain $\mathbf{k}$ and will associate a certain energy in concordance to its dispersion relation $\omega_{\mathbf{k}}$ (the branch indexes will always be neglected, but must in principle be considered).
The final state will be characterized not only by the number of phonons excited, but also by *which* phonons have been excited: $f \to n'_{\mathbf{k}_1}, n'_{\mathbf{k}_2}, n'_{\mathbf{k}_3}, \ldots$ (we have a finite number of wavevectors allowed in the Brillouin zone).
Eventually, a dependence on $\mathbf{k}$ also exist for $M(\mathbf{k})$, and thus we have $g(\mathbf{k}) = |\frac{M(\mathbf{k})}{\omega(\mathbf{k})}|^2$.
A canonical transformation (as in the Einstein phonon case) is applied (see [35]), and with the comment that Franck-Cordon overlap between the ground

state and the intermediate state follows a Poisson distribution with mean $g(\mathbf{k}) = g_{\mathbf{k}}$ (see [22]) we obtain:

$$F_{fg} \simeq T\frac{\delta_{\mathbf{q},\sum_{\mathbf{k}} n'_{\mathbf{k}}\mathbf{k}}}{z}\prod_{\mathbf{k}}[\sum_{n=0}^{n'_{\mathbf{k}}}\frac{B_{n'_{\mathbf{k}}n}(g_{\mathbf{k}})B_{n0}(g_{\mathbf{k}})}{z+(_{\mathbf{k}}g-n)\omega_{\mathbf{k}}}+\sum_{n=n'_{\mathbf{k}}+1}^{\infty}\frac{B_{nn'_{\mathbf{k}}}(g_{\mathbf{k}})B_{n0}(g_{\mathbf{k}})}{z+(g_{\mathbf{k}}-n)\omega_{\mathbf{k}}}] \quad (3.17)$$

And, again (h always setted equal to unity):

$$I(\omega) \propto \sum_f |F_{fg}|^2\delta(\omega-\sum_{\mathbf{k}} n'_{\mathbf{k}}\omega(\mathbf{k})) \quad (3.18)$$

And this is the intensity spectrum that we are going to obtain in a RIXS experiment.
Again, a few comment. It is very important to notice how, in this case, the $\mathbf{q}$ dependence is not lost. It is in fact in the Dirac delta term: given a certain transferred momentum $\mathbf{q}$, we can only have a final state $(f \to n'_{\mathbf{k}_1}, n'_{\mathbf{k}_2}, n'_{\mathbf{k}_3}, ...)$ which satisfy the condition $\mathbf{q} = \sum_{\mathbf{k}} n'_{\mathbf{k}}\mathbf{k}$. All the final states that satisfy this condition (remember that the transferred momentum is *fixed by the geometry of the experiment*) are allowed, and have a weight in the final spectrum through (3.18). We pay attention to the fact that the peak associated to each final state (which could be a single, double, triple and so on phonon state) is not, in the energy spectrum, a Dirac delta - in (3.17) we have a Dirac delta, $\delta(\omega - \sum_{\mathbf{k}} n'_{\mathbf{k}}\omega(\mathbf{k}))$, but we must account for an energy broadening due to the finite lifetime of this excited state.
Again, we suppose that in the ground state we do not have any phonon, and the number of phonons with vector $\mathbf{k}$ in the final state is denoted by $n'_{\mathbf{k}}$.

3.3 Approach to Calculations

In first place, we have to briefly discuss Einstein phonons.
Einstein introduced his model for phonons in order to explain the specific heat behaviour in solids. The two main assumptions that he made were: each atom is seen as an independent quantum oscillator and all the atoms are oscillating at the same frequency. The first assumption in particular is significant in order to accept the fact that in the framework of such a model it makes no sense to talk about a Brillouin zone: a lattice of non interacting atoms is a lattice in which a perturbation in one point (i.e. a phonon localized on one atom) does not affect in any way the behaviour ot the neighbouring atoms - we do not have a perturbation with a form such as (3.1). This means that we do not have a dispersion, and thus we have only phonons with $\mathbf{k} = 0$. This is why, by the way, only $\mathbf{q} = 0$ is allowed. We can also consider that a lattice with non interacting atoms is a lattice where we have a distance between atoms which is conceptually $a \to \infty$ (in the sense that assuming non interacting atoms is the same as assuming interacting atoms at an infinite distance), and thus the Brillouin zone is such that $(-\frac{\pi}{a}, \frac{\pi}{a}) \to 0$.
To visualize the Einstein phonons as an approximation of the optical branch

in which ω is constant all over the first Brillouin zone could be misleading. In fact, it is not the same thing - even if, for the Einstein purpose, it would work the same way.
In fact, developing the calculation for the total energy (the specific heat is the derivative of the total energy with respect to the temperature), in theory we should have (considering the phonons as bosons, which follows the Einstein-Bose statistic):

$$E_{tot} = nP_i h\omega_0 = n < n_{\mathbf{k}=0} > h\omega_0 = \frac{nh\omega_0}{e^{\frac{h\omega_0}{k_B T}} - 1} \tag{3.19}$$

Where we are considering a total number of phonons which is n (the number of atoms) times the average number of phonons on a single atom (P_i).
We would obtain the same result considering a branch of phonons with constant dispersion $\omega(\mathbf{k}) = \omega_0$ (see [26]):

$$E_{tot} = \sum_{\mathbf{k}} E_{\mathbf{k}} = \sum_{\mathbf{k}} < n_{\mathbf{k}} > h\omega_{\mathbf{k}} = \frac{nh\omega_0}{e^{\frac{h\omega_0}{k_B T}} - 1} \tag{3.20}$$

But in our case the situation is pretty different.
Eventually, the important fact here is that we expect (3.17) to fall into (3.13) (which is to say that we expect the same spectra) if we consider only phonons with $\mathbf{k} = 0$ (and thus $\mathbf{q} = 0$) - and this is different from considering a non-dispersive dispersion relation.
Our approach will consists in the following steps:

- **Fix a $\mathbf{q}_{\parallel}$**: This comes directly from the geometry of the experiment (see Chapter 2.3), and it is equivalent to say that each spectrum will be the expected one in a given experimental geometry. $q_{\parallel}$, for what we have said in Chapter 2, is the total momentum transferred into the CuO_2 plan, and is thus the total momentum that a phonon - in case of single phonon excitation and coherently with conservation laws - will have to carry (in the case of Einstein phonons, as already said, the total momentum transferred is identically zero).

- **Identify every allowed phonons combinations of the final state**: Once we have the total momentum transferred, we have to identify all the possible combinations of phonons. In the final state (that is the excited state of the material) we can have one phonon, two phonons, three phonons and so on. The allowed state (once again, a state is defined as $f \rightarrow n'_{\mathbf{k}_1}, n'_{\mathbf{k}_2}, n'_{\mathbf{k}_3}, ...$) are, as stated in (3.17), those who respect $\mathbf{q} = \sum_{\mathbf{k}} n'_{\mathbf{k}_i} \mathbf{k}$.
  This means that we can have a single phonon with $\mathbf{k} = \mathbf{q}$, every couple of phonons with $\mathbf{k}_1$ and $\mathbf{k}_2$ such that $\mathbf{k}_1 + \mathbf{k}_2 = \mathbf{q}$, and so on for higher numbers of phonons.

- **Identify the energies of each final state**: This is simply done through the dispersion relation. The energy of the state with a phonon will be $h\omega(\mathbf{k})$, if the phonons are two (with $\mathbf{k}_1$ and $\mathbf{k}_2$), then it is $h\omega(\mathbf{k}_1) + h\omega(\mathbf{k}_2)$; and so on.

- **Find the amplitude of each state**: Which is to say, through (3.17), to find $|F_{fg}|^2$, and eventually the RIXS spectrum with the help of (3.18).

3.3.1 Manipulations

As we have already said, in the first Brillouin zone we have a number of allowed vectors $\mathbf{k}$ (N_k) which is equal to the number of unitary cells in the sample, at the power of the number of dimension that we are considering (N_d). This is a huge number, both when developing the product in (3.17) and searching all the possible couples of phonons for a given $\mathbf{q}$ (which is in the order of $N_{\mathbf{k}}^{N_d}$) - and we should also consider the "triplets" of phonons (which number goes as $N_{\mathbf{k}}^{2N_d}$), and so on.

In first place, we have to overcome the problem of the product, which obviously is impossible to compute, even for a reduced number of N_k.
The units in which the intensity will be expressed are arbitrary: and this is because of the terms NT^2 in (3.17), which we do not compute.
What really matter is the *relative intensity* of a peak with respect to the others. When we talk about the intensity of a peak, we are talking about the term $|F_{fg}|^2$.
We have $f \to n'_{\mathbf{k}_1}, n'_{\mathbf{k}_2}, n'_{\mathbf{k}_3}, ...$ and

$$I_{RIXS}(E) = \sum_f |F_{fg}|^2 \delta(E - E_f) \tag{3.21}$$

It is convenient to define the element inside the product in (3.17) with respect to their "phononic occupation number" (n'_k). This means, for zero phonons with $\mathbf{k}$:

$$A(\mathbf{k}) = \frac{B_{00}(g_{\mathbf{k}})B_{00}(g_{\mathbf{k}})}{1 + g\omega_{\mathbf{k}}/z} + \sum_{n=1}^{\infty} \frac{B_{n0}(g_{\mathbf{k}})B_{n0}(g_{\mathbf{k}})}{1 - \frac{(n-g_{\mathbf{k}})\omega_{\mathbf{k}}}{z}} \tag{3.22}$$

For one phonons with $\mathbf{k}$:

$$A^*(\mathbf{k}) = \sum_{n=0}^{1} \frac{B_{1n}(g_{\mathbf{k}})B_{n0}(g_{\mathbf{k}})}{1 - \frac{(n-g_{\mathbf{k}})\omega_{\mathbf{k}}}{z}} + \sum_{n=2}^{\infty} \frac{B_{n1}(g_{\mathbf{k}})B_{n0}(g_{\mathbf{k}})}{1 - \frac{(n-g_{\mathbf{k}})\omega_{\mathbf{k}}}{z}} \tag{3.23}$$

For two phonons with $\mathbf{k}$:

$$A^{**}(\mathbf{k}) = \sum_{n=0}^{2} \frac{B_{2n}(g_{\mathbf{k}})B_{n0}(g_{\mathbf{k}})}{1 - \frac{(n-g_{\mathbf{k}})\omega_{\mathbf{k}}}{z}} + \sum_{n=3}^{\infty} \frac{B_{n2}(g_{\mathbf{k}})B_{n0}(g_{\mathbf{k}})}{1 - \frac{(n-g_{\mathbf{k}})\omega_{\mathbf{k}}}{z}} \tag{3.24}$$

And so on.

This allows us to rewrite the amplitudes. In the case of a phonon with $\mathbf{k}_3$ (from (3.18), (3.22), (3.23), (3.24)):

$$F_{fg} = \frac{T}{z} A(\mathbf{k}_1)A(\mathbf{k}_2)A^*(\mathbf{k}_3)...A(\mathbf{k}_N) \tag{3.25}$$

If we have two phonons with, respectively, $\mathbf{k}_1$ and $\mathbf{k}_3$:

$$F_{fg} = \frac{T}{z} A^*(\mathbf{k}_1)A(\mathbf{k}_2)A^*(\mathbf{k}_3)...A(\mathbf{k}_N) \tag{3.26}$$

Or for two phonons with $\mathbf{k}_1$:

$$F_{fg} = \frac{T}{z} A^{**}(\mathbf{k}_1)A(\mathbf{k}_2)A(\mathbf{k}_3)...A(\mathbf{k}_N) \tag{3.27}$$

As we said, all our intensities will be in arbitrary units (for example $[NT^2] \equiv 1$). If we consider two final states, the difference in their final amplitude will be given only by the terms of the product which are occupied.
We can formalize this concept by expressing the intensity (which is directly proportional to the modulus squared of the terms (3.25), (3.26), (3.27)) in units of:

$$\frac{NT^2}{(\prod_{\mathbf{k}} A(\mathbf{k}))^2} \equiv 1 \tag{3.28}$$

This imply an heavy simplification, since, in this basis, we can write our amplitude terms as (from (3.21), (3.25), (3.28)), for example in the case of a phonon with $\mathbf{k}_3$:

$$F_{fg} = \frac{T}{z} \frac{A^*(\mathbf{k}_3)}{A(\mathbf{k}_3)} \tag{3.29}$$

Or, if we have two phonons with $\mathbf{k}_1$ and $\mathbf{k}_3$:

$$F_{fg} = \frac{T}{z} \frac{A^*(\mathbf{k}_3)A^*(\mathbf{k}_1)}{A(\mathbf{k}_3)A(\mathbf{k}_1)} \tag{3.30}$$

In this way we get rid of the product. The price to pay is to set absolutely awful units, but that is not a big deal, since already at the start we did not have useful units ($NT^2 = 1$). Moreover, as we said earlier, what we are really interested in is the *relative* intensity of a peak respect to each other, which is a dimensionless quantity.
(3.28) also imposes other limitations, which we will see more in detail in Section 3.3.3.

3.3.2 More Comments on Calculations

Another problem that emerges during calculations is that the number of couples of phonons allowed is proportional to the number of wavevectors - and

of course we cannot account for all the wavevectors and all the couples which really exist in the Brillouin zone.
Moreover, if we consider the total amplitude of the peak associated to the two phonons final states (the sum of the intensities of all the peaks associated to each single couple of phonons in the final state), this is directly proportional to the number of couples, and it grows with $N_{\mathbf{k}}$, eventually resulting incredibly bigger than the single phonon peak intensity (if we consider a realistic number of wavevectors) - even if the amplitude of a double phonon event by itself is always smaller than the amplitude of a single phonon one (this is because we always have $\frac{A^*}{A} < 1$: an important and promising fact). The same goes for the three phonon peak (the number of so called "triplets" grows as $N_{\mathbf{k}}^{2N_d}$) with respect to the two phonon peak, and so on. We have a divergent (and thus non-physical) behaviour of the system.
We account for this by introducing a normalization, as prescribed by the density of states present in the Fermi Golden rule for second order transitions, which is the starting point of the Kremers-Heisenberg equations (2.7). The intensity relative to each couple of phonons, $|F_{fg}|^2$, is divided by the numbers of wavevectors N_k (which also directly proportional to the number of couples allowed) before being summed into the total intensity. This can be viewed as a way to keep into account the fact that the more couples are allowed, the less is likely to excite a precise one. In one dimension we have:

$$I = |F_{single}|^2 + \frac{1}{N_k} \sum_{couples} |F_{couples}|^2 + \frac{1}{N_k^2} \sum_{triplets} |F_{triplets}|^2 \tag{3.31}$$

This provides in both avoiding the explosion of the intensity for high numbers of wavevectors allowed (the intensity converge to a finite quantity for $N_{\mathbf{k}} \to \infty$) and in obtaining an intensity of the two phonons peak smaller than the intensity of the single phonon peak,at least in most of the cases (see Figure 3.1).

In (3.21) we have that every possible final state contributes as a Dirac delta to the RIXS spectrum. That would be true only in the case in which the final state is a stable state, i.e. it does not decade in a finite time. But since it is an excited state, it does - and we have to account for an energy broadening of the peak in the shape of a Lorentzian (the overall intensity will remain the same, due to the implicit normalization of the Lorentzian curve). Indicatively, we chose a broadening of about 10 meV - and this associate a lifetime for the excited state of hundreds of femtoseconds.
Moreover, we will consider only one branch. Theoretically, we should consider all the branches (see (3.1.1)). This would mean to have one single phonon peak for every branch, and the combinations of two phonons allowed would grow in a factorial proportionality with the branches. Still, to consider only one or two branches could be a good approximation (for more details, see Chapter 4) - and in any case, our simulated spectrum should be considered as the contribution of the single branch to the overall spectrum.
One last detail is that, considering a couple of phonons, we account two times for its intensity: we have in fact two possible orders in which the phonons

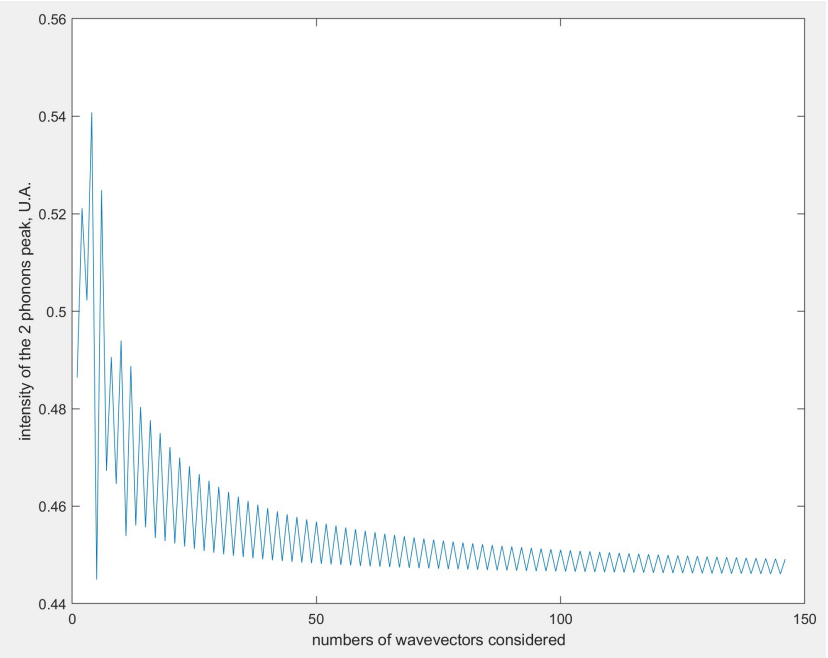

FIGURE 3.3: Total intensity of the second peak, in U.A., as simulations were done with an increasing number of wavevectors in the first Brillouin zone. It is evident how we have a stable and finite intensity for a number of wave vector greater than, indicatively, one hundred.

are created (two possible excitation channels, more technically). If the couple of phonons is instead made by two identical phonons, we count it only once.

3.3.3 Validity of the Results

As we said in the previous chapter, the price to pay to get rid of the product in (3.17) is to introduce an odd sets of units: (3.28).
We must pay the attention to the dependences of $A(\mathbf{k})$. From (3.22):

$$A = A(M(\mathbf{k}), \omega(\mathbf{k}), z) \tag{3.32}$$

with, again, $z = (h\omega - E_n) + i\Gamma = \Delta E_{det} + i\Gamma$.
This means that, once the calculations are done, the units of the intensity in which the result is expressed are themselves functions of those parameters - once we have taken a decision on which values $(M(\mathbf{k}), \omega(\mathbf{k}), z)$ to use, we have set our arbitrary units.
It follows that two intensities obtained with different values of $M(\mathbf{k}), \omega(\mathbf{k})$ or z are not comparable.
Let's suppose for example to compare the intensity of the single phonon peak obtained with different $M(\mathbf{k}), \omega(\mathbf{k})$ or z - in both cases setting the same units in energy (but even if the energy units were different that would not be a problem, we would just need to multiply the result for a scaling factor $\frac{\omega_0}{\omega_1}$, where ω_0 or ω_1 are the energy setted equal to unity in each case), the ratio will not be dimensionless, but will be in units of:

$$\frac{I_{1_1}}{I_{1_2}} \longmapsto \frac{NT^2}{(\prod_{\mathbf{k}} A(M_1(\mathbf{k}), \omega_1(\mathbf{k}), z_1))^2} \frac{(\prod_{\mathbf{k}} A(M_2(\mathbf{k}), \omega_2(\mathbf{k}), z_2))^2}{NT^2} = \\ = \frac{(\prod_{\mathbf{k}} A(M_2(\mathbf{k}), \omega_2(\mathbf{k}), z_2))^2}{(\prod_{\mathbf{k}} A(M_1(\mathbf{k}), \omega_1(\mathbf{k}), z_1))^2} \tag{3.33}$$

Anyway, ratios between one phonon and two phonons peaks are really non dimensional, since they are calculated with the same $M(\mathbf{k}), \omega(\mathbf{k})$ and z, and thus it makes sense to compare ratios calculated with different choice of parameters. Results obtained with different total momentum transfers are comparable, too, since a different choice of $\mathbf{q}$ does not influence the units in which the results are expressed (always according to (3.28) - the choice of $\mathbf{q}$ does not enter in the product, see (3.17)).
To recap, it is meaningful to study:

- $$\frac{\frac{I_2}{I_1}(M_1, \omega_1, z_1)}{\frac{I_2}{I_1}(M_2, \omega_2, z_2)} \Longleftrightarrow \frac{I_2}{I_1} = f(M, \omega, z) \tag{3.34}$$

  The evolution of the ratio between single phonon and two phonons peak with different choices of parameters.

- $$\frac{I_{1,2}(M, \omega, z)|_{\mathbf{q}_1}}{I_{1,2}(M, \omega, z)|_{\mathbf{q}_2}} \Longleftrightarrow I_i(M, \omega, z) = f(\mathbf{q}) \tag{3.35}$$

  The evolution of a peak at different total momentum transfers.

There are parameters good enough to attempt to have experimental feedback.
Moreover, the shape of the peaks is also, in principle, reliable. The units is impossible to compute (3.28) (since here we have again our product over all the possible $\mathbf{k}$), but it is, of course, a constant, once $M(\mathbf{k}), \omega(\mathbf{k})$ and z are fixed - the shape of the spectra is not modified, only its overall amplitude is.

3.4 1D

We will use the 1D case as an instructive case, to later apply what we have learned to the more significant 2D case.
A first point is which to branch to consider. This is immediately non trivial, since we have defined $g(\mathbf{k}) = |\frac{M(\mathbf{k})}{\omega(\mathbf{k})}|^2$ - choosing the acoustic branch would also mean having a coupling M which goes to zero for $\mathbf{k} \to 0$, in order to avoid divergence. So, we will work with an optic branch, whose maximum energy (found at $\mathbf{k} = 0$) sets the unity of the energy (typically around 80 meV), which are the ones found on the coordinates in the spectra that we will have as a result of the calculations. Also from an experimental point of view, the most energetic phonons are the more interesting, since are the ones which are better distinguishable from the elastic peak.
We will try different shapes for $M(\mathbf{k})$, to see how the spectrum is affected. We will specify it each time - more consideration about this coupling factor, in the more realistic 2D case, are found in Section 3.5.2.
The program implemented in MatLab accepts as input the following parameters:

- Γ: the energy broadening of the intermediate state. Usually taken as 5 (remembers that the unity is setted by the dispersion relation, it is assumed to be around 400 meV) - and it means to have a lifetime of the intermediate state of about ten femtoseconds.

- Γ_{int}: the energy broadening of the phonon final state energy; in general it is set at about 5 meV. This parameter changes the shape of the peaks, but not their overall intensity, since the Lorentzian is normalized to the unit. The response of the one phonon peak to a change of Γ_{int}, in term of shape change, is quite different from the two phonons peak one: its broadening is more striking - but this is normal, since the two peak phonons is the sum of many Lorentzian, while the one phonon peak is just a Lorentzian.

- **Detuning**: together with Γ, defines z. It is the difference between the energy of the photon and the system resonant energy. It will be a main parameter in the discussion of the experimental results in Chapter 4.

- **Phonons' combination allowed**: This parameter decides if we want to consider only the single phonon or also the couples, adding or removing in this way a part of the resulting spectra. In 1D, the program is also build to find and calculate the amplitudes of triple phonons event.

- $\mathbf{N_k}$: The number of wavevectors to be considered in the first Brillouin zone. In the 2D case, in the first Brillouin zone there will be $N_{\mathbf{k}}^2$ possible vectors. To understand the importance of this parameter, see 3.3.2.

In order to have coherent simulation, we want an high number of $N_{\mathbf{k}}$ (again, see Figure 3.1). A small $N_{\mathbf{k}}$ will provide inaccurate, but still instructive results (also, if we want to consider triple phonon events, we must use a small $N_{\mathbf{k}}$ to overcome computational problems).

- **q**: The total momentum transferred into the CuO_2 plane. It sets the allowed final states.

The dispersion relation and the coupling are defined inside functions that are often called by the main program.

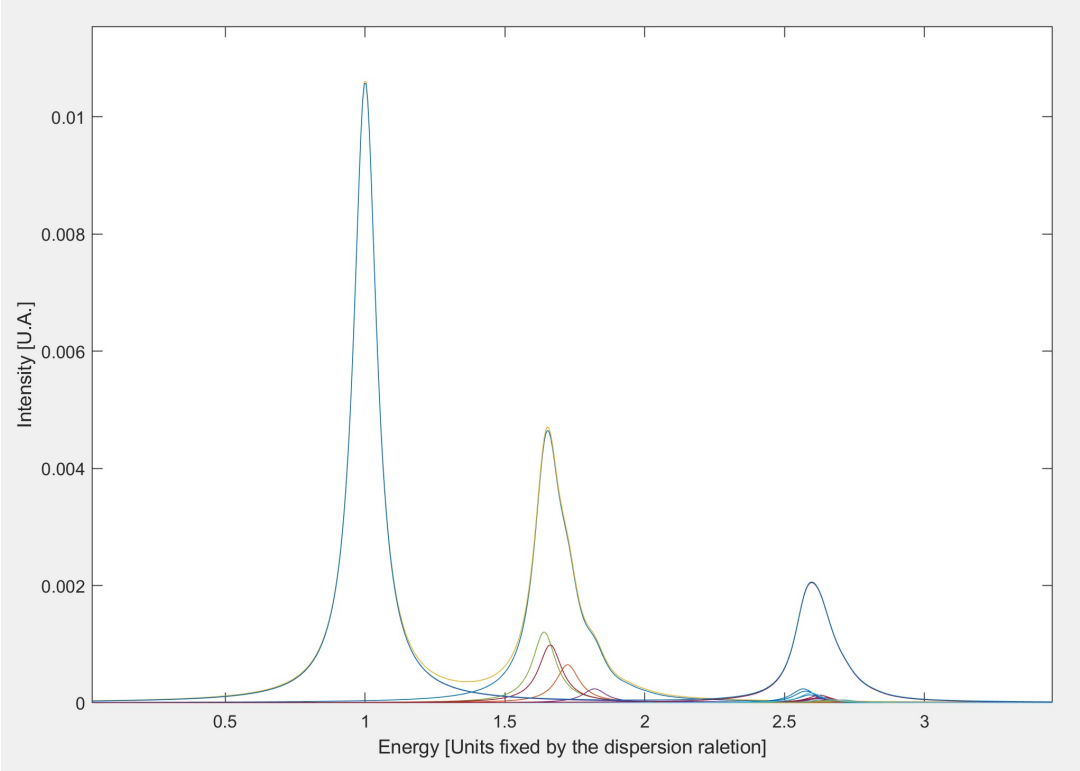

FIGURE 3.4: Example spectrum obtained as a result of the calculations. The energy unit is setted by the top of the optical branch. The parameters used are: $\Gamma = 5$, $\Gamma_{int} = 0.05$, Detuning$= 0$, $\mathbf{N_k} = 10$, $\mathbf{q} = 0$. The coupling i discussed in the text. Calculations were also made for triplets of phonons (they are visible at energies higher than 2.5).

In Figure 3.4 we have an example of the outcome of the calculations. For this example, we considered a 1D case with coupling $M(k) = 0.6 + \frac{k^2}{1+0.5k^2}$ and an acoustic branch with the characteristic shape $\omega(k) = (1 - \alpha \sin(k))$.
This spectrum is to be intended as the energy loss of the outgoing photon. We have used a small number of wavevectors, in order to be able to calculate, at least in this first example, the triplets (as we will call from now on the

spectra associated to triple phonon events) absorption spectra (which will be normalized to $N_{\mathbf{k}}^{2N_d}$, according to Section 3.3.2).
We can think of every peak in the figure as the amplitude relative to a single final state. With $\mathbf{N_k} = 10$ (technically there are eleven wavevectors, k=0 is always present) and $\mathbf{q} = 0$ we have five possible pairs. For each couple we develop the calculations, find an amplitude (and thus an intensity) centred at an energy dictated by the dispersion relation and then overlap it to a Lorentzian. The same goes for the single phonon (the only possibility is **q**=**k**), and all the possible combinations of three phonons. Considering the shape of the coupling, the dispersion relation, and the fact that, besides the very complex form of (3.17), the greater is $g_{\mathbf{k}}$ the greater is the coupling and thus the intensity, we can get an intuitive confirmation of the relative intensity of the two phonons peak (which are $(-\pi, \pi)$, $(-\frac{\pi}{2}, \frac{\pi}{2})$, ...).
In Figure 3.5 we zoom in order to distinguish each triplet (whose intensity is too small to be distinguishable respect to the single and two phonons peaks). Each intensity is normalized according to Paragraph 3.3.2. We notice how, even in a simple case with $\mathbf{N_k} = 10$ we have an high number of possible triplets which satisfy the momentum conservation.

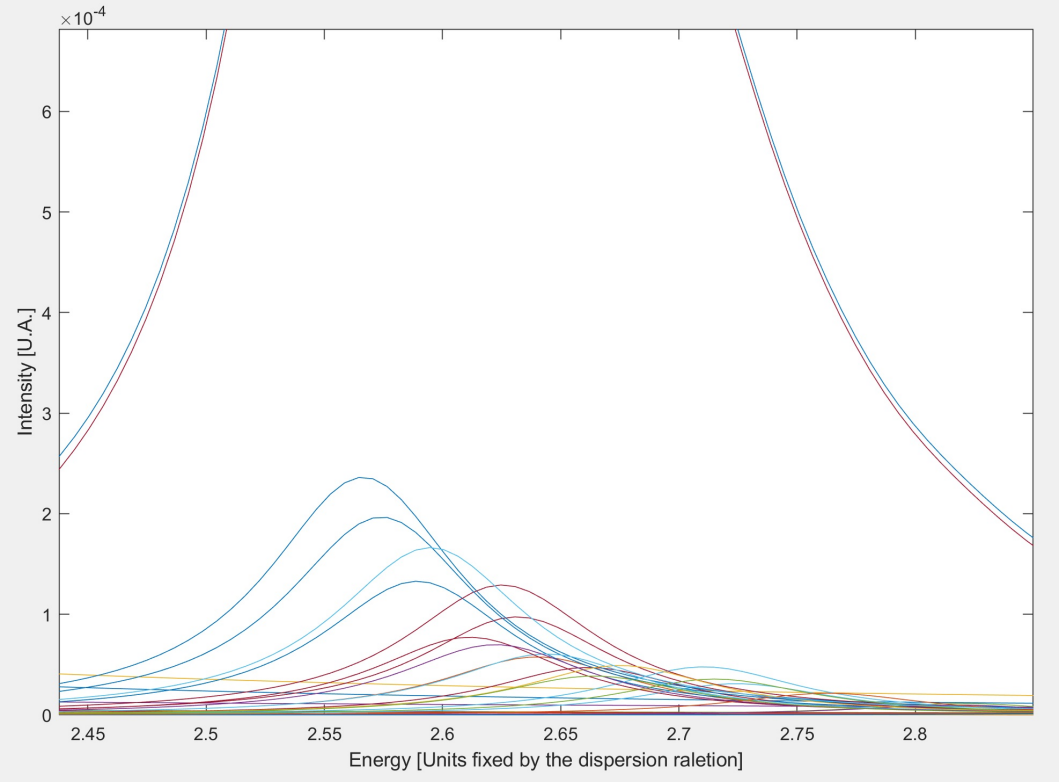

FIGURE 3.5: Zoom of Figure 3.4. The peaks are associated to triplets of phonon, the overlying line is their sum (and thus it is what we call the total intensity of the three phonon peak). The same goes for Figure 3.4.

3.4.1 Programming

All the codes for the 1D case can be found in Appendix A. For the 2D case, the codes are found in Appendix B.
To be more specific, first we find all possible combination of couples of triplets which satisfy the momentum conservation. Once the couples and the triplets are returned to the main function, we run the calculation for (3.17). In particular, we calculate (3.22), (3.23), (3.24) with the corresponding function call ("A, A-star, A-double-star"). The dispersion relation, the coupling and the Frank-Cordon factor are also calculated though the call of respective functions ("Dispersion, Coupling, B"). We then associate a Lorentzian to each peak, sum the peaks and plot. In order to obtain the effective RIXS spectrum, we should do the convolution between our spectrum and a Gaussian with full width at half maximum equal to the experimental resolution (indicatively 35 meV).

3.4.2 Results And Comments

From now on, we will not consider the triplets of phonon (which intensity is always smaller than the single or the two phonons peak). We will use $\mathbf{N_k} = 200$, and Γ_{int}=0.05.
There are many aspects of the RIXS phonons features behaviour that we can consider, even with our one dimensional calculations. Brief discussion for each of them will follow.

- **Einstein Phonons** The first thing that we can try to do is to check that, as explained in Section 3.3, the dispersive phonons peaks fall into the Einstein phonons' ones once we consider only $\mathbf{k} = 0$, and thus a constant dispersion ($\omega_0 = 1$) and a constant coupling too ($M = 5$) - of course, in order to be coherent, we also need to consider a null total momentum transfer.

  Figure 3.6 and 3.7 show, respectively, the calculated spectrum in the case of Einstein phonons and in the case of dispersive phonons for a null total momentum transfer. Now, the ratio between the first and the second peak in Figure 3.6 and 3.7 is the same. The two figures differs only for a rescaling factor - but this is due to the normalization that we are using in the case of dispersive phonons (again, (3.28)). If working with only $\mathbf{k} = 0$, that rescaling factor (which is implicit in the normalization) is easily computable, and once we account for it we find that Figure 3.6 and 3.7 coincide (they would be now expressed on the same basis, $NT^2 = 1$).
  Eventually, we have that the dispersive phonon case converge with the Einstein phonon approximation when considering only phonons with $\mathbf{k} = 0$ - thus non dispersive phonons with constant coupling and fixed energy. All this is coherent with the discussion which allowed us to derive (3.19) and (3.20), and is also striking comparing equations (3.16) and (3.17).

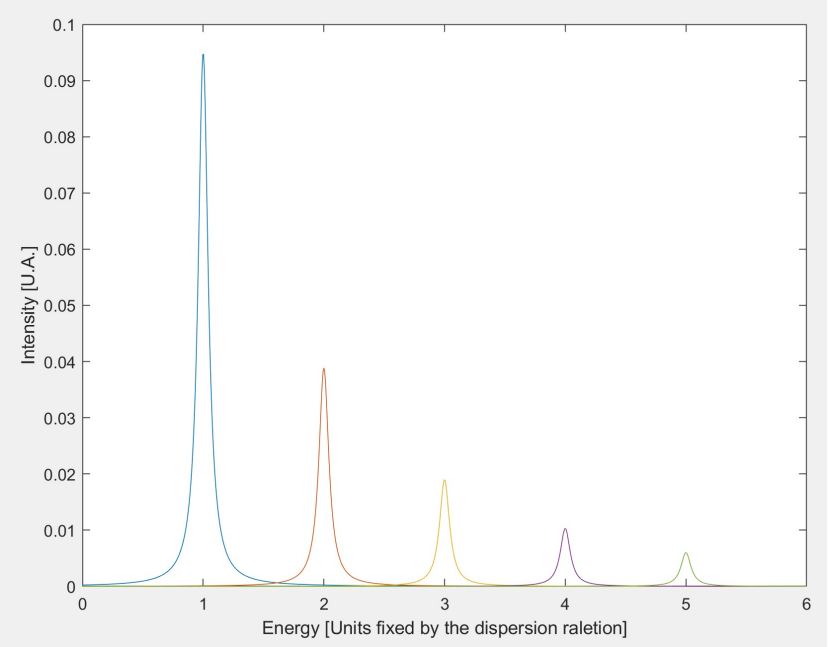

FIGURE 3.6: Here we have the spectrum resulting from the Einstein Phonon case, according to formula (3.16). We have that every peak is centred exactly at a multiple of the single phonon energy, since we do not have dispersion.

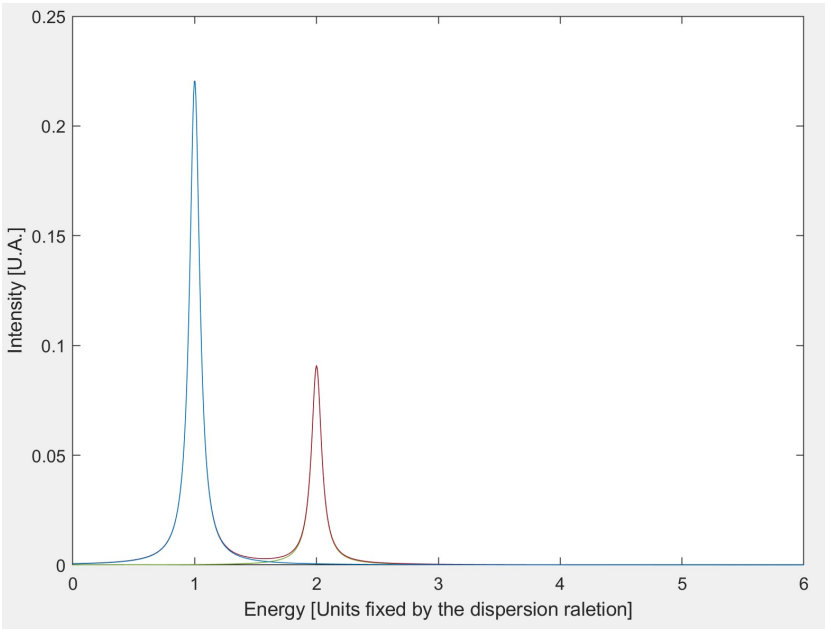

FIGURE 3.7: Here we used formula (3.17), for the dispersive phonons intensities, together with the assumptions specified in the text. We only calculated single and double phonon peaks intensity.

- **RIXS spectra for different couplings, detunings and total momentum**

transfer What we can do now is a study of the different shape of the attended RIXS spectrum in terms of the two phonons peak. In fact, considering different configurations of the energy dispersion and of the coupling, we will have that different couples of phonons (remember that the allowed couples will be fixed by the total momentum transfer) will be endued with different amplitudes.
We will always use, in this section, a dispersion relation $\omega(k) = (1 - \alpha \sin(k))$, which is the classical shape for the optical branch. Considering an acoustic branch, in order to avoid a divergent behaviour of the parameter M, would force us to also consider a coupling which vanishes for $\mathbf{k}$ approaching zero (this will anyway be the interesting case - for more details see chapter 4).
We can immediately notice that, until the total transferred moment is null, the single phonon peak will always be centred at zero energy, and its amplitude will be proportional to the coupling at $\mathbf{k} = 0$.
Also, a non null detuning will in general depress the intensities of both the single and double phonons peak, but there is no a priori reason to expect them to decrease at the same rate - for further considerations, again, see chapter 4.
A very important result is that the shape of the two phonon peak (and, of course, its intensity) is directly dependent on the coupling shape - even if, at the state of art, it is impossible to actually distinguish it in a realistic RIXS spectrum (see Figure 2.2 or 2.9).
Way more interesting, in this sense, is the total momentum transfer dependence of the spectra, as well as the detuning one, as we will later see.
We considered a coupling in the form $M(\mathbf{k}) = 0.6 + 1.5|\sin(\mathbf{k})|$ since we want a coupling which is non null for $\mathbf{k} = 0$, (again, we would otherwise lose the single phonon peak for zero total momentum transfers).

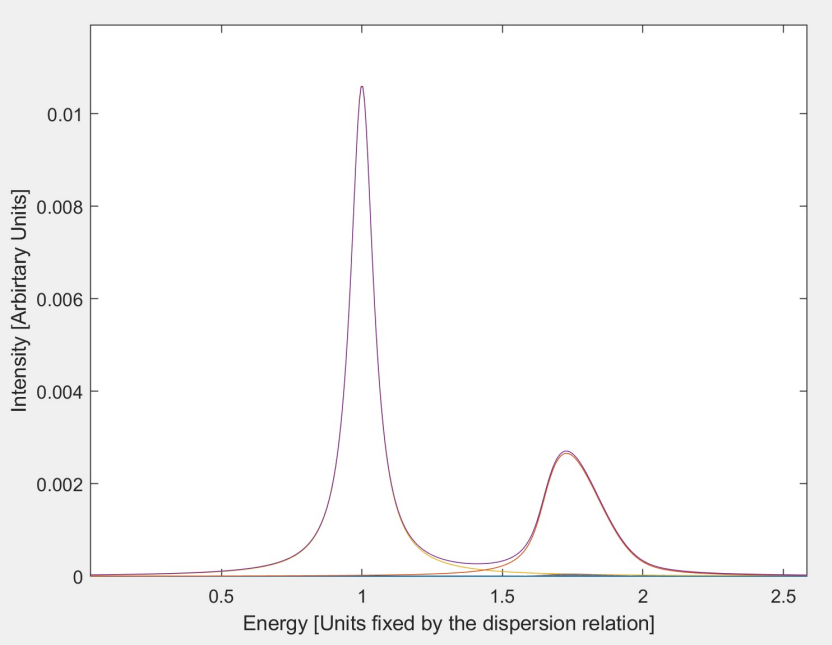

FIGURE 3.8: Here we have used a coupling $M(\mathbf{k}) = 0.6 + 1.5|\sin(\mathbf{k})|$ and $\mathbf{q} = 0$. Since the coupling is stronger for phonons with higher $\mathbf{k}$, and the phonons with greater $\mathbf{k}$ have, in our assumptions, smaller energies, we will find our two phonons peak translated to lower energies.

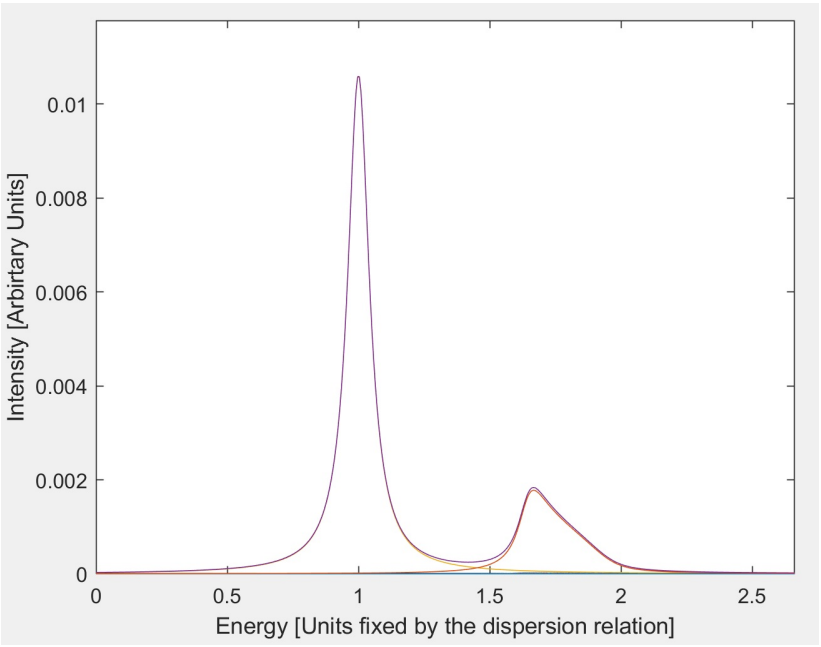

FIGURE 3.9: Here we have used a coupling $M(\mathbf{k}) = 0.6 + \frac{\mathbf{k}^2}{0.2+\mathbf{k}^2}$ and $\mathbf{q} = 0$. What we said for Figure 3.8 is also true here, but is important to notice how the effective shape of the two phonon peak is changed from the previous case - as consequence of the different coupling.

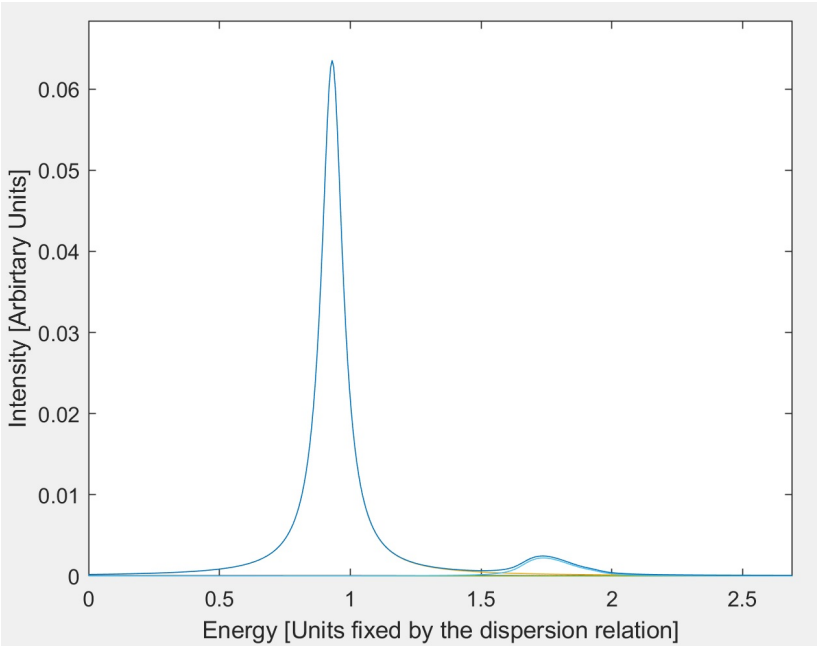

FIGURE 3.10: Here we have used a coupling $M(\mathbf{k}) = 0.6 + 1.5|\sin(\mathbf{k})|$ and $\mathbf{q} = \frac{\pi}{4}$. This is, basically, the same case as Figure 3.9, but with a non null total momentum transfer. Here is important to not be mislead by the intensity scale - the single phonon peak grows of a factor 6 (since the coupling grows for bigger $\mathbf{k}$), and it is found at smaller energies - while the two phonon peak still grows, but of a much smaller ratio (about 1.1). In the case of the two phonon peak, in fact, we must account both for a bigger coupling and for a smaller number of couples allowed - the more $\mathbf{q}$ approaches the Brillouin zone edge, the fewer are the allowed couples of phonons.

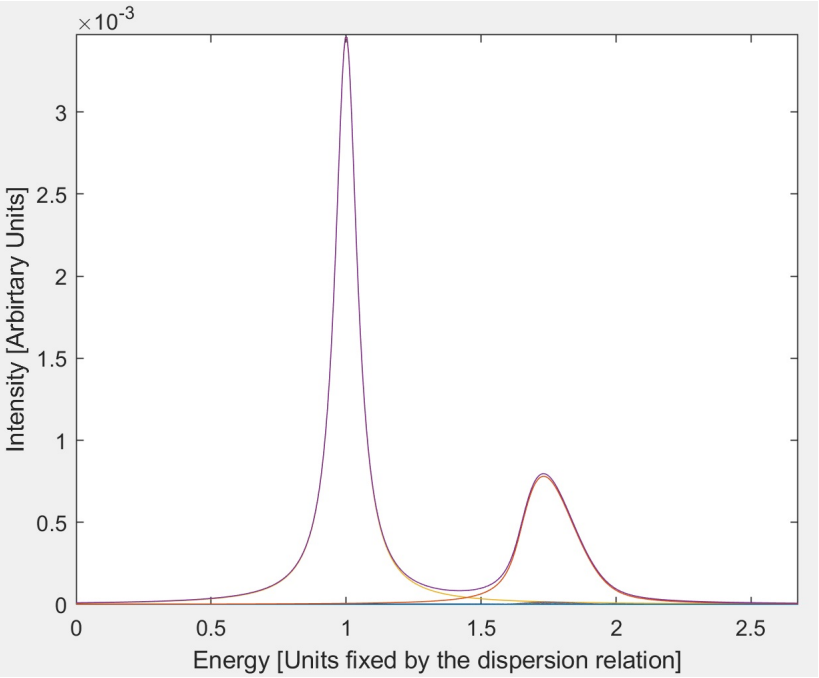

FIGURE 3.11: Here we have used a coupling $M(\mathbf{k}) = 0.6 + 1.5|\sin(\mathbf{k})|$ and $\mathbf{q} = 0$, but we also supposed a detuning of 5 energy units (which, as always, are fixed by the top of the optical dispersion relation, and are equivalent to 400 meV). We have a general depression of the intensities of both the single and double phonon peak (again, pay attention to the scale, much smaller than the one in figure to Figure 3.9), but the shape and the ratio between the intensities are unchanged - and it is reasonable, since what we are doing is to get away from the resonance, and thus we are reducing the overall RIXS cross section.

For more considerations about detuning, see Chapter 4.

- **Characteristic curves** We consider the ratio between the intensity of the single and the double phonon peak (where, from now on, we will intend the intensity of a peak as its area, coherently with the intuitive notion of an overall cross section for that excitation). We notice that an universal curve can be deduced - in particular, the ratio $\frac{I_2}{I_1}$ plotted against the parameter $(\frac{M}{\Gamma})^2$ results to be a constant for whatever g we choose (g, again, is defined as $(\frac{M}{\omega})^2$). The physical meaning of this universality is not striking at all, considering also that g itself is dependent on M - we are saying that the possibility to excite two phonons is not dependent from the absolute values of the parameters M, ω, Γ, but rather on their ratios. A big lifetime (with respect to the value of the coupling) enhance the possibility to generate couples of phonons, and the same goes for an high ratio $(\frac{M}{\omega})$ - different triplets of values can associate the same ratio $\frac{I_2}{I_1}$.
  It is also noteworthy that this universality does not depend on the total momentum transfer, which will instead affect the overall ratio value itself, as we can see from Figure 3.13. This is, though, easily understood: while the single phonon peak intensity is only affected by how the coupling changes along **k**, the two phonon peak is also affected by the total number of available couples, which becomes smaller with higher **q** - but apart from this, that can be considered as a scaling factor - the dependence from the coupling strength, energy and lifetime ratios is left unchanged.

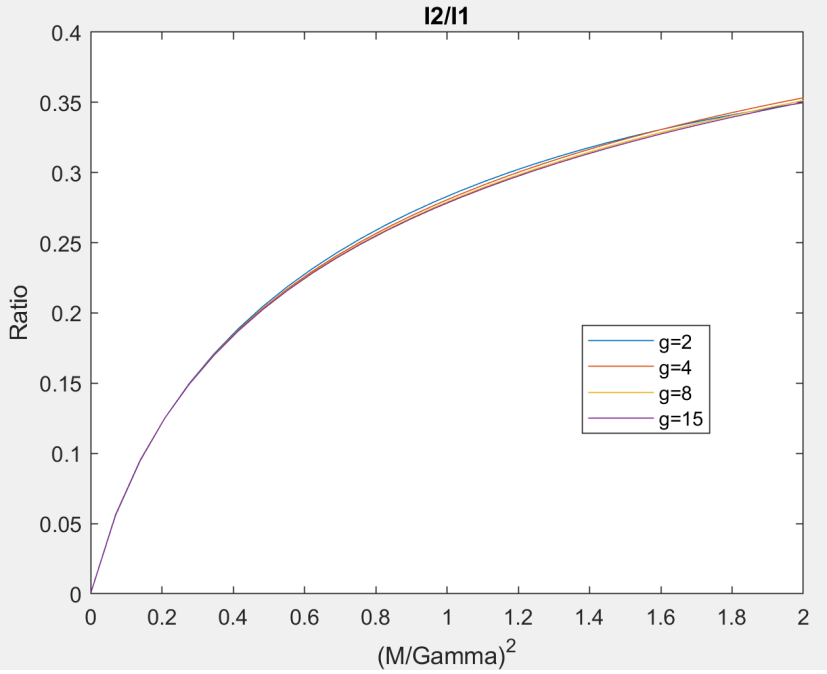

FIGURE 3.12: Here we have the ratio $\frac{I_2}{I_1}$ for different values of the parameter $g = (\frac{M}{\omega})^2$. As we have said, it is found to be universal - here we have plotted four possible values of g. We have used $N_k = 100$ and $\mathbf{q} = 0$

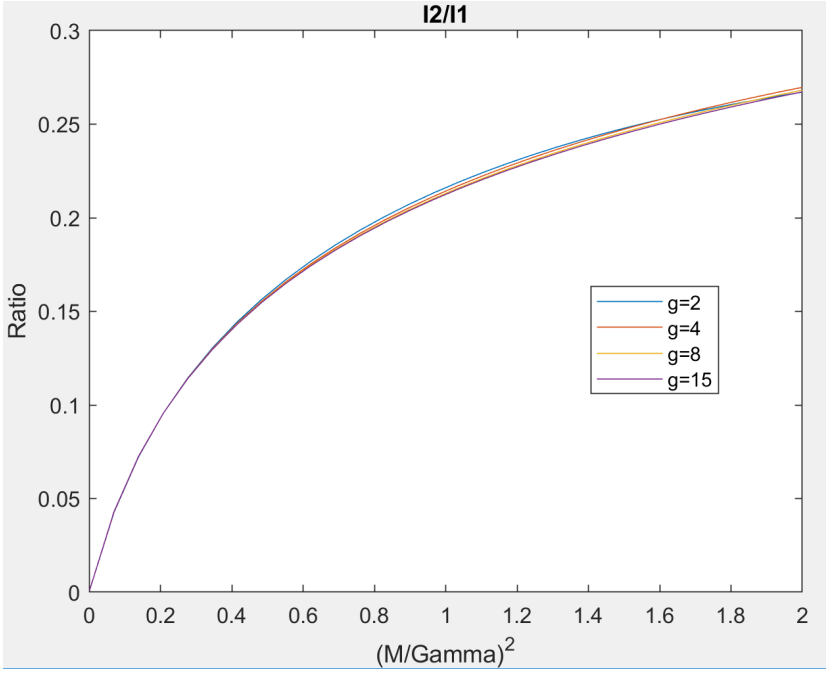

FIGURE 3.13: Here we have the same plotting of Figure 3.12, but in this case we have used $\mathbf{q} = \frac{\pi}{2}$. As it is discussed in the text, the double phonon peak intensity is smaller than at $\mathbf{q} = 0$.

- **Systematic study of the ratio between one phonon and two phonons peaks intensity** One last interesting thing that we can do is to deal with a systematic study of the ratio $\frac{I_2}{I_1}$ (one of the good parameter to study through our calculations, see (3.3.3)) along different shapes of coupling and dispersions, and for different choices of the parameter Γ. This can be thought as a sort of generalization of what we have done in the previous point.
  In particular, before extracting some general result, we can immediately recognize how those situations in which the two phonon peak is bigger than the single one are non-physical, in the sense that we always expect the overall cross-section of a second order event to be smaller than the one of a first order one; we thus discard the parameters choice which leads to such a situation.
  This study has been very useful in order to understand which coupling can be considered realistic. More considerations about the effective coupling will follow in section 3.5.2 - for now it is enough to say that the difficulties arise from the definition (3.6), which prevent us, due to its intrinsic complexity, from having a closed and tractable expression for the electron-phonon coupling.

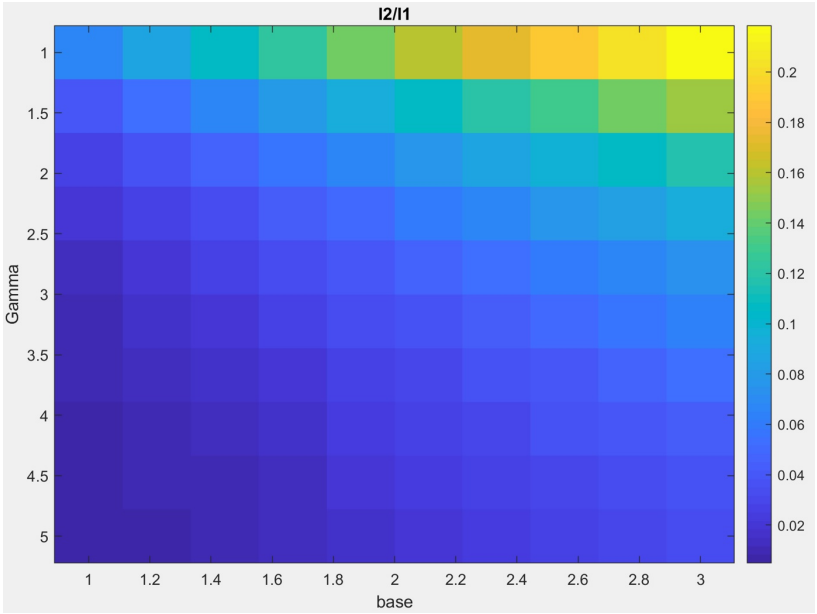

FIGURE 3.14: In this simulation, we have supposed a dispersion relation in the form $\omega(\mathbf{k}) = 1 - 0.2\cos(\mathbf{k})$, and a coupling $M(\mathbf{k}) = base \cdot e^{-\frac{2}{\pi}|k|}$. *base* is a generic name which we gave to the paramater enhance the whole function. This parameter is thus responsible for the variation (in an overall strength sense) of the coupling - the bigger is, the bigger the coupling. Γ, as we have already said, is the energy broadening due to the short lifetime of the intermediate state. Here we have supposed a null total momentum transfer. We can notice how the two phonons peak is enhanced by a long lifetime of the intermediate state ($\Gamma = 1$) and a strong coupling. We can imagine that every point of this surface is associated to a spectrum like the one in FIgure 3.8.

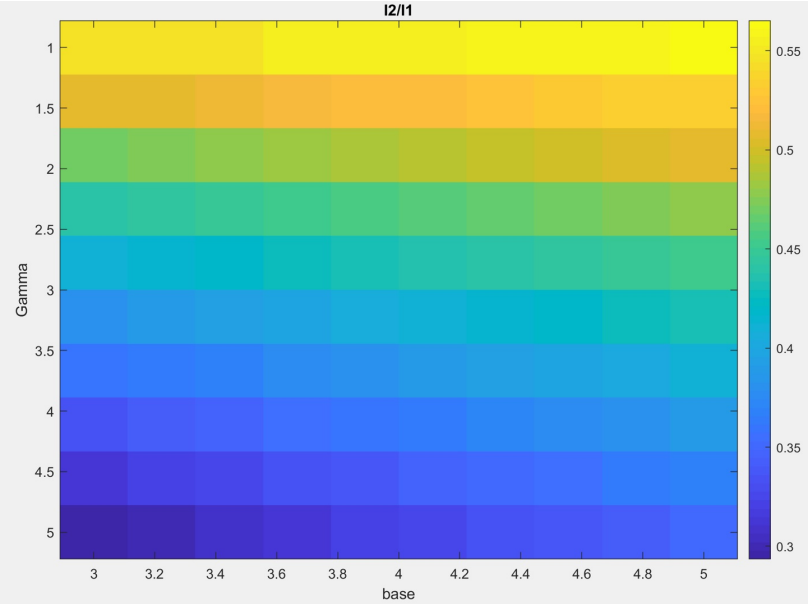

FIGURE 3.15: Here we have supposed a dispersion relation in the form $\omega(\mathbf{k}) = 1 - 0.2\cos(\mathbf{k})$, as before , and a coupling $M(\mathbf{k}) = \sqrt{2}|\sin(\mathbf{k})| + base$. Again, *base* has the same meaning of Figure 3.14, and so will be for the next Figures. We can see that this choice of parameters greatly enhance the two phonon peak. Here we supposed, again, a null total momentum transfer.

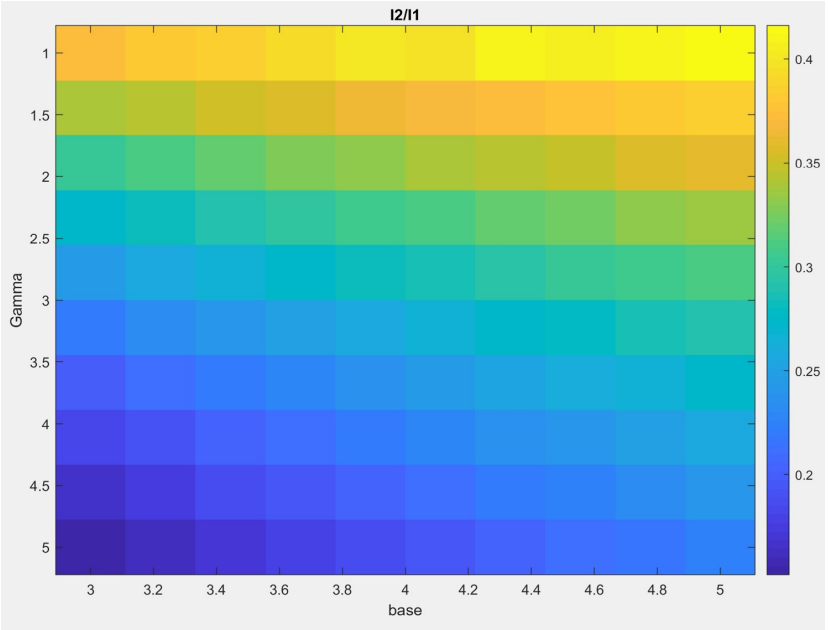

FIGURE 3.16: In this simulation we used the same parameters of Figure 3.15, but this time we supposed a total momentum transfer $\mathbf{q} = \frac{\pi}{2}$. Paying attention to the scale, we can immediately notice that the ratio is smaller, for every combination of Γ and *base*. Otherwise, the dependence of the ratio from the parameters is left substantially unchanged.

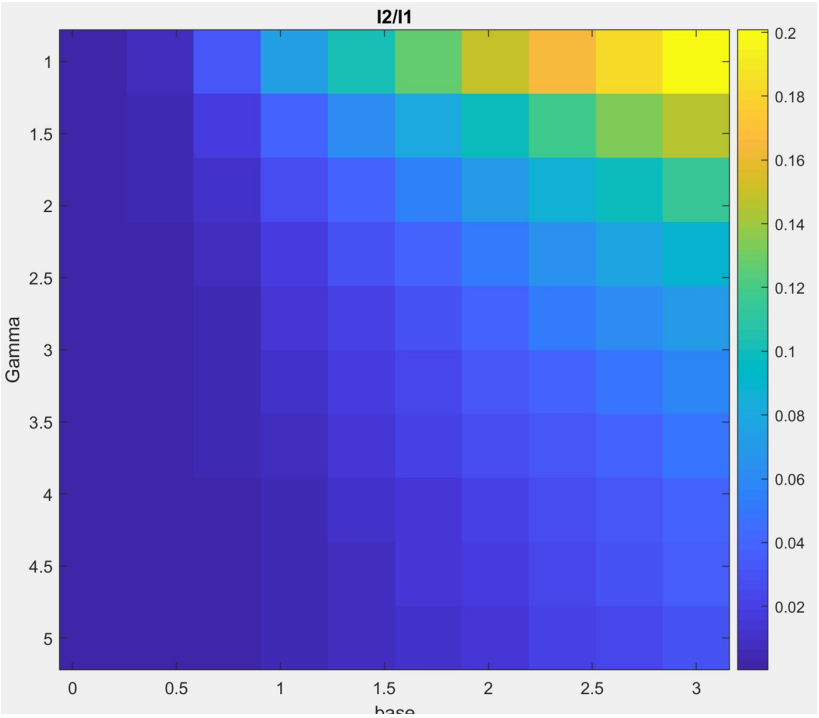

FIGURE 3.17: In this example we have considered the same dispersion relation of the previous figures, but with a coupling $M(\mathbf{k}) = base \cdot \sin(\mathbf{k})$. In order to be have a single phonon peak, we also needed to consider $\mathbf{q} = \frac{pi}{2}$, since for $\mathbf{k} = 0$ the coupling is null. What we can see is that a pure sinusoidal coupling (without any constant component, like in Figure 3.13) drastically reduces the overall two phonons peak intensity, all over the parameters range.

3.5 2D

Now we make a step further, and we proceed in bringing our calculations in a two dimensional environment. Conceptually, this is not very challenging - it is just a question of accounting for a bi dimensional Brillouin zone instead of a mono dimensional one - but still it is much more interesting than the one dimensional case, mainly because the cuprates, which we are investigating along this thesis, are "quasi 2D materials" [11] (see Chapter 1). This follows from the fact that the relevant physics is played in the CuO_2 plane, and the coupling between different planes is, in first approximation, negligible.
We can thus think that also the relevant phonon physic take place in the CuO_2 plane, and our two dimensional calculations have some hope to catch some insight of the real experimental results.
Our main limitations, throughout the whole work, is that we consider only one branch of phonons, which can be thought of - we will see this in Chapter 4 - as a justifiable assumption, especially if we are not interested in very low energetic excitations (indicatively phonons mode with energy below 40 meV).
More specifically, we will only consider the breathing mode [36].

3.5.1 Programming

Again, the whole code is found in appendix B. Nothing has really to be added from the one dimensional case. Now both $\mathbf{k}$ and $\mathbf{q}$ are vectors, and so we will have their component along both the axis - our functions will in general need to accept one more parameter. The complexity arise when we are looking for the possible couples and triplets (the program, by the time i am writing this thesis, still misses the part dedicated to the counting of triplets). Their number will grow quadratically (for the couples, coherently with what we said in Section 3.3.2) and there will be one dedicated function which will find them ("Contare"). The number N_k will indicate the number of wavevectors considered along a direction, which means that the effective number of wave vectors in the first Brillouin zone will be N_k^2.
We will call the two dimensions, intuitively, x and y.
The output of the program will be conceptually the same as shown in Figure 3.4 - the phononic part of a RIXS spectrum.

3.5.2 Theoretic Considerations About Coupling

But at this point we are also interested in a definitive form for our coupling, touse in our 2D calculations. In the previous sections we have run some simulations in order to understand how our RIXS spectrum would change on the basis of different couplings, but the overall dependence is not very strong and we cannot prefer one coupling to another relying only on those considerations.
We have basically two different approaches, one from [22], which consider

a localized electron during the RIXS intermediate state, and one from [37], where the electron is considered as itinerant.
In the first approach, the excited electron is considered to be bond to the core hole (which happens to be a very good approximation at Cu L-edge [38]). This means that the electron-phonon Hamiltonian is localized at R_i, and it follows the discussion which brought us to (3.6).
The second approach considers the photo-excited electron as promoted into conduction band, and assumes that the most interesting phonons are coupled to mobile charges - i.e. valence electrons.
We are interested, for the moment, only in the most energetic branch, which is the breathing mode [34][39]. The breathing mode is an acoustic branch which embodies the dispersion relation of the in plane oxygen atoms, oscillating in a direction parallel to the their bonding with Cu atoms. In general, we can say that oxygen modes are more energetic than the modes related to Cu oscillations, since Cu atoms are much heavier. Another interesting mode, the second most energetic, is the buckling - again, it is an oxygen mode, but this time the in plane oxygens oscillations are found in a direction perpendicular to their bounding with Cu atoms.
The first approach, as we said, which is conceptually simpler and also more adequate in the case of Cu L edge (in particular in case of charge transfer insulators, parents compounds of high T_c materials, where a single ion model is a suitable model, see [11]), leads to (3.16). Unfortunately, such an expression is not useful - its intrinsic complexity prevent us from obtaining an adequate function. The potential appearing in (3.16) is the potential function for the electrons when the atoms are in their equilibrium positions, which form a periodic potential in the crystal [33]. It is problematic: the use of a pseudo potential is smost of the time adopted (always [33]), since a naive bare ion potential would lead to a divergence behaviour of the coupling in case of $\mathbf{q} = 0$ for both the optical and the acoustic branches. We preferred not to follow such a path.
The second approach, instead, offers a simple and clear formula for the coupling of the breathing mode to our intermediate state - we will follow this approach from now on. The formula for the coupling also happens to be independent from the electron momentum - or better, it results to be weakly dependent (remember that this model is relying on itinerant electrons), and we have a pre factor that can be setted to a constant solely to have an overall magnitude estimation ([40], relying on calculations made in [37]). Once this approximation is done, the important thing is the shape of this coupling - which can also be used in our single ion L Cu picture, at least as a first order approximation:

$$M_{br}(\mathbf{k}) = [\frac{g^o_{br}}{2}\sqrt{\sin^2(k_x) + \sin^2(k_y)}]^2 \tag{3.36}$$

Where g^o_{br}=87 meV. The first thing to notice is that the coupling grows in different ways as we move along different directions of the Brillouin zone. Thus it will be interesting to study the beahvior of the single phonon and two phonons peak along the directions $[0, \pi]$ and $[\pi, \pi]$.

Also, we notice how the coupling is null for $\mathbf{k} = 0$. This means that, for a null total momentum transfer, we will not have any single phonon peak.
If we had considered also the buckling mode, we would have found a coupling to the electron which goes as $\cos(\mathbf{k})$, and thus in an opposite fashion with respect to the breathing mode coupling: stronger at the center of the zone and weaker at the edges.
The dispersion that we are going to use is given, for the breathing mode, in [40]:

$$\omega(\mathbf{k}) = \Omega_{br}[1 - 0.18\sqrt{\sin^2(\frac{k_x}{2}) + \sin^2(\frac{k_y}{2})}] \tag{3.37}$$

Where Ω_{br}=85 meV. This will also fix the unit of energy in all the Figures from now on.

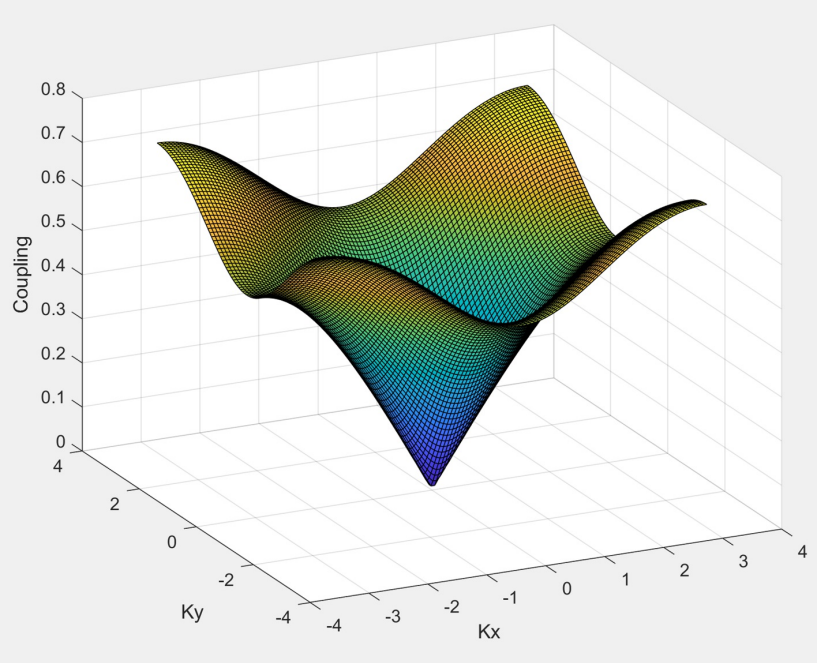

FIGURE 3.18: Breathing mode coupling intensity, according to (3.36), plotted over the first Brillouin zone. As it is easily seen, the phonon coupling is enhanced as we move towards the edges of the Brillouin zone, and more in particular is enhanced moving along the direction $[\pi, \pi]$.

3.5.3 Results And Comments

We are now going to study the intensity of the peaks in the directions $[0, \pi]$ and $[\pi, \pi]$: all the other high symmetry directions are equivalent, for the high symmetry of our model (here the symmetry is given by the coupling, but it is the same of an effective CuO_2 plane).
Still, since for small $\mathbf{q}$ we have two phonon peak with a greater intensity than the single phonon peak, we would like to check that this behaviour is not divergent - and thus that the intensity of the three phonons peak is smaller than

the one of the two phonons peak. We check this in one dimension (the important thing is to exclude a pathological behaviour of the coupling), and what we obtain in Figure 3.19 empathizes the good behaviour of our calculations.

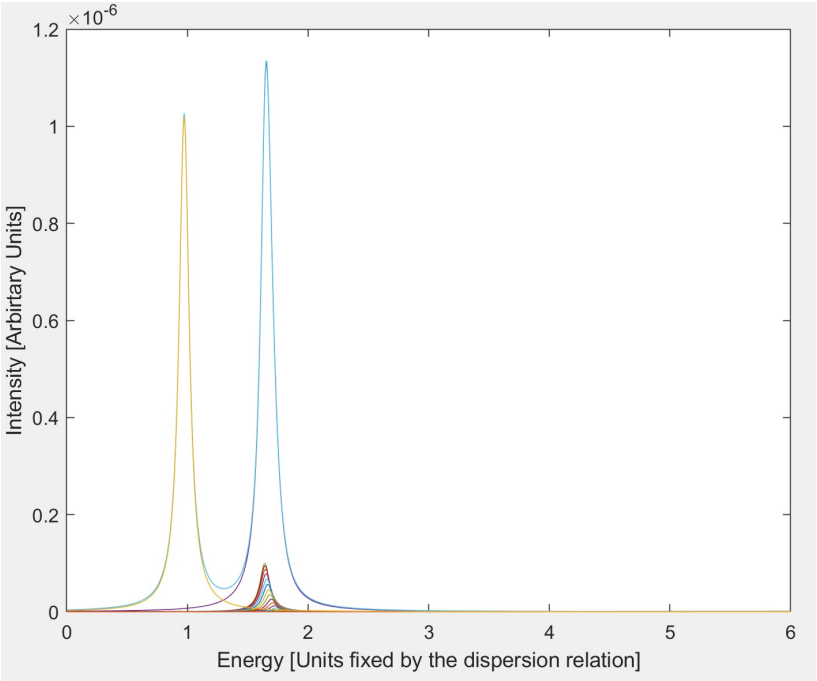

FIGURE 3.19: Here we have the results for a simulation in 1D where we have used the coupling choosen with (3.36). We used $\Gamma = 5$, $N_k = 50$ and $\mathbf{q} = 0.3$. The three phonon peak is too small to be seen, but it is present. This means that, even if the two phonon peak is bigger than the single phonon peak, the behaviour of our model is not divergent, and the two phonon event is really the biggest contribution to the phononic RIXS cross section.

Moreover, we have to keep in mind that the comparision between the intensities along $[0, \pi]$ and $[\pi, \pi]$, in order to be interesting, must be done at the same distance from the centre of the Brillouin zone - which is to say that we have to consider a factor $\sqrt{2}$ between the components of $\mathbf{q}$ projected along $[0, \pi]$ and those projected along $[\pi, \pi]$.
We are going to focus primarily on the proximity of the centre of the Brillouin zone (Figure 3.20: we will restrict our investigation to about a quarter of the first Brillouin zone), and then we will look at the whole zone (Figure 3.21). This is needed because the two phonon peak intensity, at the edge of the Brillouin zone, results to be at least one order of magnitude larger than the the two phonons peak one. Anyway, as said in Chapter 2, the edges of the first Brillouin zone are not accessible through RIXS investigation.
In Figure 3.22, 3.23 we have a comparison between the intensities of the peaks along different directions. In Figure 3.24, the ratio between the intensity of the single phonon peak and the double phonon peak as a function of the total momentum transferred is plotted for different values of the parameter Γ - the energy spread of the intermediate state due to its finite lifetime. The result

that we find is that the bigger is Γ (and thus the smaller is the lifetime of the intermediate state), the closer to the centre of the zone is the point where the single phonon and the double phonon peak have the same intensity. This is another way to say that the possibility to excite two phonons is somehow related to the lifetime of the intermediate state - and it is reduced for short lifetimes. But this are concept on which we will return in Chapter 4, and that we expressed breafly in the previous Chapters.

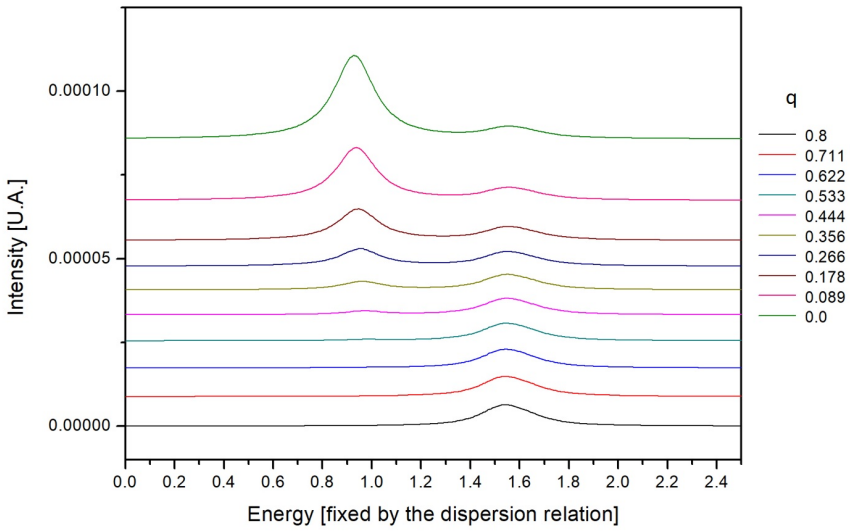

FIGURE 3.20: Here we have a stack plot with the results of the simulations made at different total momentum transfer: we are thus moving in the Brillouin zone, and in particular along $[\pi, \pi]$. When we set $\mathbf{q}$, we imply $k_x = \frac{|\mathbf{q}|}{\sqrt{2}}$ and $k_y = \frac{|\mathbf{q}|}{\sqrt{2}}$. What we can notice is pretty striking: due to the form of the coupling, the single phonon peak is suppressed near the centre. Still, here we can found a non null two phonon peak, which will also show a little dispersion, accordingly to (3.37).

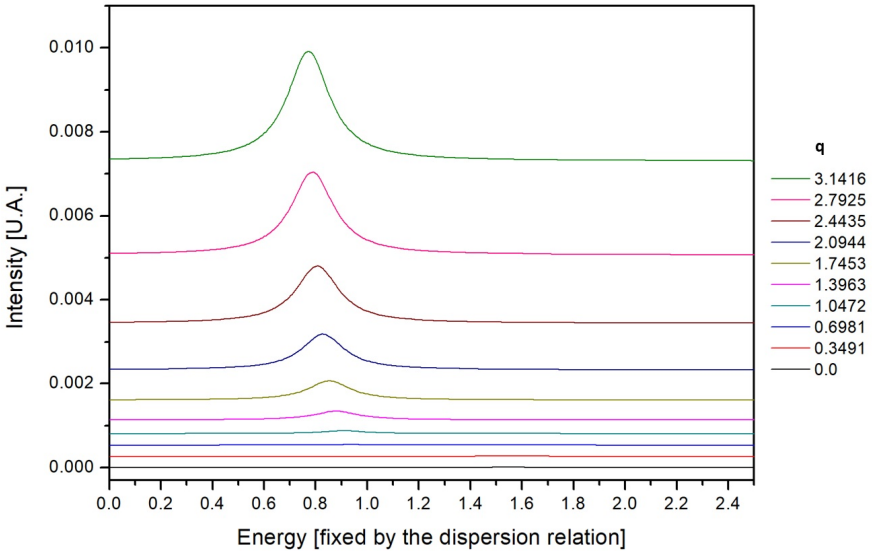

FIGURE 3.21: This can be thought as a prolongation of Figure 3.18, again along $[\pi, \pi]$ and with the same value of **q**. The magnitude of the single phonon peak near the edge of the zone is too big to be comparable with the intensities of the peak near the centre of the zone.

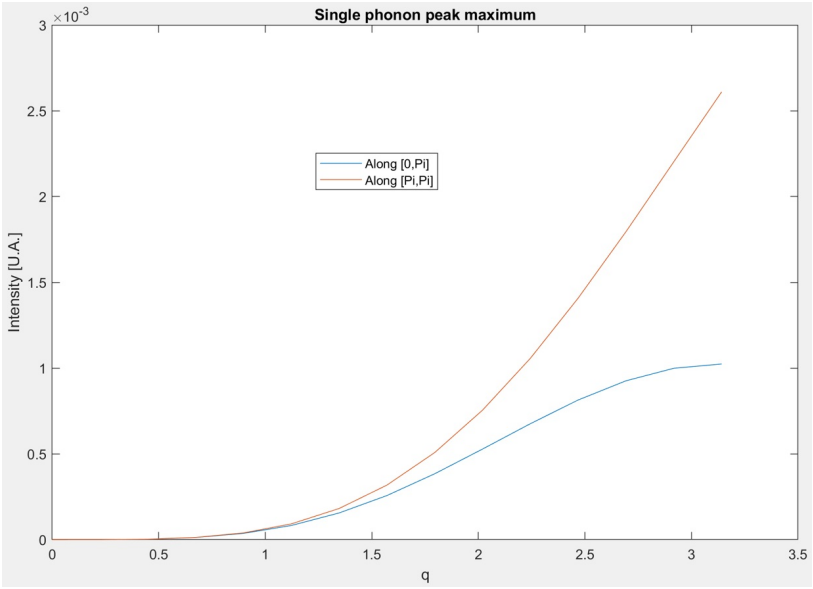

FIGURE 3.22: here we are plotting the intensities of the single phonon peak (once again intended as its total area), calculated along different directions. The total momentum transferred refers to its modulus, as specified in Figure 3.18. The peak along $[\pi, \pi]$ is bigger, because the coupling is here stronger - there is nothing surprising in this result. Still, what we can notice is that in the portion of the Brillouin zone interested by the RIXS investigation (see Chapter 2) the difference in intensity between the two directions is, at least in a first approximation, negligible.

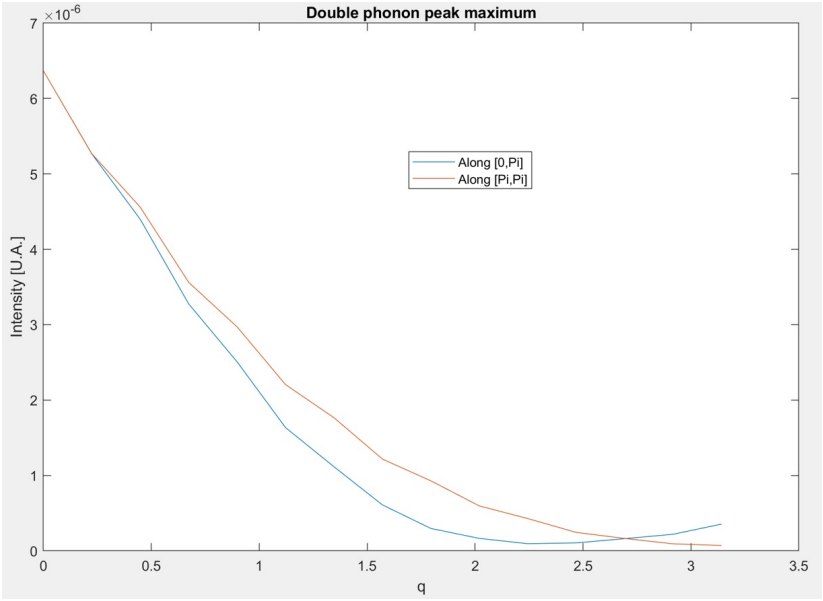

FIGURE 3.23: In this case the intensities are comparable all over the Brillouin zone. The peak along the direction $[\pi, \pi]$ is in general stronger than the one along $[0, \pi]$, but we have two peculiarities: the first one is that the general trend of the intensity to became smaller for higher $\mathbf{q}$ is inverted near the edge of the Brillouin zone along the direction $[0, \pi]$ (and we can have an intuitive understanding of this - the fewer number of couples accessible is compensated by the greater coupling), while the second one is that for high transferred momentum we also have that the peak along $[0, \pi]$ is more intense than the one along $[\pi, \pi]$.

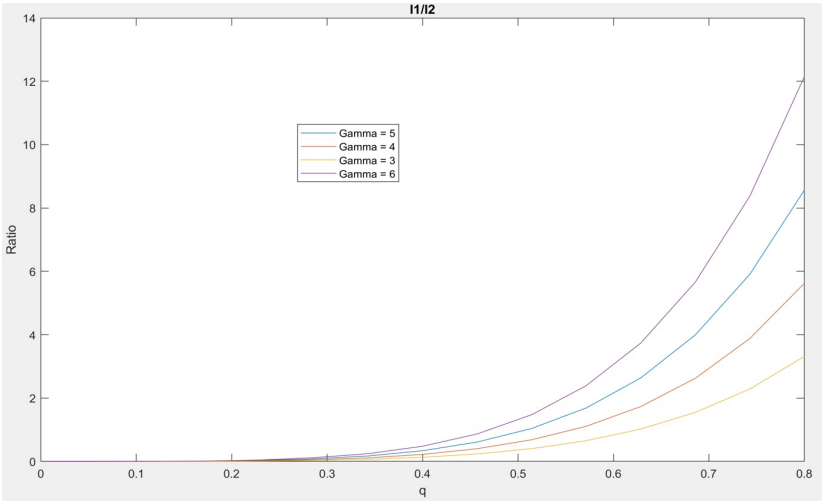

FIGURE 3.24: Here we have plotted the ratio between the intensities of the single and the double phonon peak, along the direction $[0, \pi]$, for different values of the parameter Γ. The point at which the intensities of the single and the double phonon peak are equal ($\frac{I_1}{I_2} = 1$) is found to be closer to the center of the Brillouine zone for bigger values of Γ.

Chapter 4

Experimental Results Analysis

4.1 Experiment Description

As we said, we realized our experiment at beamline ID32 at ESRF [31]. We had in total 96 hours of beam time.

FIGURE 4.1: In this Figure we can see the sample holder preparation. From the top to the bottom, we have La_2CuO_4 with $T_c = 22K$, La_2CuO_4 antiferromagnetic - and thus insulating - and again La_2CuO_4, but with a non measurable resistance, thinner than the others and endued with a larger Rocking Curve (Rocking Curve analysis reveals the broadening of the diffraction peaks - which is a way to evaluate the quality of the sample, see Section 2.3).

Once we have prepared the samples, we proceed to the alignment of the beamline, which is carried out by the local scientists. This operation allows the reach of optimal resolution and energy calibration (since we are using a CCD detector, we need to have a $\frac{meV}{pixels}$ ratio conversion in order to read the results data of our experiments).

In order to do this, the elastic diffused photons from a carbon taped are used - its spreading in energy is a measure of the actual resolution. We found a conversion ratio of $18.182 \frac{meV}{pixel}$ and a FWHM (full width at half maximum) of the elastic peak (the broadening due to finite resolution is in a preponderantly gaussian shape) of 1.97, which sets our resolution to 35 meV (see Figure 4.2).

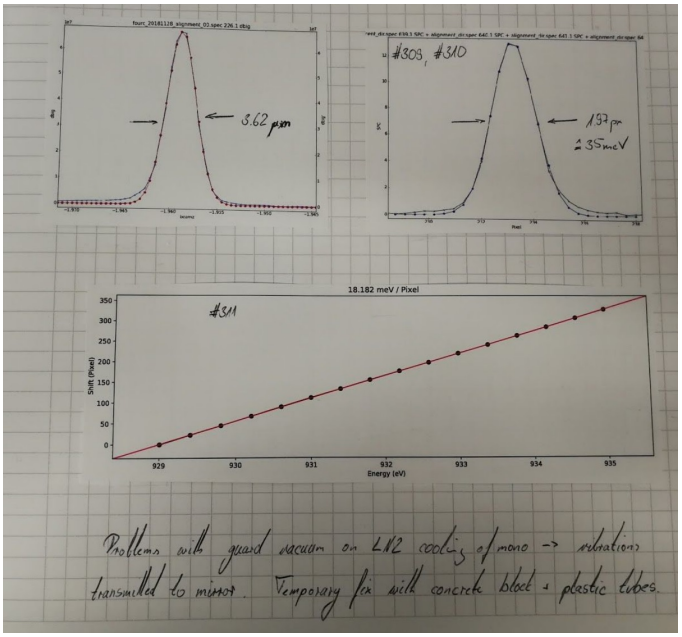

FIGURE 4.2: Picture of the beamline logbook, in which the final resolution and conversion rate are shown.

Eventually, we cool down our sample to 20 K, and we start with the angles offset measurement (see Section 2.3). Each sample will be characterized by its position and its offset angles (which are different for each sampels, since they are dependent on the sample).
We also take a XAS measure, in order to observe the resonance edges and adjust the photon energy at the exact resonance edge (or, if we want to do a detuning measurement, to know exactly at which detuning we are operating). More in general, taking a XAS before any measure is a good practice if we think that the beamline could not be stable in energy calibration.
Before any measure, moreover, we also collect an image of twenty second of the specular reflection (a Bragg reflection generated by a plane [0,0,N], where, adopting r.l.u. units, N is an integer), in order to have a reference for the energy resolution, which could have maybe changed since the calibration.
As we said many times along the thesis, a collection of a typical RIXS spectrum requires a quite long time, due to its intrinsically small cross section. The time required is even higher if we are working at detuning, where the cross section is smaller (see next Section). Of course, the time required will also depend on the site where the experiment is taking place - and thus on the brilliance of the synchrotron radiation source - and on the quality of the spectrum that we want to obtain. The higher is the acquisition time, the higher

the accumulated counting rate, and thus the better our statistic - in the sense that the overall real signal will emerge from the statistical noise, which is naturally always present. More in detail, we can not just collect a long image (where with image we intend the signal collect by the CCD detector) - for a technical reason related to the double photons event, we must collect an adequate number of images with relatively small acquisition time, and sum them together in a second moment [11].
At resonance, for example, as we move through the Brillouin zone, during the experiment we choose to obtain a spectrum as the sum of sixty images, each one realized with a two minute acquisition time. This means that for every spectrum we need a total acquisition time of two hours - and for detuning they will require even more. We thus chose, when dealing with detuning spectrum, to accept more noisy results in order to low the needed acquisition time.
Overall we collected different spectra for the antiferromagnetic samples (the middle one in figure 4.1) along the direction $[\pi, \pi]$ and $[\pi, 0]$ and the detuned ones in the point $[0.4, 0]$ (in r.l.u.). We are gonna to study all those spectra in the Section 4.3.
We can choose the polarization (σ or π, see Section 2.3) of the incoming photons, but it is not an information that we are going to use during our investigation (it is only relevant for the XAS spectrum analysis).
We also collected spectrum for the underdoped samples, but they are not going to be studied along this thesis.

4.2 Theory and Approximations

The main idea behind our experiments at the beamline ID32 at ESRF was to probe the electron phonon coupling. This can be done, theoretically, through a study of the dependence of the phonon intensity from the detuning. What we generally expect from a detuning (a situation in which the energy of the incoming photon will be slightly different from the resonant peak) is a general reduction of the intensity of the RIXS spectrum. From the formula (2.12), and rewriting the denominator as $z = h\omega_{\mathbf{k}_{in}} - E_{res} + i\Gamma$ (as we have done in (3.12), the meaning of each symbol can be found in Chapter 3) we can clearly see that a detuning different from zero (in which case we would find $z = i\Gamma$) means to increase the denominator of the overall cross section.
But when we are talking about phononic RIXS cross section (3.16), we also notice a new term in the denominator of the overall cross section - g, which we already defined as $(\frac{M}{\omega})^2$. This term does not show up in magnons or *dd* orbital excitations (see [11]), but it is what allow us to extract the parameter g from the intensity decay of phonons excitations as a function of detuning (as we will see in a moment).
We can think of this as a consequence of phononic RIXS being an *indirect* event (see Chapter 2). Magnon or *dd* excitations are products of the final state of the RIXS process (they are perturbation introduced in the system by the final state of the electron), while phonons are created in the intermediate state. Even if, as we have seen in Chapter 2, in a first approximation phonons

only slightly modify the electron state (and in fact we consider two dipole transitions as to and from the same intermediate state), we notice that the dynamic of the intermediate state somehow (more specifically, by virtue of the canonical transformation (3.11)) enters the cross section calculation through the number of phonons generated in it (see (3.12) or (3.16)):

$$\frac{d^2\sigma}{d\omega d\Omega} \propto \sum_f |F_{fg}|^2 \delta(\omega - n'\omega_0) = \\ = NT^2 \sum_{n'=0}^{\infty} | \sum_{n=0}^{n'} \frac{B_{n'n}(g)B_{n0}(g)}{z + (g-n)\omega_0} + \sum_{n=n'+1}^{\infty} \frac{B_{nn'}(g)B_{n0}(g)}{z + (g-n)\omega_0} |^2 \delta(\omega - n'\omega_0) \tag{4.1}$$

To consider a non zero detuning means to, in a very naive and intuitive picture, to consider an shorter lifetime of the intermediate state, and we can think at the lifetime of the intermediate state as to a factor which enhances the cross section for a phonon creation - the shorter the lifetime, the smaller the cross section; and this proportionality passes through the coupling strength, since, as we have seen in Chapter 3, only the relative magnitude of those parameters matter, and not their absolute value (this is not true, for example, in the case of magnons: in that case the overall cross section is only reduced by the fact that the absorption of the photon itself is less probable).
Rigorously, thought, things are not so easy and intuitive, since to reach an excited state through a photon which is not exactly tuned to the resonance energy does not associate a shorter lifetime of the intermediate state - still, it means to change its property ([35] [41]), and thus to affect the phonon overall cross section in a more complex way than in magnons or dd orbital excitations case. If everything could be explained through an "effective lifetime", then we could enclose both the intermediate state (Γ) and the detuning (Ω) into an unique parameter: the "effective lifetime" would be given by Γ added, through a certain constant of proportionality, to Ω.
But in Figure 4.3 is evident how this cannot be done - Γ and Ω must be regarded as independent factors.

So: in the case of phonons the intensity detuning dependence is dictated not only from the photon absorption probabilities, but also from the properties of the intermediate state, which are altered by the detuning. And this dependence, as we see from (3.16) and more clearly in Figure 4.3, pass through g.
In a very practical way: what we obtain is that the detuning dependence of the single phonon feature will depend on g - the smaller g, the fastest is the decay. Once we have obtained experimentally this dependence, we have a way to determine g.
The last thing that we have to notice is that we are considering the non dispersive phonons derivations (i.e. (3.16)), which is immediately reflected in the fact that we consider g and not $g(\mathbf{k})$. This is simply why, even if Chapter 3 of this thesis is dedicated to the study of the theoretical phononic RIXS

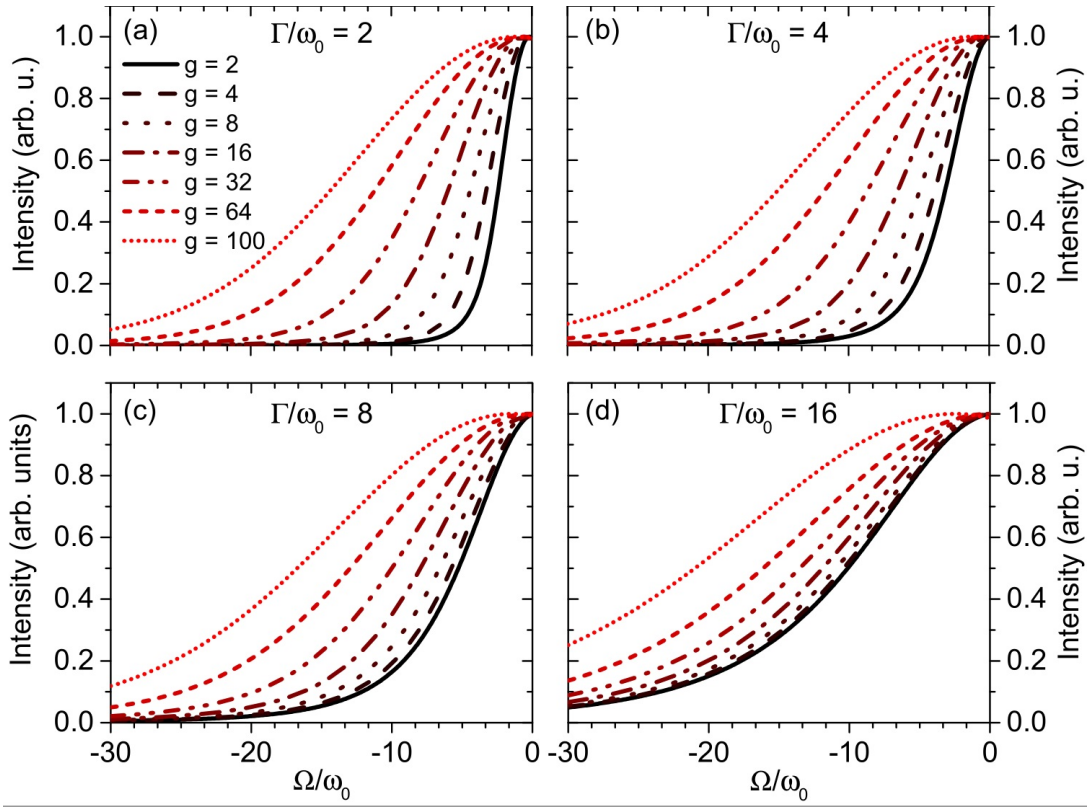

FIGURE 4.3: Here we have the dependence of the intensity of the single phonon peak as a function of the detuning (Ω), for different values of the intermediate state lifetime (Γ - for the L edge of Cu is in the scale of hundreds of meV) and, most importantly, of $g = (\frac{M}{\omega})^2$. Figure by Matteo Rossi.

spectra generated by the creation of dispersive phonons, the grasp on the non dispersive phonons theory is more solid. The main differences are that we do not have to consider the dependence of the coupling from the transferred momentum and that, in calculating the intensity of the double phononic peak, we do not have to account for all the possible couples - we do not have to search for all possible combinations such that $\mathbf{k}_1 + \mathbf{k}_2 = \mathbf{q}$. And of course those are also the major drawback of that approximation (as I have already written in Sections (3.2.1) and (3.2.2)): it means that we are considering only $\mathbf{q} = 0$, and that approximating a spectrum obtained with $\mathbf{q} \neq 0$ is, in principle, erroneous. But still, we will be interested only in single phonon peak intensity fall - the different dynamic of the double phonon peak will not concern us (for example, we do not account for the fact that the closer we are to the edge of the Brillouin zone, the fewer the couples of phonons available are, and we do not account for the different amplitude relative to each possible couple: in non dispersive calculations we are basically considering only one single couple, the one with $\mathbf{k}_1 = \mathbf{k}_2 = 0$).
We will consider the results obtained with non dispersive phonons calculations as a first order approximation ([22], again) - from them we can obtain the order of magnitude of the electron phonon coupling, while its shape can

be deduced (again, in first approximation) by the single phonon peak behaviour when we move along different directions in the Brillouin zone ($[\pi, \pi]$ or $[\pi, 0]$).

4.3 Data Analysis

As we said in Section 4.1, we want to study the spectra of the antiferromagnetic sample, and in particular the spectra obtained along the directions $[\pi, \pi]$ e $[\pi, 0]$ and the detuned spectra acquired at the fixed $[0.4, 0]$ position.
For what concerns the spectra obtained along the different directions of the Brillouin zone, what we are interested in is the behaviour of the coupling - i.e. is the coupling growing with a bigger transferred momentum? To have an answer, we just look and the intensities of the phonon peak along those directions (as we said in Section 4.2, we only look at single phonon peak - also because the double phonon peak is suppressed by the noise).
From the detuning, instead, we want to obtain an estimate of the absolute strength of that coupling. Thus what we are really interested in is the ratio at which the intensity decay happens (again, see Figure 4.3).
All the spectra that are showed in this pages are corrected for self-absorption (the self absoprtion correction is different in case of crossed or not crossed polarization) and are normalized to the sample current.
The experimental spectra are showed in Figure 4.4, 4.5, 4.6, 4.7, 4.8.
As we can immediately notice, we have some noisy spectrum in the phonons' region for detuned spectra, and in particular for the spectra with a detuning between 0.05 eV and 0.20 eV (see Figure 4.8). As we said, we accepted to have less statistic on the detuned spectra (a smaller acquisition time), in order to collect more data and have more informations.

Once we have our spectra, we proceed with the fitting. The main idea is that we know which features we expect to find in our spectra (2.1.3), and which shape they should have. What we do not know is their intensities. We thus fit those features with their expected characteristic shapes, leaving the intensity as a parameter to be fitted. The best fitting, which is the one which once subtracted to the experimental spectrum leaves the smaller - and ideally only noisy - intensity, is the more realistic. The intensities associated to the best fitting can be considered as the real intensities of the features.
In Figure 4.9 we have an example of a fitted spectra.

The features that we have fitted are:

- **Elastic Peak**: we assumed a Gaussian shape:

$$I(E) = A \cdot e^{-\frac{4\log(2)(E-E_0)^2}{\sigma}} \tag{4.2}$$

  Here σ is the full width half maximum. In the case of the elastic peak, it is our resolution - and for every measurement we take we also collect the specular reflection, with the purpose to measure it. In all our

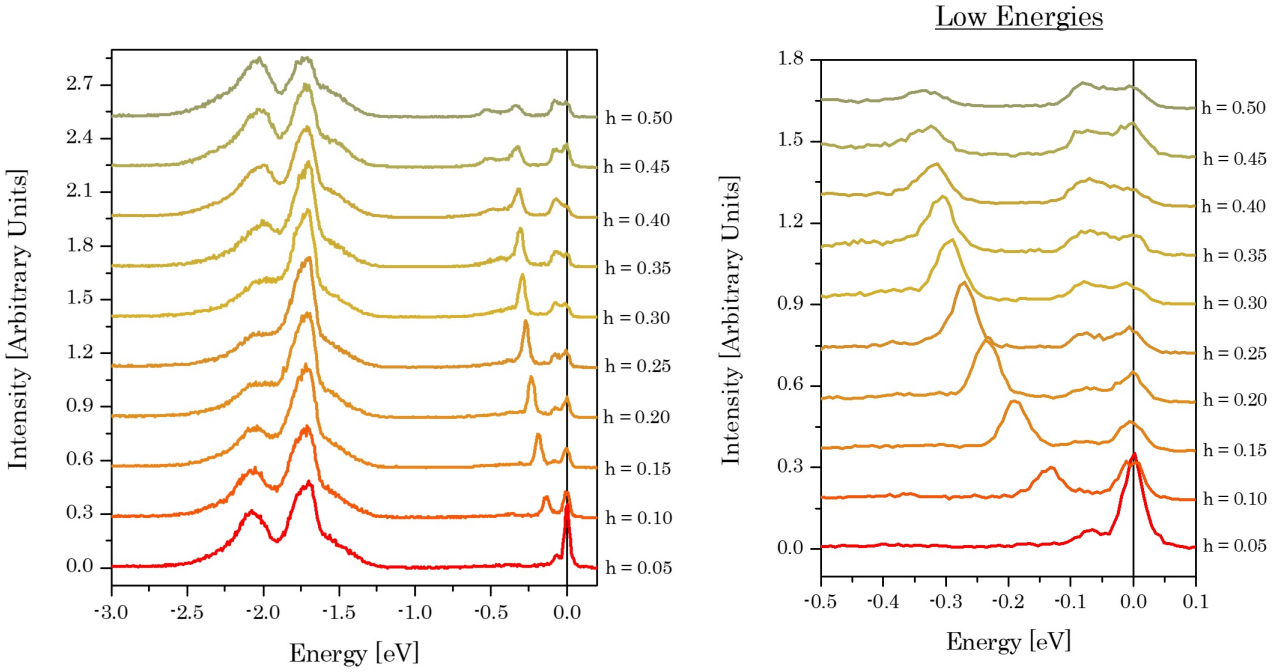

FIGURE 4.4: Stack plot along the direction $[\pi, 0]$, for the antiferromagnetic LCO. On the left we have the full spectra, while on the right we have a zoom on the low energies scale, where the magnon dispersion is clearly visible.

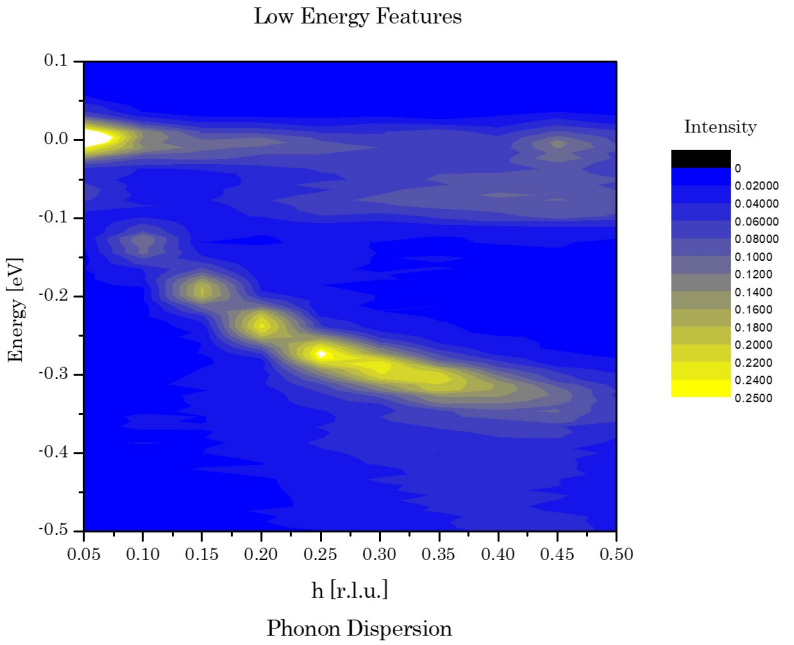

FIGURE 4.5: The same data as in figure 4.4, but plotted through a color map. The magnon dispersion relation is even more evident. We can also notice how the phonons (approximately identified by the intensity between 0 and 100 meV) seem to grow approaching higher values of the transferred momentum.

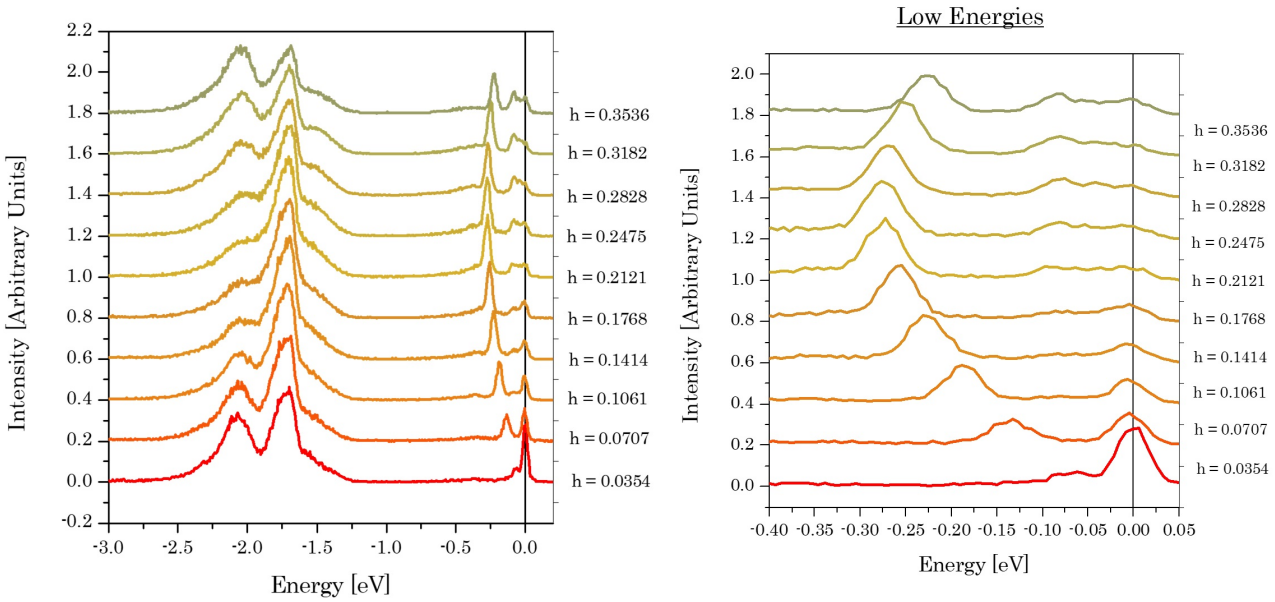

FIGURE 4.6: Stack plot along the direction $[\pi, \pi]$, again for the antiferromagnetic LCO. The associate total transferred momentum is $\mathbf{q} = [h, h]$. Here is interesting to notice, among the other features, the dispersion of the magnon: moving along this direction we cross the magnetic Brillouin zone.

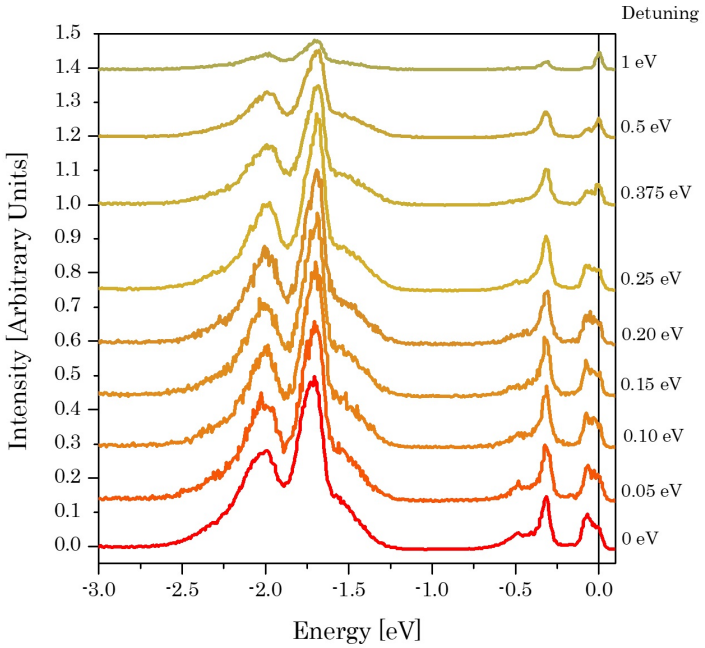

FIGURE 4.7: All the spectra are collected in the point $[0.4, 0]$ (r.l.u.). The overall effect of the detuning is striking - the intensity of the spectrum drops with greater detuning for all the features, since the cross-section itself is reduced.

fitting, we use a resolution which is an average (with an insignificant variance) of the resolution at which the different spectra were acquired. It is in general worse than the one found during the initial calibration

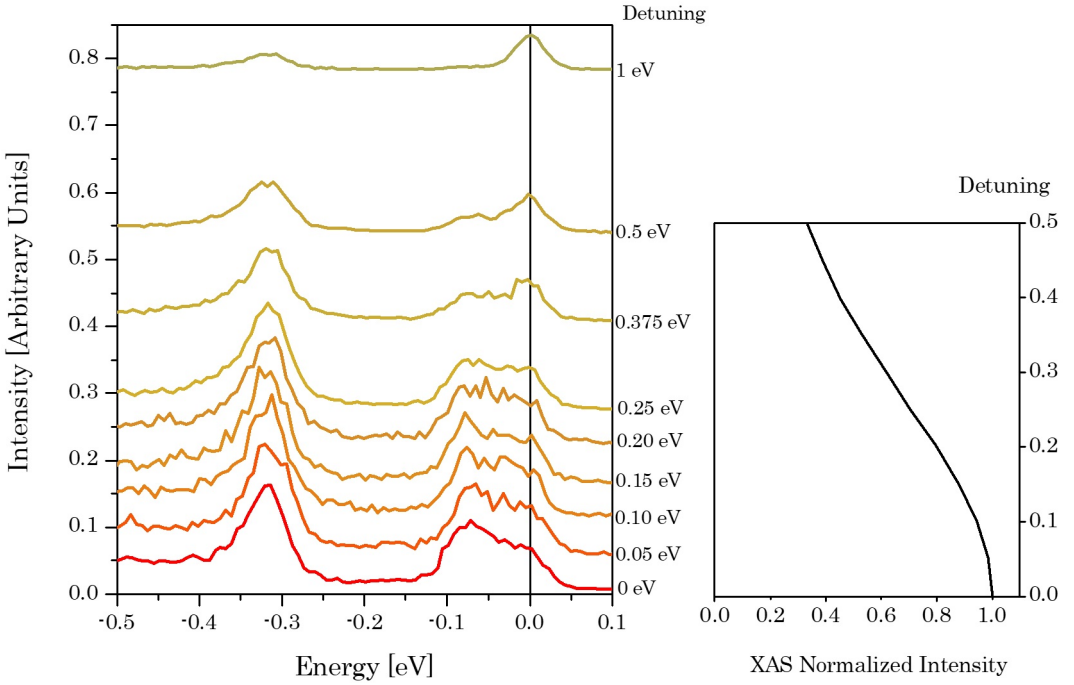

FIGURE 4.8: Low Energy scale of Figure 4.7. Here we also plotted the XAS absorption normalized to the resonance value, for comparison (see Section 4.2).

procedure: it is around 41 meV. The parameter E_o fix the position of the peak in the spectrum. We expect, of course, to find the elastic peak at 0 meV, but sometimes a small displacement (in the order of units of meV) is found.
Eventually, A is what really fixes the intensity. Once we fix σ, the area of the cure only depends on it.

- **Phonons**: concerning the phononic part of the spectra, we choose to fit it with two phonons peaks - one at high energy and one at low energy. The phonon with the higher energy peak, which we systematically place between 75 meV and 85 meV, can be thought as to be really associated to the highest phononic mode (and thus the breathing optical mode, [36]).
But for the low energy phononic peak (which we place between 35 meV and 45 meV) such a naive picture is not adequate. In fact, we cannot ignore that in this range of energy we have an high density of phononic modes. We must think at this phononic peak as a peak in which the overall intensity is the result of the contributions of many phononic modes of low energy (the energetically lower phononic modes, associated to the copper modes, cannot be distinguished from the ealstic contribution to the spectrum) - and those are mainly buckling modes. In principle, moreover, we should account for the fact that every phononic mode is endued with its particular coupling (in (3.17) we have already suppressed the branch index, but it is always meant to be present).

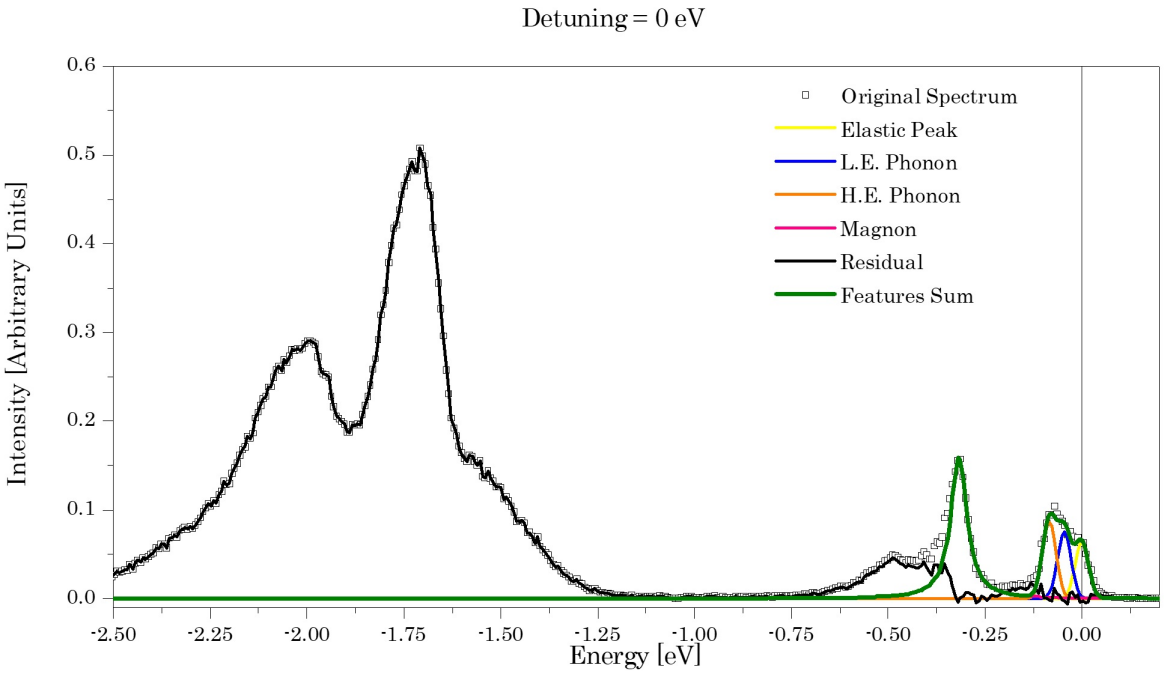

FIGURE 4.9: Example of fitted spectra. In particular, this is the first spectrum of Figure 4.8. An important track is given by the residual, especially in the low energy region - if its mean value is different from zero (as it is supposed to be for the noise) then we are probably leaving an excitation unfitted. In this case, as in all the fitting made in this thesis, the non-noisy residual at around 120 meV can be attributed to the double and triple phonons events - which, as we said in Section 4.2, we decided not to consider.

Still, we once again rely on the fact that what we are doing is a reasonable zero order approximation - we are looking for the *general* behaviour of the phononic coupling, and the intensity dependence of this low energy phononic peak from the total transferred momentum is an indicator of the average coupling dependence along those middle energy modes.
In principle the energy broadening of the phononic excitations should follow a Lorentzian shape, since it is due to the finite lifetime of the excited state. But this broadening is smaller than the experimental resolution, and so we once again use a Gaussian shape (in the exact form of (4.1)) - we are resolution limited.

- **Magnons**: In order to fit the single magnon peak, we used a Lorentzian shape - this time, no more resolution limited. The exact shape that we used is:

$$I(E) = \frac{A}{\pi}\left[\frac{\Gamma}{\Gamma^2 + (E - E_o)^2}\right] \tag{4.3}$$

The intensity is once again fixed by the parameter A, since this expression for the Lorentzian distribution is normalized to one.
The energy broadening is dictated by the parameter Γ, which is anyway always included between 0.021 and 0.024. E_o, again, set the energy position of the peak. In the case of magnons, it will display an evident dispersion.

- **Bimagnons**: in the case of bimagnon, we do not perform a proper fit. In fact, we just take the integral of the residual intensity - the intensity which is left after we subtract from the experimental spectrum all the previous fittings - in the region where bimagnons, at least in La_2CuO_4, are expected [42]. this means to take the integral between 300 meV and 900 meV energy loss.

- **dd excitations**: for the dd (or orbital) excitation we follow the same track given by bimagnons - we integrate the residuals between 1 eV and 3 eV of energy loss. This is not useful for our purpose, but it is

Once we have fitted every spectrum, we just have to plot all the intensities as functions of transferred momentum (for the maps along different Brillouin zone directions) or of the detuning.
In figure 4.10, 4.11, 4.12, 4.13, we have the plots.

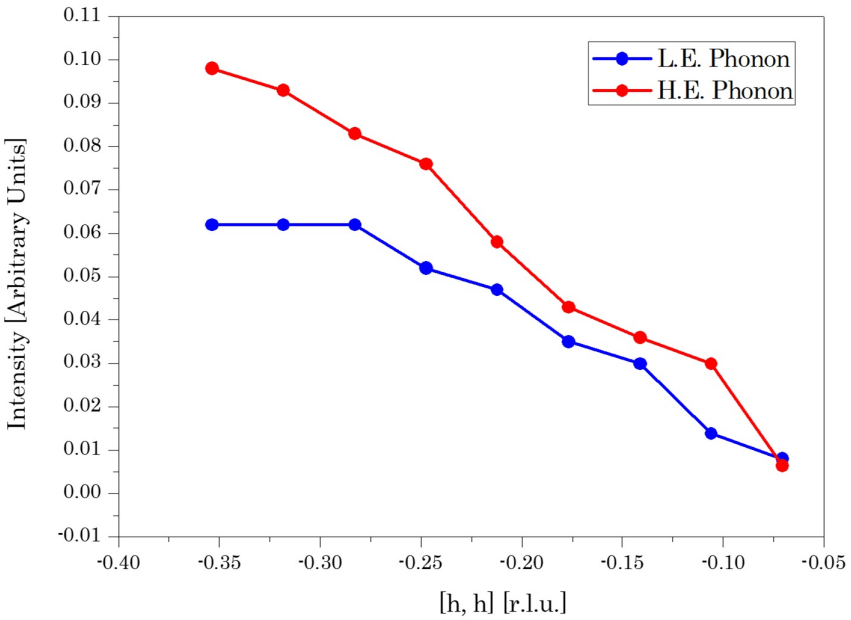

FIGURE 4.10: Phonons' intensities along diagonal direction in the Brillouin zone - all the data are extracted from the spectra in Figure 4.6. Both the lower energy phonon and the higher energy one are shown.

From Figure 4.10 and 4.11, we can immediately notice the trend of our coupling dependence. What we supposed in the previous Chapter - a coupling dependence which goes as the sin of the total transferred momentum

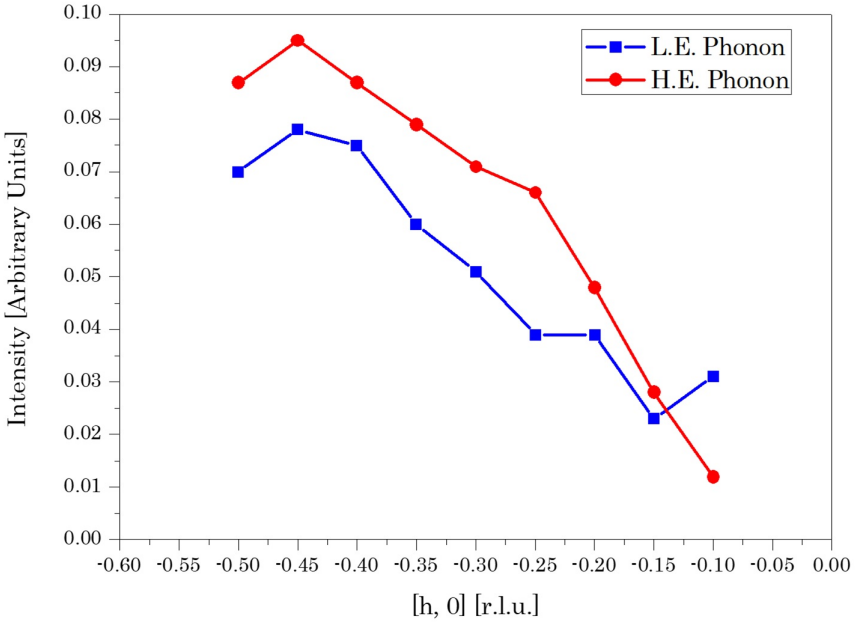

FIGURE 4.11: Phonons' intensities along diagonal direction in the Brillouin zone. In this case, data are extracted from the spectra in Figure 4.4.

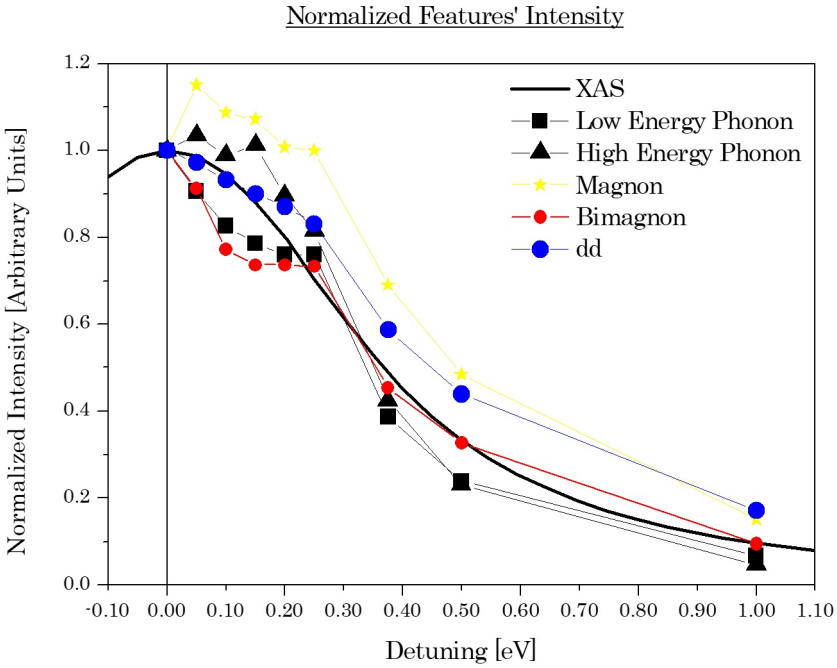

FIGURE 4.12: intensities for different values of detuning energy. All the intensities are normalized to their value at (supposed) zero detuning, which should be maximized by the greatest overall cross section (see Section 4.2). Evidently, things are way more complicated, as it is discussed in the text.

- is plausible: at least, the intensity of the phonons peaks really goes to zero moving towards the centre of the Brillouin zone and grows as we approach

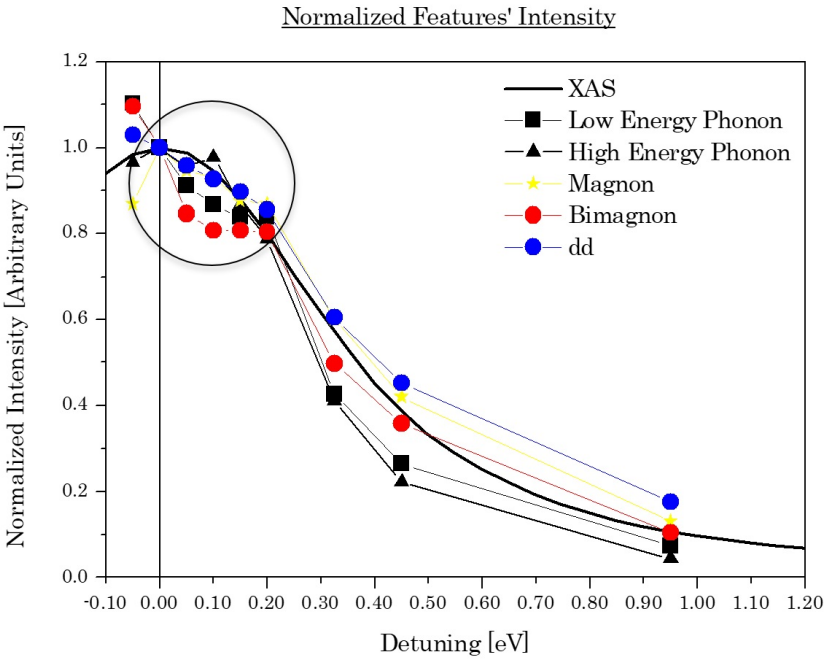

FIGURE 4.13: Again, features' intensity for different values of the detuning, but this time the intensities are normalized to their value at 0.05 eV detuning - this imply that the energy that we supposed to be at resonance is slightly out of it. The red circle highlight the spectra which are evidently more noisy (see Figure 4.7 - 4.8)

the borders.
The intensities of the peaks along different directions are rather comparable, and this is very coherent with Figure 3.20 - accounting for the fact that in RIXS we are able to investigate about half of the Brillouin zone, and that in Figure 4.10 and 4.11 (a vector $[0.35, 0.35]$ has a modulus which is $\simeq 0.5$) we arrive only at a $\mathbf{q} \simeq 5$, which correspond to $\mathbf{q} = 1.57$ in Figure 3.20.
Moreover, we can also notice that the higher energy phonon is always more intense than the low energy one - where all the precautions about really considering the low energy one as a single phonon are implicit. Anyway, this would suggest that the high energy phonons have a stronger coupling to the electrons than the low energy ones.
In Figure 4.12 and 4.13 we have the intensity dependence from detuning. The situation is more complicated than expected - and it is evident, at first glance, from the fact that the intensities of magnons' features in Figure 4.12 seems to grow with detuning. This is a non-sense, for what we have said in Section 4.2.
In first place we have to recall that, between 0.05 eV and 0.20 eV we are dealing with quite noisy spectra. The intensity values are plausible, but they are definitely not incontrovertible.
Considering Figure 4.12, the overall dependence follows the XAS intensity, as we expected. Still, we have an anomalous intensity from the high energy phonon and the magnon. If for the phonon we could also accept that our

simple fitting, in which we use only two phononic peaks, is subject to errors, for the magnon the error can not be due to errors in fitting and the result will have to be explained in a different way (see Figure 4.8).
This said, is hard to find a plausible physical explanation for what happens in the first experimental fitting points of Figure 4.12. More interesting (and somehow comforting) is what happens in the next points, which also are the cleanest (in the sense that here we have a remarkably smaller noise). We have a clear behaviour of the "intermediate state dependant" features (in the sense of the previous section) which consists in a faster intensity decay for growing energy detuning. The features which are generated in the final state of our RIXS process, as it is seen, follow more strictly the XAS detuning dependence, which is the only explicit dependence of their overall cross-section.
This trends should be eventually confronted to the calculations in Figure 4.3, paying attention to the parameters which enter this simulations - an evidently important factor is the intermediate state lifetime (which associate a certain energy broadening $\Gamma = \frac{h}{\omega_o}$). A reasonable choice is a Γ between 0.5 eV and 0.8 eV (a lifetime of tens of femtoseconds) - which means $\frac{\Gamma}{\omega_o}$ of around 8 for the high energy phonon and of 16 for the low energy one. $\frac{\Omega}{\omega_o}$ also change for the two phonons: the higher energy one will be in a range 0-12, while the low energy one will be in the range 0-25.
Figure 4.13 is another way to consider the anomalies in the small detuning region, and in particular the magnon intensity which is greater than at resonance. In this picture we suppose that the true resonance was where we supposed to be at 0.05 eV detuning, which is, as we can see from Figure 4.12, the point in which the magnon fits give the greatest intensity. This could be explained with the fact that the XAS peak relative to the Cu L_3 edge is not a properly simple peak, but it is associated, inside its Lorentzian shape, to more than one state - and this can complicate the detuning dependence of the spectrum collected at such edge.

In the end, a preliminary fitting of our results with the figure 4.3 returns a coupling strength of 210 meV for the higher energy mode (nominally the breathing mode) and of 190 meV for the lower energy one. This means, once we fix a plausible value for Γ (which we already discussed), to identify the coupling strength which better approximated the experimental intensity loss at different value of detuning. We are referring to the strength of the coupling as to the parameter $M(\mathbf{K})$ in the equation (3.17). As we have said, since we are considering non dispersive phonons, the momentum dependence is clearly lost.

Bibliography

[1] J. George Bednorz and K. Alex Müller. "Possible highT c superconductivity in the Ba-La-Cu-O system." In: *Zeitschrift für Physik B Condensed Matter 64.2* (1986).

[2] Matteo Rossi. "Resonant inelastic X-ray scattering on spin-orbit-induced correlated-electron systems: scientific applications and instrumental developments". PhD thesis. Universitè Grenoble Alpes, 2016.

[3] Greta Dallea. "Collective excitations in high temperature superconducting cuprates studied by renonant inelastic x-rays scattering". PhD thesis. Politecnico di Milano, 2016.

[4] Leon N. Cooper Bardeen John and J. Robert Schrieffer. "Theory of Superconductivity". In: *Physical Review 108.5 (1957): 1175.* (1957).

[5] C. C. Tsuei and J. R. Kirtley. "Pairing symmetry in cuprate superconductors". In: *Rev. Mod. Phys.* 72 (4 2000), pp. 969–1016. DOI: 10.1103/RevModPhys.72.969. URL: https://link.aps.org/doi/10.1103/RevModPhys.72.969.

[6] B. Keimer et al. "High Temperature Superconductivity in the Cuprates". In: *arXiv e-prints*, arXiv:1409.4673 (2014), arXiv:1409.4673. arXiv: 1409.4673 [cond-mat.supr-con].

[7] Maddury Somayazulu et al. "Evidence for Superconductivity above 260 K in Lanthanum Superhydride at Megabar Pressures". In: *Phys. Rev. Lett.* 122 (2 2019), p. 027001. DOI: 10.1103/PhysRevLett.122.027001. URL: https://link.aps.org/doi/10.1103/PhysRevLett.122.027001.

[8] R. O. Jones. "Density functional theory: Its origins, rise to prominence, and future". In: *Rev. Mod. Phys.* 87 (3 2015), pp. 897–923. DOI: 10.1103/RevModPhys.87.897. URL: https://link.aps.org/doi/10.1103/RevModPhys.87.897.

[9] John Hubbard. *Electron correlations in narrow energy bands.* 1963.

[10] G. A. Sawatzky Zaanen J. and J. W. Allen. *Band gaps and electronic structure of transition-metal compounds.* 1985.

[11] Marco Moretti Sala. "Magnetic and Inelastic soft x-rays scattering". PhD thesis. Politecnico di Milano, 2011.

[12] S. Blundell. *Magnetism in Condensed Matter*. Oxford Master Series in Condensed Matter Physics. OUP Oxford, 2001. ISBN: 9780198505914. URL: https://books.google.it/books?id=0GhGmgEACAAJ.

[13] T. Timusk. "The mysterious pseudogap in high temperature superconductors: an infrared view". In: *Solid State Communications* 127.5 (2003), pp. 337 –348. ISSN: 0038-1098. DOI: https://doi.org/10.1016/S0038-1098(03)00371-5. URL: http://www.sciencedirect.com/science/article/pii/S0038109803003715.

[14] William Witczak-Krempa et al. "Correlated Quantum Phenomena in the Strong Spin-Orbit Regime". In: *Annual Review of Condensed Matter Physics* 5.1 (2014), pp. 57–82. DOI: 10.1146/annurev-conmatphys-020911-125138. eprint: https://doi.org/10.1146/annurev-conmatphys-020911-125138. URL: https://doi.org/10.1146/annurev-conmatphys-020911-125138.

[15] Øystein Fischer et al. "Scanning tunneling spectroscopy of high-temperature superconductors". In: *Rev. Mod. Phys.* 79 (1 2007), pp. 353–419. DOI: 10.1103/RevModPhys.79.353. URL: https://link.aps.org/doi/10.1103/RevModPhys.79.353.

[16] Matteo Minola. "Magnetic, Orbital and Charge fluctuations in layered cuprates studied by resonant soft x-rays scattering". PhD thesis. Politecnico di Milano, 2013.

[17] G. Seibold, M. Grilli, and J. Lorenzana. "Stripes in cuprate superconductors: Excitations and dynamic dichotomy". In: *Physica C Superconductivity* 481 (2012), pp. 132–145. DOI: 10.1016/j.physc.2012.03.072. arXiv: 1202.1615 [cond-mat.str-el].

[18] K. Yamada et al. "Doping dependence of the spatially modulated dynamical spin correlations and the superconducting-transition temperature in $La_{2-x}Sr_xCuO_4$". In: *Phys. Rev. B* 57 (10 1998), pp. 6165–6172. DOI: 10.1103/PhysRevB.57.6165. URL: https://link.aps.org/doi/10.1103/PhysRevB.57.6165.

[19] A Gabovich et al. "TOPICAL REVIEW: Charge and spin-density-wave superconductors". In: *Superconductor Science Technology - SUPERCONDUCT SCI TECHNOL* 14 (Apr. 2001). DOI: 10.1088/0953-2048/14/4/201.

[20] Leon N. Cooper. "Bound Electron Pairs in a Degenerate Fermi Gas". In: *Phys. Rev.* 104 (4 1956), pp. 1189–1190. DOI: 10.1103/PhysRev.104.1189. URL: https://link.aps.org/doi/10.1103/PhysRev.104.1189.

[21] T. Cuk et al. "A review of electron-phonon coupling seen in the high-Tc superconductors by angle-resolved photoemission studies (ARPES)". In: *physica status solidi (b)* 242.1 (), pp. 11–29. DOI: 10.1002/pssb.200404959. eprint: https://onlinelibrary.wiley.com/doi/pdf/10.1002/pssb.200404959. URL: https://onlinelibrary.wiley.com/doi/abs/10.1002/pssb.200404959.

[22] Luuk Ament. "Resonant inelastic x-ray scattering studies of elementary excitations". PhD thesis. Instituut-Lorentz for Theoretical Physics, Leiden Institute of Physics, Faculty of Science, Leiden University: Leiden University, 2010.

[23] Akio Kotani and Shik Shin. "Resonant inelastic x-ray scattering spectra for electrons in solids". In: *Rev. Mod. Phys.* 73 (1 2001), pp. 203–246. DOI: 10.1103/RevModPhys.73.203. URL: https://link.aps.org/doi/10.1103/RevModPhys.73.203.

[24] Luuk J. P. Ament et al. "Resonant inelastic x-ray scattering studies of elementary excitations". In: *Reviews of Modern Physics* 83 (2011), pp. 705–767. DOI: 10.1103/RevModPhys.83.705. arXiv: 1009.3630 [cond-mat.str-el].

[25] L. Braicovich et al. "Momentum and polarization dependence of single-magnon spectral weight for Cu L_3-edge resonant inelastic x-ray scattering from layered cuprates". In: *Phys. Rev. B* 81 (17 2010), p. 174533. DOI: 10.1103/PhysRevB.81.174533. URL: https://link.aps.org/doi/10.1103/PhysRevB.81.174533.

[26] N.W. Ashcroft and N.D. Mermin. *Solid State Physics*. Philadelphia: Saunders College, 1976.

[27] J. Zaanen, G. A. Sawatzky, and J. W. Allen. "Band gaps and electronic structure of transition-metal compounds". In: *Phys. Rev. Lett.* 55 (4 1985), pp. 418–421. DOI: 10.1103/PhysRevLett.55.418. URL: https://link.aps.org/doi/10.1103/PhysRevLett.55.418.

[28] M. P. M. Dean. "Insights into the high temperature superconducting cuprates from resonant inelastic X-ray scattering". In: *Journal of Magnetism and Magnetic Materials* 376 (2015), pp. 3–13. DOI: 10.1016/j.jmmm.2014.03.057. arXiv: 1402.5423 [cond-mat.supr-con].

[29] P. M. Platzman and E. D. Isaacs. "Resonant inelastic x-ray scattering". In: *Phys. Rev. B* 57 (18 1998), pp. 11107–11114. DOI: 10.1103/PhysRevB.57.11107. URL: https://link.aps.org/doi/10.1103/PhysRevB.57.11107.

[30] J.J. Sakurai. *Advanced Quantum Mechanics*. Always learning. Pearson Education, Incorporated, 1967. ISBN: 9788177589160. URL: https://books.google.it/books?id=lvmSZkzDFt0C.

[31] N.B. Brookes et al. "The beamline ID32 at the ESRF for soft X-ray high energy resolution resonant inelastic X-ray scattering and polarisation dependent X-ray absorption spectroscopy". In: *Nuclear Instruments and Methods in Physics Research Section A: Accelerators, Spectrometers, Detectors and Associated Equipment* 903 (2018), pp. 175 –192. ISSN: 0168-9002. DOI: https://doi.org/10.1016/j.nima.2018.07.001. URL: http://www.sciencedirect.com/science/article/pii/S0168900218308234.

[32] L. Pintschovius et al. "Phonon anomalies in La2NiO4". In: *Physica C: Superconductivity* 153-155 (1988), pp. 276 –277. ISSN: 0921-4534. DOI: https://doi.org/10.1016/0921-4534(88)90590-4. URL: http://www.sciencedirect.com/science/article/pii/0921453488905904.

[33] G.D. Mahan. *Many-Particle Physics*. Physics of Solids and Liquids. Springer US, 2000. ISBN: 9780306463389. URL: https://books.google.it/books?id=xzSgZ4-yyMEC.

[34] A. Anderson. "Canonical Transformations in Quantum Mechanics". In: *Annals of Physics* 232 (1994), pp. 292–331. DOI: 10.1006/aphy.1994.1055. arXiv: hep-th/9305054 [hep-th].

[35] Faris Gel'mukhanov et al. "Duration of x-ray Raman scattering". In: *Phys. Rev. A* 59 (1 1999), pp. 380–389. DOI: 10.1103/PhysRevA.59.380. URL: https://link.aps.org/doi/10.1103/PhysRevA.59.380.

[36] D. Reznik. "Giant electron-phonon anomaly in doped La2CuO4 and other cuprates". In: *arXiv e-prints*, arXiv:0909.0769 (2009), arXiv:0909.0769. arXiv: 0909.0769 [cond-mat.supr-con].

[37] S. Johnston et al. "Systematic study of electron-phonon coupling to oxygen modes across the cuprates". In: *Physical Review B* 82, 064513 (2010), p. 064513. DOI: 10.1103/PhysRevB.82.064513. arXiv: 1007.3451 [cond-mat.supr-con].

[38] Maurits Haverkort. "Spin and orbital degrees of freedom in transition metal oxides and oxide thin films studied by soft x-ray absorption spectroscopy". PhD thesis. Universität zu Köln, 2005. URL: https://kups.ub.uni-koeln.de/1455/.

[39] C. Thomsen and G. Kaczmarczyk. "Vibrational Raman Spectroscopy of High-temperature Superconductors". In: (2006). DOI: 10.1002/0470027320.s6305. eprint: https://onlinelibrary.wiley.com/doi/pdf/10.1002/0470027320.s6305. URL: https://onlinelibrary.wiley.com/doi/abs/10.1002/0470027320.s6305.

[40] T. P. Devereaux et al. "Directly Characterizing the Relative Strength and Momentum Dependence of Electron-Phonon Coupling Using Resonant Inelastic X-Ray Scattering". In: *Phys. Rev. X* 6 (4 2016), p. 041019. DOI: 10.1103/PhysRevX.6.041019. URL: https://link.aps.org/doi/10.1103/PhysRevX.6.041019.

[41] Zbigniew W. Gortel, Robert Teshima, and Dietrich Menzel. "Time-dependent theory of the Auger resonant Raman effect for diatomic molecules: Concepts and model calculations for N_2 and CO". In: *Phys. Rev. A* 58 (2 1998), pp. 1225–1246. DOI: 10.1103/PhysRevA.58.1225. URL: https://link.aps.org/doi/10.1103/PhysRevA.58.1225.

[42] V. Bisogni et al. "Bimagnon studies in cuprates with resonant inelastic x-ray scattering at the O *K* edge. I. Assessment on La_2CuO_4 and comparison with the excitation at Cu L_3 and Cu *K* edges". In: *Phys. Rev. B* 85 (21 2012), p. 214527. DOI: 10.1103/PhysRevB.85.214527. URL: https://link.aps.org/doi/10.1103/PhysRevB.85.214527.